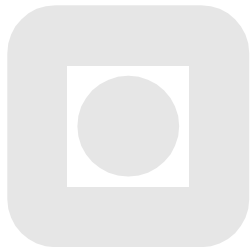


# Optimal Wrist Prosthesis Kinematics: Three-dimensional Rotation Statistics and Parameter Estimation

Dr. ing. thesis  
**Øyvind Stavdahl**



Report 2002:9-W  
Department of Engineering Cybernetics  
Norwegian University of Science and Technology  
NO-7491 Trondheim, Norway  
2002



# Summary

This thesis presents new theoretical results related to the statistical analysis of three-dimensional rotational data, as well as experimental results on the rotational kinematics of exoskeletal prosthetic wrist joints.

The statistical methods that are traditionally applied to rotational data are inadequate for rotations that have an arbitrary range. A set of rotation-specific statistical operators, referred to as the *cosine statistics*, are presented and interpreted from a geometrical point of view. The resulting cosine average operator is equivalent to the maximum likelihood estimator for the mean of a matrix Fisher distribution. A strong feature is that it is isotropic in its function, completely decoupling its value from the choice of reference coordinate frame. The novel concept of *definity* constitutes a measure of the degree of rotational symmetry in a given data set, providing a confidence measure for the cosine average. The operators related to data dispersion are simpler than those previously presented.

An experiment is designed and conducted in order to provide new insight into the utilization of the human wrist joint. Eight healthy subjects are instrumented and their range of elbow and finger motion is mechanically restricted to that obtainable with a commercial hand prosthesis. This construct is denoted a *simulated prosthesis*. The freedom of motion at the wrist is kept intact. Data on forearm and hand movement are recorded during the performance of activities of daily living (ADL) and subsequently analysed with respect to wrist motion.

Simple kinematic models are fitted to the data, and an ANOVA-inspired analysis is carried out. Considerable variability is found in wrist utilization between the different activities, while between-subject variations are only moderate.

For the zero-Degree-of-Freedom (0-DoF) prosthetic wrist, the overall optimal orientation is found to imply a slight pronation, extension and ulnar deviation. In the 1-DoF case, the overall optimal axis of rotation closely resembles that of a prosupination movement, which is the functionality offered by most commercial electric wrist prostheses. In some activities, however, the optimal axis of rotation exhibits significant obliquity with respect to the forearm and hand, indicating that there is potential for a better adaptation of prosthesis kinematics to these tasks.



# Preface

This thesis is submitted in partial fulfilment of the requirements for the degree Dr.ing. (Doktor ingeniør) at the Norwegian University of Science and Technology (NTNU). The research has been carried out at the Department of Engineering Cybernetics during periods from 1994 to 2002.

I am an engineer. Engineers are known to be notoriously preoccupied with technical solutions, sometimes to the point where the focus on the real problem is lost. In writing this thesis it has become ever more clear to me how many problems are *not* addressed and how many relevant questions still remain unanswered. This is one of the real benefits of a research project: it leaves a new set of defined areas and subjects to be researched in the future. Still, at each stage of research, new significant knowledge should be revealed, and the goal of future research should be updated to reflect the new knowledge. It is my personal hope that the work presented in this thesis will be a contribution to the design of prosthetic components that better suit the needs of those who choose to use them. While a modern powered prosthesis is an advanced mechatronic device, its area of application is still very demanding when used by intelligent individuals to carry out everyday tasks. Even if the formal language of a doctoral thesis tends to “objectify” these individuals as “subjects” or “amputees”, they should and will be thought of as those they really are: friends, neighbours, spouses or colleagues, ordinary people who are respected and loved.

This project has been a truly multidisciplinary one, and without virtually unlimited professional and personal support from a number of people the completion of the project would have been impossible. Therefore, I would like to dedicate this preface to those who have helped me through this riveting period. A comprehensive list of all contributors would be far too voluminous, thus I have selected just a few individuals and institutions that have been especially important for this project:

My dear friend **Sigbjørn Rønning** for sharing his personal experience with prosthetic components and for his enthusiasm and patience.

**Svein Sivertsen, K. Tomm Kristensen, Rolf Sørbye** and their respective staffs for introducing me to the field of prosthetics and sharing their experience and contacts; Svein and Tomm for a long and fruitful cooperation; Tomm and his Mette for being good friends and a source of inspiration – and delicious meals.

**Lennart Philipson, Peter J. “DA” Kyberd** and **David Gow** for their tremendous hospitality and for sharing their experience with me. **DA** for a truly modern friendship. Our E-mail chats have kept me optimistically on track while also providing some of the everyday variation needed to stay motivated.

Assistant Professor **Klara Jakobsen** of the Department of Occupational Therapy, School of Health Education, Sør-Trøndelag University College and **Tordis Magne**, OT, of the Department of Prosthetics and Orthotics, University Clinic of Trondheim, for invaluable cooperation and enthusiastic support in conjunction with the experimental design.

My supervisor Professor **Kjell E. Malvig** and my adviser Professor Emeritus **Jens G. Balchen**, both of the Department of Engineering Cybernetics, Norwegian University of Science and Technology, are acknowledged for providing the advice and motivation needed for releasing the grant and getting me started with the work, for always being there when needed, for invaluable advice throughout the project and for being good friends and colleagues.

**Stewart Clark** also of the Norwegian University of Science and Technology for his linguistic advice and English-language editorial assistance on a draft version of this thesis.

In addition I am indebted to my friends and colleagues for valuable comments to this manuscript and for their support throughout the project.

The majority of the work presented in this thesis has been financed by the **Research Council of Norway** under grant 109533/320. Additional funding, components and services for the research have been provided by **Norsk teknisk ortopedi AS, Cypromed AS, Centri AB** and **Trøndelag ortopediske verksted**. **TINE Midt-Norge AS** provided empty milk cartons for some of my experiments. My present employer, **SINTEF Electronics and Cybernetics**, has been overwhelmingly patient and generous in facilitating the completion of this work. All contributions are acknowledged and highly appreciated.

**My parents** and **my sister** for always backing me up and showing interest in my work. My **mother** for leading me to the understanding of the binary number system close to three decades ago, and my **father** for being my pal and a very creative and stimulating person; an engineer by birth. Thanks to my **sister** for asking the questions I needed to be asked in order to fully understand what I am doing, questions that originate from a truly brilliant and curious mind.

Finally, thanks to my magnificent bride and my wonderful brood, of whom I am utterly proud.

After all, you are all I need.

Trondheim, Norway, 28 October 2002  
Øyvind Stavdahl



# Contents

<b>Summary</b>	<b>i</b>
<b>Preface</b>	<b>iii</b>
<b>Contents</b>	<b>vii</b>
<b>List of Figures</b>	<b>xiii</b>
<b>1 Introduction</b>	<b>1</b>
1.1 Motivation .....	1
1.2 Scope of the Thesis .....	2
1.3 Contributions .....	3
1.4 Guidelines for the Reader .....	4
<hr/>	
<b>Part I The Distal Upper Limb and its “Replacement”</b>	<b>7</b>
<b>2 Anatomy and Biomechanics of the Human Upper Limb</b>	<b>9</b>
2.1 Motivation .....	9
2.2 Terminology .....	10
2.2.1 The Standard Anatomical Position .....	11
2.2.2 Anatomical Planes .....	11
2.2.3 Relative Positions, Directions and Sides .....	11
2.2.4 Clinical Angles .....	12
2.3 Structural Description .....	12

2.3.1	Elbow and Forearm .....	12
2.3.2	Wrist and Hand .....	13
2.3.3	Muscles and Tendons .....	15
2.3.4	Neuromuscular Structures and Mechanisms .....	17
2.4	Kinematics of the Hand and Wrist .....	18
2.4.1	Kinematics of the Fingers .....	19
2.4.2	Kinematics of the Thumb .....	20
2.4.3	Functional Anatomy of the Wrist .....	21
2.4.4	A Kinematic Model of the Wrist .....	22
2.5	Modes of Operation .....	26
2.5.1	Non-prehensile Movements .....	26
2.5.2	Prehensile Movements .....	27
<b>3</b>	<b>Upper-limb Prostheses</b>	<b>29</b>
3.1	A Brief Introduction .....	29
3.2	Principal Functions Impaired by Transradial Amputation .....	29
3.3	Principal “Anatomy” of Upper-limb Prostheses .....	30
3.4	Overview of Prosthetic Solutions .....	32
3.4.1	The Residual Limb as a “Prosthesis” .....	32
3.4.2	Cosmetic Prostheses .....	33
3.4.3	The Krukenberg Procedure .....	33
3.4.4	Body-powered Prostheses .....	33
3.4.5	Externally Powered Devices .....	34
3.4.6	Suspension .....	36
3.4.7	Control Aspects .....	37
3.5	Elaboration of the Scope .....	39
3.5.1	The Focus: Kinematic Constraints .....	39
3.5.2	The Unavoidable Restrictions .....	40

<b>Part II Materials and Methods</b>	<b>43</b>
<b>4 Experimental Design</b>	<b>45</b>
4.1 Introduction .....	45
4.1.1 Compensatory Movements .....	45
4.1.2 The Simulated Prosthesis .....	46
4.1.3 Restatement of the Purpose .....	47
4.2 Materials and Methods .....	47
4.2.1 Brief Overview .....	47
4.2.2 Selection and Performance of Activities .....	47
4.2.3 Choice and Design of Utensils .....	50
4.2.4 Selection and Preparation of the Subjects .....	51
4.2.5 Motion Measurement .....	52
4.2.6 Coordinate Frames and Transformations .....	58
<b>5 Rotational Foundations</b>	<b>63</b>
5.1 Motivation .....	63
5.1.1 Human Joints Rotate .....	63
5.1.2 Conventional Methods are Not Applicable .....	64
5.2 Terminology .....	64
5.2.1 A Rigid Body's Degrees of Freedom .....	64
5.2.2 Orientation of a Joint .....	65
5.2.3 Parallelity of Coordinate Frames .....	66
5.2.4 Orientation vs. Rotation .....	66
5.2.5 Orientation, Attitude and Posture .....	66
5.3 The Rotation Matrix Space: SO(3) .....	67
5.3.1 Topology .....	67
5.3.2 Parameterizations of SO(3): Special Phenomena .....	69
5.3.3 Properties of the Full Matrix Representation .....	70
5.3.4 Angle/Axis Parameterization .....	70

5.3.5	Metric on SO(3); Rotational Distance .....	71
5.3.6	Equivalent Axis of Rotation .....	72
5.3.7	Euler Angles .....	72
5.3.8	The Orientation Vector .....	72
5.3.9	Euler Parameter Representation .....	73
5.4	Kinematics of the Restricted Wrist .....	74
5.4.1	Introduction .....	74
5.4.2	Model of the Single-Degree-of-Freedom Wrist .....	74
5.4.3	Model of the Two-Degree-of-Freedom Wrist .....	77
5.4.4	On the Uniqueness of Solutions .....	78
<b>6</b>	<b>Orientation Statistics</b>	<b>81</b>
6.1	Previous Research .....	81
6.1.1	Parameterizations Frequently Used in Biomechanics .....	81
6.1.2	Orientation Statistics .....	82
6.2	The Problem of Averaging Orientations .....	83
6.2.1	Arithmetic Attempts and their Shortcomings .....	83
6.2.2	The Least Squares Average .....	84
6.2.3	A Class of Average Operators for Samples on Groups .....	86
6.3	The Cosine Average .....	88
6.3.1	Geometric Interpretation .....	89
6.3.2	Existence .....	90
6.3.3	Uniqueness Properties .....	91
6.3.4	Calculation Formulae .....	92
6.3.5	Definity .....	93
6.3.6	SO(3) is Distributive over the Cosine Average Operation .....	94
6.4	Comparative Assessment of Cosine Average Performance .....	95
6.4.1	Application to Simulated Data .....	95
6.4.2	A Real-World Case .....	96
6.5	Variance and Standard Deviation of Orientations .....	99

---

6.5.1	Relative Cosine Variance . . . . .	102
6.6	Kinematic Models Revisited: Estimating Optimal Parameters . . . . .	103
6.6.1	The Maximum Cosine Estimate . . . . .	103
6.6.2	Reparameterization . . . . .	105
6.6.3	Assessment of a Numeric Solver . . . . .	105
6.7	Appendix: Symmetry and Rotational Neutrality . . . . .	108
6.8	Appendix: Generalizations and Applications . . . . .	113
6.8.1	The Cosine Average as an Orthogonalization Operator . . . . .	113
6.8.2	Filtering of Ordered Series of Rotations . . . . .	113
6.8.3	Discrete Simulation of Rigid Body Orientation . . . . .	114
6.8.4	Dynamic State Estimation . . . . .	115
 <hr/>		
<b>Part III</b>	<b>Optimal Wrist Prosthesis Kinematics</b>	<b>117</b>
<b>7</b>	<b>Experimental Results</b>	<b>119</b>
7.1	Introduction . . . . .	119
7.2	Optimization: A Bird's Perspective . . . . .	120
7.3	The 0-DoF Problem . . . . .	120
7.3.1	Grand Average Wrist Orientation During ADL . . . . .	120
7.3.2	Intra- and Inter-Group Variations . . . . .	121
7.4	The 1-DoF Problem . . . . .	124
7.4.1	Terms and Conventions . . . . .	124
7.4.2	Grand Optimal Kinematics . . . . .	124
7.4.3	Intra- and Inter-Group Variations . . . . .	127
7.5	Range of Motion . . . . .	128
7.6	Measurement Error Quantified . . . . .	133
<b>8</b>	<b>Discussion and Conclusion</b>	<b>137</b>
8.1	Rotation Statistics . . . . .	137
8.1.1	Differential Rotations vs. General Rotational Data . . . . .	137

8.1.2	Suggestions for Future Research . . . . .	138
8.2	Wrist Prosthesis Kinematics . . . . .	138
8.2.1	People are Alike but Activities are Different . . . . .	138
8.2.2	Validity of the Results . . . . .	139
8.2.3	Suggestions for Future Research . . . . .	142
<b>References</b>		<b>143</b>
<b>A Tabulated Experimental Results</b>		<b>A-1</b>
A.1	0-DoF Optimal Wrist . . . . .	A-2
A.1.1	Subject-based Analysis . . . . .	A-2
A.1.2	Activity-based Analysis . . . . .	A-4
A.1.3	Subject/Activity-based Analysis . . . . .	A-6
A.1.4	Age Group-based analysis . . . . .	A-7
A.1.5	Sex-based Analysis . . . . .	A-8
A.2	1-DoF Optimal Wrist . . . . .	A-9
A.2.1	Subject-based Analysis . . . . .	A-9
A.2.2	Activity-based Analysis . . . . .	A-12
A.2.3	Age Group-based Analysis . . . . .	A-15
A.2.4	Sex-based Analysis . . . . .	A-17

# List of Figures

2.1	The standard anatomical position with planes and directions. . . . .	10
2.2	Principal functions of the elbow and forearm. . . . .	13
2.3	The bones and joints of the human wrist and hand. . . . .	14
2.4	The major intrinsic muscles of the hand, viewed from the palmar side. . . . .	16
2.5	Thumb CMC model of Hollister et al. (1992). . . . .	21
2.6	Kinematic model and clinical angles of the wrist. . . . .	24
3.1	Transradial amputee with a body-powered split-hook. . . . .	34
3.2	Joints and internal structure of the so-called IBM arm. . . . .	35
3.3	Consequence for wrist cross section of an oblique axis of rotation. . . . .	41
4.1	Plaster-of-Paris sockets. . . . .	53
4.2	Calibration measurement set-up. . . . .	54
4.3	Orientation of body-fixed coordinate frames in calibration posture. . . . .	59
5.1	Illustration of a rigid body's six mechanical DoFs. . . . .	65
5.2	Orientation of a joint, exemplified by the proximal interphalangeal (PIP) joint. . . . .	66
5.3	The topology of rotation spaces. . . . .	68
5.4	A rotation matrix and its geometric interpretation. . . . .	70
5.5	Illustration of SO(3) and a fewer-dimensional subspace. . . . .	75
5.6	Actual one-dimensional subspaces of SO(3) with different rotation offsets and axes. . . .	76
5.7	Physical meaning of the 2-DoF model parameters. . . . .	77
5.8	Actual two-dimensional subspaces of SO(3) with different rotation offsets and axes. . . .	79
6.1	Sign shifts of the orientation vector and the Euler parameter vector. . . . .	84
6.2	Comparison between the square and the cosine function. . . . .	87

6.3	Geometric interpretation of the cosine average.....	90
6.4	Uniqueness modes of the cosine average: geometric interpretations.....	93
6.5	Comparison of different average operations. ....	97
6.6	Forearm and hand: instrumentation and coordinate frame definitions. ....	98
6.7	Comparison of average wrist orientation calculated using two different methods. ....	100
6.8	Distance from a point to a 1-DoF subspace on SO(3).....	104
6.9	Robustness of the 1-DoF model estimator.....	107
6.10	Rotational Neutrality; a geometric interpretation.....	109
6.11	Schematic discrete-time FIR filters for real scalar data and for rotation matrix data. .	114
7.1	Grand average wrist orientation during ADL. ....	122
7.2	Largest activity-based average deviation from the grand average orientation.....	123
7.3	Angular deviation of subject-activity average from grand average.....	123
7.4	The concept of angular distance between two axes of rotation. ....	124
7.5	Postures obtainable with the grand optimal 1-DoF wrist kinematics.....	126
7.6	Example of clinical angles during RoM activity. ....	130
7.7	Scatter plot of FEM vs. RUD angles for the data in Figure 7.6.....	131
7.8	Muscles: the four groups of wrist motors according to Saffar and Semaan (1994)....	132
A.1	Largest subject-based deviation from grand average orientation. ....	A-3
A.2	Largest activity average-wise deviation from grand average orientation. ....	A-5
A.3	Axis and postures for optimal 1-DoF parameters based on subject 3. ....	A-11
A.4	Axis and postures for optimal 1-DoF parameters based on subject 4. ....	A-11
A.5	Axis and postures for optimal 1-DoF parameters based on activity 5. ....	A-14
A.6	Axis and postures for optimal 1-DoF parameters based on activity 9. ....	A-14
A.7	Axis and postures for optimal 1-DoF parameters for subjects below 30 years of age. A-16	
A.8	1-DoF model optimized for female subjects. ....	A-18
A.9	1-DoF model optimized for male subjects. ....	A-18

# **Chapter 1**

## **Introduction**

### **1.1 Motivation**

Next to the human mind, the musculoskeletal system is what makes us what we are: it is our ability to precisely control multiple muscles and joint movements in a coordinated manner that enables us to interact with our environment by feeding, moving, actively exploring and communicating with other individuals. Human motor control is closely integrated with the mind to the extent that most movements are carried out more or less unconsciously as an automatic response to a mental intention. Because of this close relationship between mind and body, the loss of a limb may have consequences for the individual far beyond the mechanical domain. The loss of a limb, such as a hand, means the loss of an extremely adept tool for carrying out sophisticated tasks as well as the loss of an instrument for recreation and diversion, for advanced non-verbal communication and more. The loss of a limb is a loss indeed, and trying to provide an optimal “replacement” is a natural thought.

Even though some professions and extreme sports imply an increased risk of traumatic amputation, acquired limb defects strike all layers of all societies. In addition, congenital limb abnormalities are produced in approximately 3 to 6 in 10 000 live births (Hjermstad, 1996, Kyberd et al., 1997), a number of which are related to the upper limb. Land mines and acts of war keep claiming their victims, many of whom survive but with varying degrees of limb injuries. Thus there is no indication that the need for limb prostheses will disappear or even diminish.

Dental prostheses are common in industrialized countries, but a large number of other body parts also have their artificial counterpart. Providing adequate upper-limb prostheses has proven to be especially challenging because of the extraordinary properties of this limb: it is powerful and robust, yet dexterous and delicate, and it is closely integrated with the central nervous system (CNS) via motor

nerves and sophisticated sensory pathways. This combination challenges numerous fields of technology, such as material properties (weight, strength), sensor technology (user input and feedback devices), energy supply (battery size, weight and capacity), actuator technology (motor size and power, devices for sensory feedback to the CNS) and control engineering (control schemes, embedded microprocessors). Several of these areas exhibit tremendous technical progress and have been doing so for decades, yielding a well-known gap between the available technical possibilities and the devices actually available to prosthesis users.

In light of this ever-increasing unexploited technical potential, and whilst appreciating that a prosthetic device is not the best option to all potential users, the present work aims at providing bits and pieces needed for possessing some of the yet unexploited land relevant to externally powered upper-limb prostheses.

## 1.2 Scope of the Thesis

### *Transradial Cases*

The study focuses on devices for users with transradial amputation, which is the most common form of upper-limb prostheses (Atkins et al., 1996, Kyberd et al., 1997). The condition of the residual limb in these users is often well suited for controlling advanced wrist and hand devices compared to those with higher levels of amputation. Furthermore, the focus is on externally powered (i.e. motorized) prostheses, though parts of the results may be applicable even to body-powered devices.

### *Optimizing Wrist Prostheses for Weight, Size and Functionality*

Because of the inevitable space and weight limitations imposed on limb prostheses, terminal devices (that is artificial hands and other tools for prehension and manipulation) with multiple motorized joints are not frequently applied. Most motorized wrist units available provide a pronation/supination movement to rotate the terminal device about the long axis of the forearm; other but less common units employ a transversal flexion/extension movement. In this project it is hypothesized that neither of these single-degree-of-freedom (DoF) wrist prostheses is functionally optimal when used with a single-DoF terminal device. The study aims at evaluating this hypothesis by estimating the optimal single axis of rotation from real-world data related to healthy wrists.

The ultimate goal of this process is to limit the complexity of the wrist prosthesis to that of a single motorized joint under the constraint that the resulting device approximates the functional characteristics of a healthy wrist joint as closely as possible. Potential benefits of such an optimal device include reduction of com-

pensatory movements in other body parts, particularly elbow and shoulder, and consequently reduced susceptibility to load injuries, as well as better utilization of the terminal device which yields a higher level of rehabilitation.

#### ***Statistics for Rotational Data***

During the course of the project it became evident that the statistical methods commonly applied in biomechanics were insufficient for analysing the present data. Exploration, explanation and exploitation of the theoretical basis for orientation statistics were thus included in the work and represent a substantial part of the contents of the thesis.

### **1.3 Contributions**

The original and main objective of this work was to provide new insight into human wrist utilization and relate this information to the design of kinematically optimal wrist prostheses. The approach chosen was to utilize motion capture technology to collect information about the rotational movement patterns of healthy human wrists during the performance of carefully selected activities and under conditions resembling those experienced by a prosthesis user.

During the course of the work a second objective was to provide a generic basis for unbiased statistical analysis of this kind of data.

Specific contributions include:

**The Cosine Statistics:** Traditional statistical methods based on meagre parameterizations such as Euler angles, Euler parameters or related representations are sufficient when the angular spread of the data is small. In this thesis it is demonstrated how and why these methods fall short in relation to arbitrary data sets typical to those arising in biomechanics. The *cosine average* (CA) is introduced, which works on full  $3 \times 3$  rotation matrices and yields optimal results in a maximum cosines sense. The operator is equivalent to theoretical results previously published by others, but its present derivation based mainly on geometric considerations provides an alternative way to understanding its nature. The CA is not guaranteed to always exist, therefore the novel notion of *definity* is introduced as a simple measure of how far the average is from being indefinite for a given data set. Simple operators for rotational variance and standard deviation are suggested as an alternative to more complicated techniques.

**Interpretations and Generalizations:** Extensive geometric interpretations of the cosine statistics are given, and several of their fundamentally desirable properties are derived. Importantly it is shown that the cosine average is independent of the choice of reference coordinate frame, a property

referred to as isotropy. A powerful generalization is suggested which allows for isotropic discrete-time filtering of general rotational data. To my best knowledge this is a novel approach. Possible applications to dynamic state estimation of rigid-body motion are also pointed out.

**The Simulated Prosthesis:** An extensive laboratory experiment was designed in close cooperation with occupational therapist students at the Sør-Trøndelag University College. The freedom of movement of healthy subjects' hands and forearms was restricted to resemble that of a powered transradial forearm prosthesis, referred to as a "simulated prosthesis", by application of custom-made plaster sockets. By keeping the wrist joint unrestricted while performing carefully selected activities of daily living (ADL), information relevant to prosthesis kinematics was collected.

**Optimal Wrist Kinematics:** A number of kinematic parameters were derived from the simulated prosthesis data. The results provide insight into the functionally optimal alignment of a passive wrist unit. The results also have implications for the kinematic design of functionally optimal motorized wrist prostheses with a single degree of freedom. Data analysis revealed a relatively high degree of coherency across subjects and subject groups with respect to the optimal kinematic parameters, while the results differed significantly across activities performed. The major conclusion is that for some tasks the traditional wrist configuration with a pure prosupination movement is the most appropriate, while other activities may be more easily performed with an oblique wrist axis of rotation.

## 1.4 Guidelines for the Reader

This thesis comprises eight chapters and one appendix arranged in three parts. The dual scope of the project, ranging from group theory and linear algebra to experimental biomechanical research, has prompted the author to include somewhat detailed background information in both fields in an attempt to make the thesis accessible to a broader audience.

The structure of the thesis is as follows:

- **Chapter 1** (this chapter) gives a brief introduction to the scope and contributions of the work, as well as the present comments on the structure of the thesis.

**PART I** gives the basic terminology, background information and motivation for the work:

- **Chapter 2** reviews the anatomy and physiology of the healthy human elbow, forearm, wrist and hand as a background for understanding the challenges associated with prosthesis design. A simple kinematic model of the wrist is presented.
- **Chapter 3** gives an introduction to upper limb prosthetics in terms of technical challenges, a brief historical overview and recent advances in the field. This chapter sums up the original motivation for the project.

**PART II** presents the experimental design and data analysis methods used:

- **Chapter 4** presents full detail on the materials and methods used in conjunction with the laboratory experiments.
- **Chapter 5** gives an introduction to the rotation matrix space,  $SO(3)$ , and defines central terms and concepts related to rotational data.
- **Chapter 6** introduces cosine statistics and its properties, implications and applications.

**PART III** contains the results and conclusions pertaining to wrist kinematics.

- **Chapter 7** analyses the data collected in terms of parameters relevant to different prosthetic designs as well as inter- and intra-group variations.
- **Chapter 8** discusses the results in the previous chapter, draws some conclusions and outlines possible further research in this area.

**Appendix A** presents comprehensive tables and figures of the basic data analysis pertaining to Chapter 7.

A consistent chain of thought is progressively developed by first providing a motivational basis in the present field of application, outlining an experiment to address essential issues, developing the mathematical tools needed for conducting the following empirical research and finally collecting and analysing data. Issues which are considered to be important but not directly related to the main chain of thought are placed in appendix sections at the end of the respective chapters.

The reader who is mainly interested in the statistical aspects of the work may benefit from browsing in Part I before proceeding to Chapters 5 and 6, as the latter includes references to kinematic models and notions developed in the former.

To the reader who is most interested in the orthopaedic-technical and biomechanical features of the project, Parts I and III with the addition of Chapter 4 are clearly most relevant. However, if one is completely unfamiliar with the notions of rotational motion and kinematic descriptions, an initial journey through the pages of Chapter 5 is suggested.

## Part I

# THE DISTAL UPPER LIMB AND ITS “REPLACEMENT”

*We shall look in vain if we seek for movements that man can do and a monkey cannot, but we shall find much if we seek for purposive actions that man can do and a monkey cannot.*

*(Jones, 1941)<sup>†</sup>*

---

<sup>†</sup>. As quoted by Napier (1956).



## **Chapter 2**

# **Anatomy and Biomechanics of the Human Upper Limb**

### **2.1 Motivation**

Our Central Nervous System (CNS) to a large degree determines and controls our behaviour, both our basic reflexes and more advanced behaviour based upon conscious observations, experience and prediction. But in order to make an active difference in this world, the CNS needs an “end effector organ” to actually implement its intentions. There are two main types of tissue that can respond physically, in a macroscopic sense, to nervous input, namely the gland and muscle. Of these, the muscle clearly produces the more spectacular response; in fact the effect of gland secretion is often to modify neuromuscular response. If we add joints, bones and tendons, the result is a system which is capable of producing impressive outputs in the form of mechanical force, velocity and energy as well as precise movements, manipulation and communicating gestures, a system that plays an ultimate role in the “external interface” of the human organism.

Appreciation of the complexity and the ingenuity of the human upper limb is of crucial importance for anyone wishing to design and apply technical devices that mimic even a fraction of the limb’s functions. This chapter briefly introduces the reader to the astounding structures and modes of operation of the healthy human forearm, wrist and hand and its control system. The chapter also reviews the basic biomechanics terminology used in the remaining chapters of the thesis.

## 2.2 Terminology

The human skeletal system is a tree-like open kinematic chain in which the spine constitutes the trunk and the legs and toes, arms and fingers make up the branches. Standardized terminology exists that comprises notions for specific locations and directions relative to the body and its members. This terminology is described in the following paragraphs and many of the notions are illustrated in Figure 2.1.

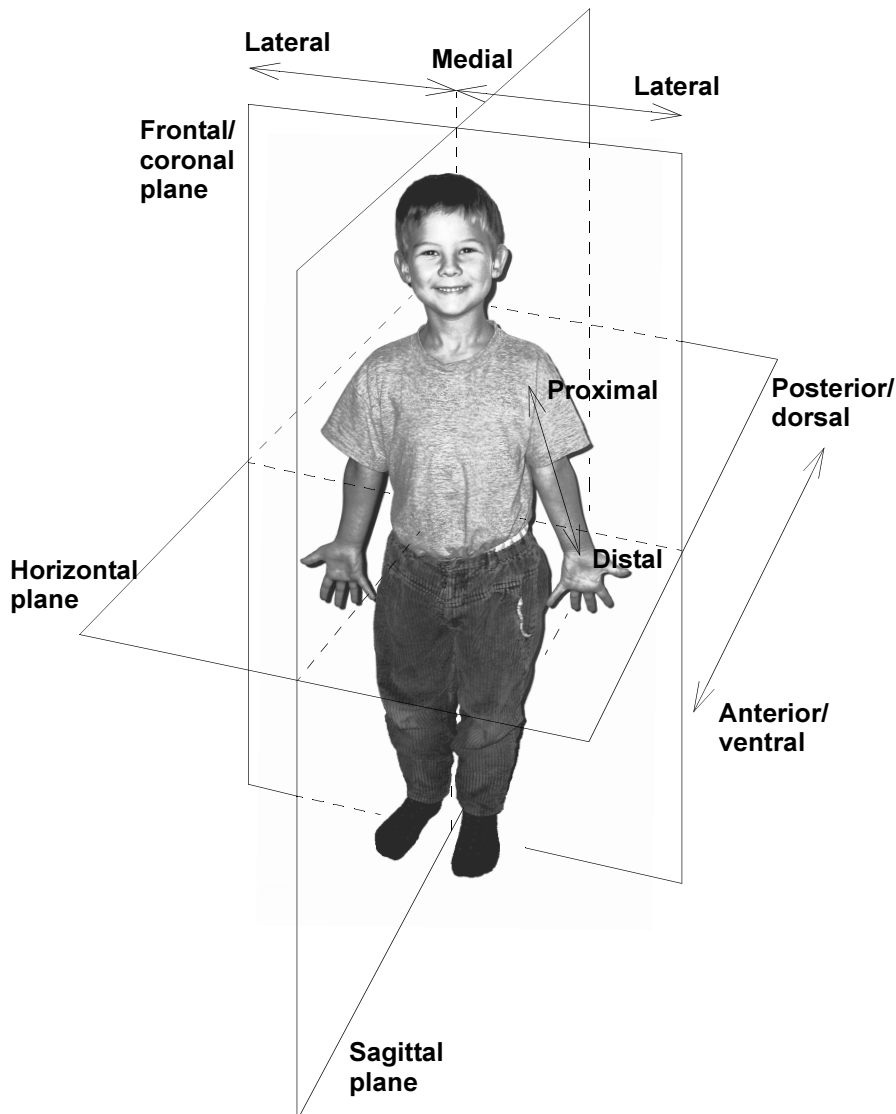


**Figure 2.1:** The standard anatomical position with planes and directions.

### 2.2.1 The Standard Anatomical Position

The standard anatomical position for the human body is as shown in Figure 2.1: subject standing straight up and facing forwards, legs straight down and toes pointing forwards, arms straight down and palms facing forwards. Most positions and directions are defined with reference to this posture.

It should be noted that in this thesis the term *posture* is generally used to denote the overall configuration of a kinematic chain (cf. Section 5.2.5 on page 66). The present use of the term “position” is an exception to this convention; it is used here because “standard anatomical position” is a well established term in pertinent literature.

### 2.2.2 Anatomical Planes

Frequently references are made to *anatomical planes*, i.e. planes defined in relation to the body. The *sagittal plane* (Lat. *sagitta* = arrow) is the plane of movement of an arrow when shot forwards from the archer i.e. the vertical plane of symmetry of the body. The *horizontal plane* is a plane dividing the body in an upper and a lower part, and the *frontal* or *coronal plane* is the plane perpendicular to the other two, i.e. the plane dividing the body in a front and back part.

### 2.2.3 Relative Positions, Directions and Sides

The term *proximal* is a relative concept meaning *closer to the trunk or point of origin*. The opposite of proximal is *distal*. Thus, the shoulder is proximal to the elbow, while the ankle is distal to the knee.

In the frontal plane, *medial* denotes closer to the body’s line of symmetry (i.e. closer to the sagittal plane) while *lateral* denotes farther away from this line. For example, in the standard anatomical position the thumbs are pointing laterally. When a location or organ is specified relatively to another, locations on the same side of the sagittal plane are denoted *ipsilateral*, while opposite sides are referred to as *contralateral*. Thus, the left foot is ipsilateral to the left hand but contralateral to the right hand.

What is generally regarded as being the front of the body, i.e. the face, chest, stomach, is denoted the *ventral* or *anterior side*. The opposite side, i.e. the rear, is denoted *dorsal* or *posterior*. Note that anatomical directions are expressed with respect to the standard position described above, so that the palm is regarded as the ventral side of the hand.

### 2.2.4 Clinical Angles

A joint's movement and orientation is frequently specified in terms of three so-called *clinical* (or *anatomical*) *angles*. These resemble a Euler angle sequence (cf. Part II), and are often perceived to coincide with anatomically significant planes of motion. We will use the shoulder as an example as this joint exhibits all three DoFs. Referring to the standard anatomical position, the lateral movement of the arm (i.e. displacing the arm laterally in the frontal plane) is denoted *abduction*, while *adduction* denotes displacement in the medial direction. Moving the arm in the ventral (anterior) direction implies shoulder *extension*, while dorsally directed movement is denoted *flexion*. Finally, rotating the palm laterally about the long axis of the arm is denoted *external rotation* or *supination*, while rotating the palm medially is called *internal rotation* or *pronation*. Similar definitions of the clinical angles apply to other joints; in the case of the wrist, abduction is frequently called *radial deviation* while adduction is termed *ulnar deviation* (referring to radius and ulna, the two bones extending the forearm along its lateral and medial side, respectively; cf. Figure 2.2).

## 2.3 Structural Description

Linscheid (1986) enframed his text in the following stately declarations:

*The wrist is the most complex joint in the body. It provides the final positioning for the hand at the end of a multilinked cantilevered effector mechanism, the arm. It has a large arc of motion, incremental adjustment capabilities, and substantial resistance to forces and torques.*

(...)

*The wrist joint is a marvellously complex structure that plays an integral part in the dynamics of the hand.*

In more technical terms, the total upper limb can be seen as a *micro-macro manipulator* (Egeland and Sagli, 1993), the arm constituting the “macro” manipulator responsible for low-frequency positioning and the wrist and hand being the high-bandwidth “micro” manipulator implementing the fast and precise part of the task. The powerful shoulder joint and upper arm will not be treated here except to note that the shoulder has three degrees of freedom and plays an important role in the overall utilization of the limb.

### 2.3.1 Elbow and Forearm

Figure 2.2 shows a simplified sketch of the elbow complex. Joints are referred to by the names of the adjacent bones. Thus, the *ulna* forms the *humero-ulnar joint* with the *humerus*. The hinge-like *humero-ulnar (HU) joint* stabilizes the elbow in the sideways direction as it only permits flexion and extension. Side by side with

ulna is the *radius*. As indicated in Figure 2.2, pronation and supination movement are implemented by radius sliding against the cylindric distal ulna, forming the *distal radioulnar (DRU) joint*. The *proximal radioulnar (PRU) joint* is also cylindric, while the *humero radial (HR) joint* is spherical, providing transversal stabilization of the proximal radius while permitting flexion and extension.

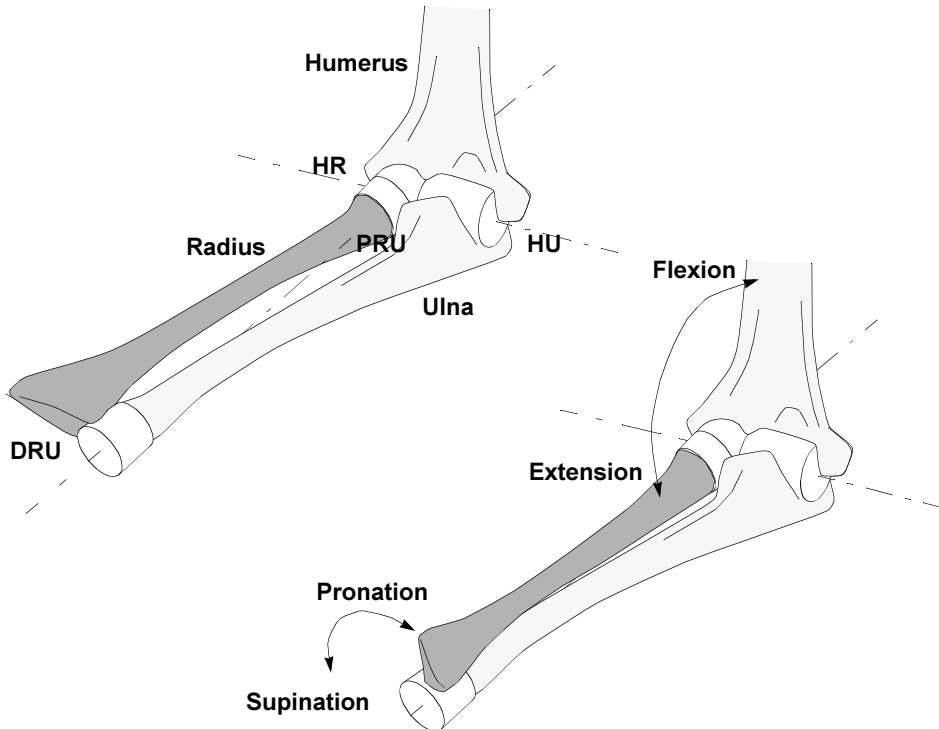
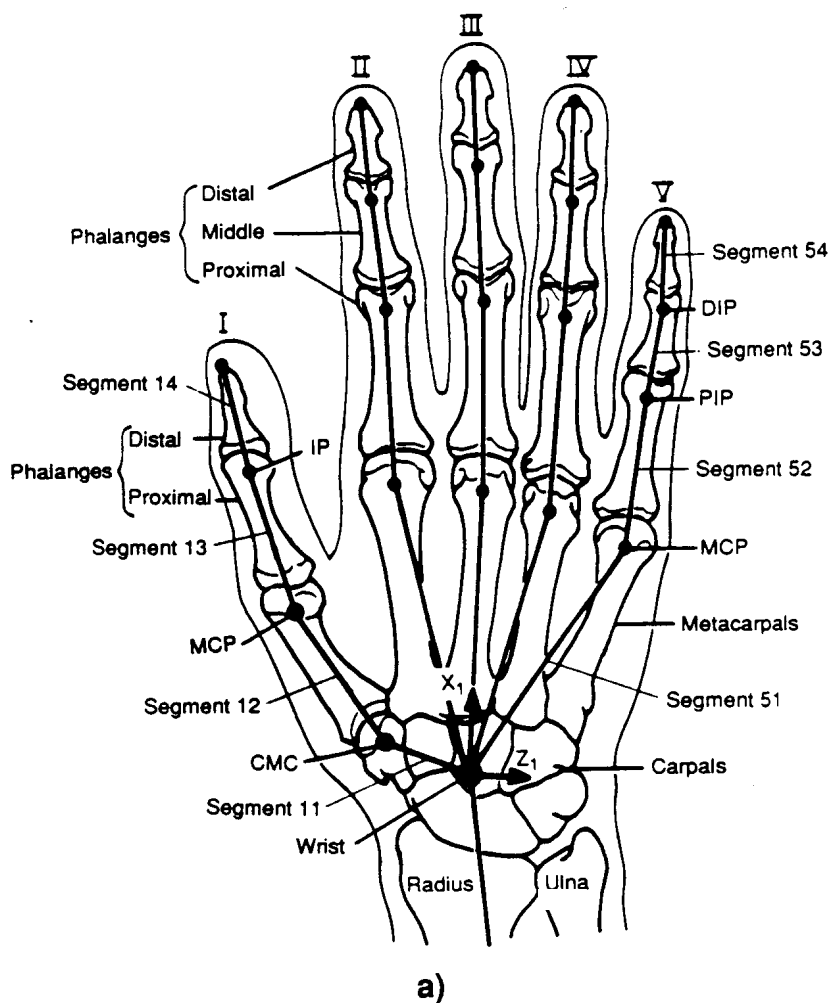


**Figure 2.2:** Principal functions of the elbow and forearm. The figure depicts a right limb.

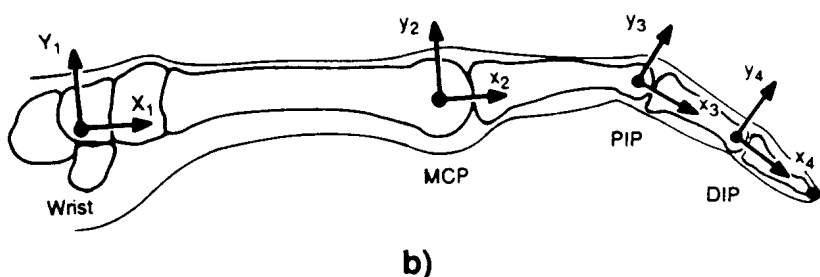
### 2.3.2 Wrist and Hand

The hand and wrist complex is among the most delicate skeletal structures in the human body. It comprises 26 bones interconnected by more than 20 joints which are actuated by more than 30 muscles and display a total of approx. 30 degrees of freedom. Figure 2.3 names and numbers these bone segments according to Buchholz and Armstrong (1992).

Just distally to the radius and ulna we find the eight *carpal bones* that together make up the *wrist joint*. The joint connecting radius and the proximal row of the carpal bones is denoted the *radiocarpal joint (RC)*. The RC joint permits flexion and a certain amount of radioulnar deviation, but is essentially locked in the pro-



a)



b)

**Figure 2.3:** The bones and joints of the human wrist and hand. From Buchholz and Armstrong (1992), © Elsevier Science. Reprinted with permission.

nation/supination direction due to powerful ligaments and the geometry of the joint itself. Thus, prosupination torque and movement of the forearm are effectively transmitted to the hand via the RC.

The palm of the hand is spanned by the five *metacarpals*, which are connected to the carpal through the *carpometacarpal (CMC) joints*.

Even if the thumb is frequently referred to as a finger, biomechanically speaking it is not because of its special geometry and function. Thus, here the term fingers denotes the index, long, ring and little finger, which each comprises three bones; the *proximal, medial and distal phalanges*, respectively. The proximal phalanges and the distal heads of the corresponding metacarpals make up the *metacarpophalangeal (MCP) joints*, while the two joints connecting the three phalanges of each finger are named the *proximal and distal interphalangeal (PIP and DIP) joints*, respectively. Having only a *proximal* and a *distal phalanx*, the joints of the thumb are denoted the *metacarpophalangeal (MCP)* and simply the *interphalangeal (IP) joint*, respectively.

### 2.3.3 Muscles and Tendons

Muscles are the motors of the body. Frequently a muscle is situated a certain distance from the joint which it actuates. Muscular force is therefore passed on to the joint via the slim and flexible but extremely strong fibrous structures called *tendons*. The elbow and forearm joints are actuated by muscles in the upper arm and forearm. The degrees of freedom of the wrist and hand are controlled by *extrinsic muscles* located in the forearm, and *intrinsic muscles* within the hand itself. Figure 2.4 illustrates some of the main muscles and tendons on the palmar side of the human hand. These structures will not be treated in detail, the purpose of the figure is to illustrate the complexity of the system.

#### ***Mechanical Properties***

According to Brand et al. (1981), the ratio of strength from muscle to muscle within the same limb is relatively constant: ‘it is not the actual *strength* that matters but *balance*’. The maximum tension developed by a muscle was found to be proportional to the cross-sectional area of all fibres that make up the muscle, while the potential excursion was proportional to muscle fibre length.

Although most skeletal muscles are identical at the microscopic level, their different high-level architecture leads to different mechanical properties. Kaufman et al. (1989) presented a simple model accounting for the angle between the muscle’s fibres and the direction of its contractile force; different angles imply different “gear ratios”.

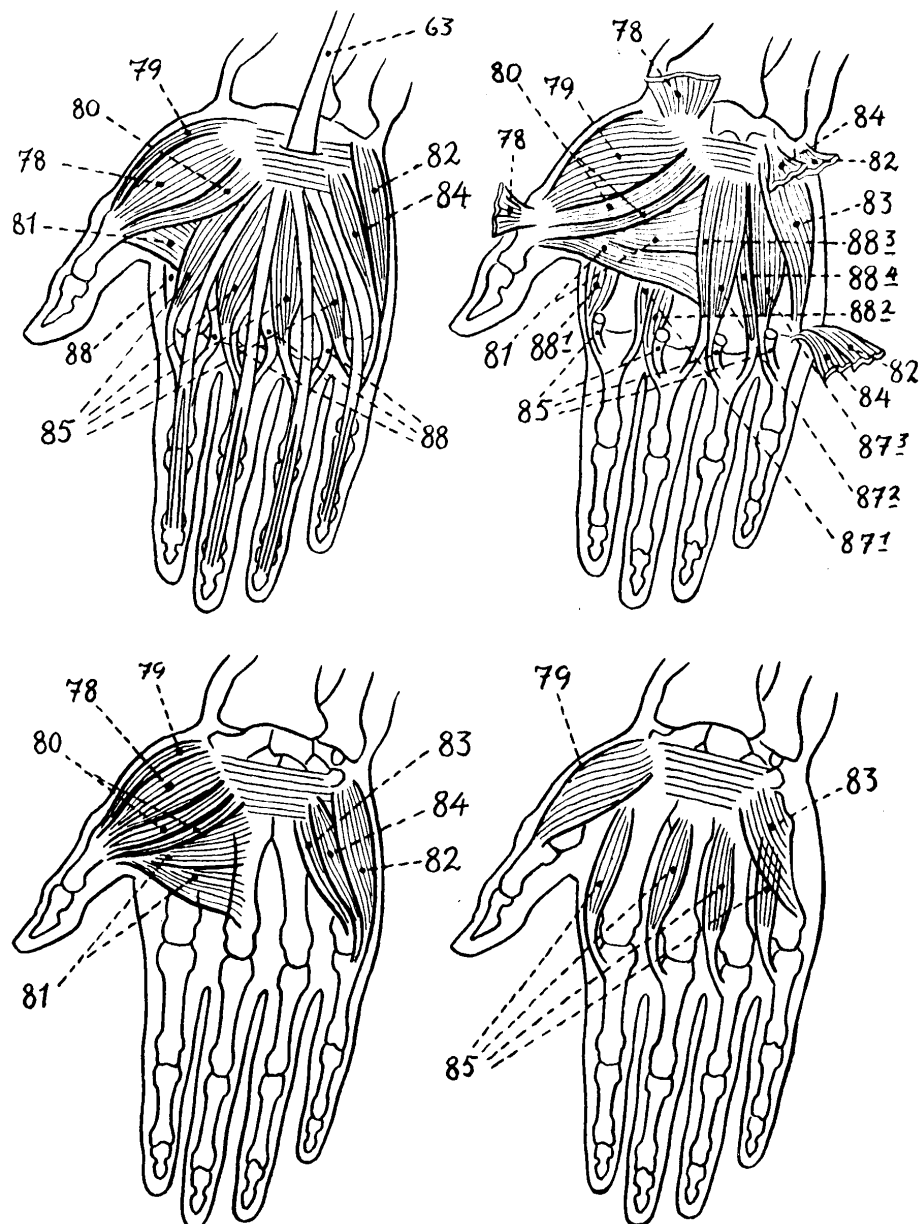


**Figure 2.4:** The major intrinsic muscles of the hand, viewed from the palmar side. The structure numbered 63 is the tendon of *Musculus palmaris longus*, one of the major extrinsic muscles responsible for flexion and incurvation of the palm. From Lie (1944).

### **Coupling between Wrist and Fingers**

As all extrinsic hand tendons pass through the wrist, there is a certain degree of coupling between wrist and finger motion. The extrinsic finger tendons are constrained to a small area close to the centre of wrist rotation, partly decoupling the functions of these tendons from those of the wrist. In contrast, the extrinsic thumb extensors cross the wrist at a significant distance from its centre of rotation and thus contribute to radial wrist deviation. The wrist motor tendons, that is the primary tendons that actuate wrist flexion/extension and radioulnar deviation, are arrayed about the perimeter of the wrist, allowing for large moments to be generated (Linscheid, 1986).

The distribution of flexor forces to each individual finger has been reported to be independent of the orientation of the wrist while the magnitude of the total force varies with wrist orientation, with the greatest total force exhibited in ulnar wrist deviation (Hazelton et al., 1975). In contrast, Lamoreaux and Hoffer (1995) found that grip force is weakened during deviation. This apparent contradiction might be due to different experimental conditions; however, similar discrepancies are evident in many other publications related to the wrist and hand, and might be attributable to the limb's complexity and individual variations.

Armstrong and Chaffin, (1978) presented a simple model of the relationship between wrist flexion angle and the accompanied extrinsic finger flexor excursion. Their model predicts an average excursion of about  $0.25\text{mm}/{}^\circ$  of wrist flexion/extension for both major flexor tendons, and their data indicate a fairly linear relationship throughout the range of wrist motion.

#### **2.3.4 Neuromuscular Structures and Mechanisms**

An introduction to this subject can be found in Deutsch and Deutsch (1993); for a more detailed treatment the reader is guided to pertinent literature in the field of Neurophysiology.

##### **Motor Units**

Skeletal muscles are controlled by so-called  $\alpha$ -motoneurons. The nucleus of an  $\alpha$ -motoneuron is situated within the spinal cord, but its *axon* (nerve fibre) extends all the way to a skeletal muscle where it branches and terminates on a set of muscle fibres. The  $\alpha$ -neuron and its connected muscle fibres make up a *motor unit*. Neurons emit series of discrete impulses called *action potentials (AP)*; each time an AP from a neuron reaches the muscle, all fibres of its motor unit generate a *twitch* of contractile force. By modulating the AP pattern of each motor unit the CNS controls the postures and movements of the body.

### Sensory Receptors

Specialized neural receptors, such as muscle *spindles* and *Golgi tendon organs*, provide feedback paths to the spinal cord that ensures dynamic stability and prevents mechanical overload of the musclotendon system. Skin receptors provide information about contact forces, surface texture and slip conditions, while *kinesthetic receptors* transduce information about joint angles. All this information is fed back to the CNS and make up what is known as *physiological proprioception*<sup>†</sup>. These neural pathways are believed to be of crucial importance for our ability to perform fine motor tasks.

In what may be referred to as the “steady state” of a neuron, the concentrations of K<sup>+</sup> and Na<sup>+</sup> ions inside the cell are different from that on the outside. A neural AP is triggered as a shift in the electric potential across the cell membrane opens certain selective ion channels. Positive ions slide down their concentration gradients through these channels, further adding to the electric potential shift and opening even more ion channels. Once this process is triggered it causes a chain reaction that propagates the AP throughout the length of the axon. When the AP reaches a muscle fibre, it triggers a similar process that causes the aforementioned twitch of force. A single motor unit may comprise several thousands of muscle fibres, so the AP as observed in the vicinity of the muscle (denoted the *motor unit action potential, MUAP*) has a significantly higher amplitude than that which can be observed around the motor axon. The MUAPs of all active motor units add up to what is known as the *myoelectric signal* or *electromyogram (EMG)*, which can be monitored by means of intramuscular needle electrodes or even with extracutaneous surface electrodes. The amplitude of the EMG signal depends on the degree of muscle contraction, and extracutaneous voltages can amount to a few mV during extreme contractions. EMG measurements are used routinely as an aid in neuromuscular diagnostics, for research purposes and as a control input to externally powered prostheses.

## 2.4 Kinematics of the Hand and Wrist

The term *kinematics* denotes that which is related to the geometry of a mechanism. In the present context, interesting geometric quantities are the positions of joint centres of rotation, the ranges of motions of joints and attitudes of the joint axes of rotation, the length of bone segments, the moment arms of the tendons relative to the joint centres and finally the relationship between tendon excursions and joint angles. A brief review of these properties is presented to get a glimpse of the mechanical principles employed in the distal upper limb.

---

<sup>†</sup>. The degree to which each of these types of afferent information reaches conscious levels in the brain, has been and remains a controversial topic.

### 2.4.1 Kinematics of the Fingers

#### *Finger Joints*

An early description of the MCP joint of a normal finger was made by You et al. (1978). They investigated the joint's active and passive range of motion (i.e. that which can be achieved by voluntary muscle contractions and the range permitted when the joint is passively moved by an external force). Measurements were made both in the *flexion-extension movement (FEM)* and the *radioulnar deviation (RUD)* direction, and indicated that the active range of all four fingers are between  $145^\circ$  and  $152^\circ$  for the FEM and between  $38^\circ$  and  $57^\circ$  in the RUD plane. The passive ranges recorded were in the intervals  $151^\circ - 172^\circ$  and  $53^\circ - 68^\circ$  for the FEM and RUD, respectively, while the centres of rotation of the joint could be regarded as fixed, coinciding and centrally located in the metacarpal head. The axial rotation of the phalanges was negligible, indicating that the MCP joint only exhibits two degrees of freedom. In a frequently cited article, An et al. (1979) published a “normative” hand model comprehensive enough to allow for biomechanical analysis without clinical facilities and anatomical studies. They investigated ten hands and reported averaged one-dimensional data on the positions of the joint centres of the MCP, PIP and DIP joints as well as the lengths of the phalanges of all four fingers. An et al. (1983) followed up this study by reporting empirical data on the ranges of motion of all three joints of the index finger. Despite general agreement with You et al. (1978), their results for the FEM plane showed an average range of only  $85.3^\circ$ . Buchholz et al. (1992) constructed a normative model that included the joint centre positions in the FEM plane. A major improvement over the model of An et al. (1979) was that the geometry was reported relatively to the wrist centre, yielding a more complete description of the hand. Buchholz et al. concluded that the centre of rotation of the PIP or DIP joints can generally be estimated as the centre of curvature of the proximal joint surface, a handy estimate that is not applicable to the thumb.

#### *Tendons and Pulleys*

The mechanical torque generated by a tendon about a joint is proportional to the tendon tension and to the distance from the tendon to the joint's centre of rotation (i.e. the “moment arm” of the tendon).

Brand et al. (1975) studied the flexor tendons and pulleys at the MCP joints of cadaver hands by applying a constant tension to the flexor tendon of choice and recording the resulting force at the finger tip as well as the tendon excursion for the full range of joint angles. Brand et al. fitted the following mathematical model to their data:

$$E = a\Theta^b \quad (2.1)$$

where  $E$  is the excursion of the tendon [mm],  $\Theta$  is the joint angle ( $^{\circ}$  relative to total extension), while  $a$  and  $b$  are constants to be fitted. In all reported cases the parameter  $b$  was close to unity, yielding a fairly linear tendon excursion-joint angle relationship. This leads to the expectation that the moment arms of the investigated tendons can be regarded as constant. Armstrong and Chaffin (1978) used a similar methodology to evaluate three alternative joint models. The model that best fitted the recorded data was the so-called Landsmeer Model I, which is linear and therefore confirms the findings of Brand et al. (1975). This contradicts the assumption by An et al. (1979) that at each joint, the tendon can be represented by a straight line joining one fixed point on the proximal bone and one on the distal. Armstrong and Chaffin also established a simple mathematical model for predicting the tendon moment arms at all three finger joints from externally measured joint thicknesses. In the same volume of the same journal, You et al. (1978) published estimated moment arms of the extrinsics and excursion of both extrinsic and intrinsic tendons at the MCP joint. Their excursion data agreed well with those of Armstrong and Chaffin, while the figures for the moment arms showed significant deviation. In particular, You et al. reported up to 50 % raise in the moment arms of the extrinsic flexor tendons at full flexion. As for the intrinsic tendons, these were found to have significant RUD moment arms at neutral FEM angle, but hardly any at full flexion. None of the extrinsic tendons were found to have any moment arms in the RUD direction. These findings were essentially confirmed by An et al. (1983).

Interestingly, Hahn and Krimmer (1995) found that an unresisted “normal” finger displays proportionality between the PIP and DIP joint angles,  $1^{\circ}$  of PIP flexion causing  $0.79^{\circ}$  of DIP flexion on an average for all fingers. This relationship is caused by a “tendon linkage”, and implies that in unresisted motion, the two interphalangeal joints can be modelled as having a single common degree of freedom. A grasping finger, however, was found to display a far less consistent relationship between these angles.

### 2.4.2 Kinematics of the Thumb

The kinematics of the thumb bones was described by Buchholz et al. (1992), who reported estimated bone lengths and normalized joint centre positions. These authors assumed the CMC joint to have three coinciding axes of rotation, and the position of the axes’ point of intersection was assumed to be at the centre of curvature of the trapezium (the carpal bone adjacent to the thumb metacarpal).

These assumptions were contraindicated by Hollister et al. (1992), who found that the CMC has exactly two non-intersecting axes that are fixed and are not perpendicular to each other or to the bones; in fact one axis is located within the trapezium while the other runs through the metacarpal base. Figure 2.5 illustrates this geometry by two hinges that are connected by a virtual link.

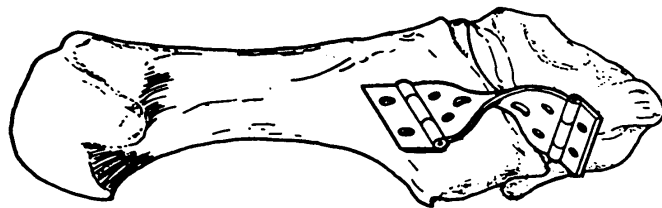


**Figure 2.5:** Thumb CMC model of Hollister et al. (1992). The left bone is the metacarpal, while the small bone to the right is the trapezium. Reprinted with permission.

### 2.4.3 Functional Anatomy of the Wrist

#### Bones and Joints

Traditionally the wrist joint is regarded as consisting of the eight carpal bones, but the bones of the forearm, in particular radius, play an important role in wrist function. The distal aspect of radius forms the *radiocarpal joint (RC)* with the *proximal carpal row*. Connecting the proximal and *distal carpal rows* is the *intercarpal joint (IC)*. The scaphoid is not member of either row; instead it is commonly perceived as bridging the two carpal rows (Linscheid, 1986).

#### Degrees of Freedom

Some of the functions and notions introduced in the following paragraphs are illustrated in Figure 2.6a, page 24.

#### Axial Rotation

As illustrated in Figure 2.2, pronation–supination or just *ProSupination Movement (PSM)* is a feature of the forearm rather than of the wrist. It occurs in the HR, PRU and DRU joints about an axis through the proximal head of the radius and distal head of the ulna.

The DRU joint is intimately involved in several important features of the wrist (see e.g. Palmer and Werner (1984)), and some authors therefore regard PSM as a wrist function (Linscheid, 1986). This view will be adopted even in this thesis, for two additional reasons. Firstly, it is frequently lost or greatly impaired following traumatic transradial amputation. Secondly, the most common kinds of sockets for transradial prostheses are partly suspended in the epicondyles and the olecranon, which in effect forces the prosthesis to follow the movements of the ulna. Thus, even if a pronation/supination ability is preserved in the residual limb, the typical below-elbow prosthesis will not follow this movement.

### Flexion

*Flexion-Extension Movement (FEM)* is rotation about an axis crudely parallel to the palmar plane and perpendicular to the forearm, that is movement in the same plane as the flexion and extension of the fingers. Flexion is sometimes called palmar flexion, while extension may be denoted dorsal flexion. FEM mainly involves the radiocarpal and the intercarpal joints (de Lange et al., 1985, Linscheid, 1986).

### Deviation

The third and final DoF of the wrist occurs about an axis perpendicular to the palmar plane, and is denoted *RadioUlnar Deviation (RUD)*. Radial deviation denotes rotation towards the radius and the thumb, while ulnar deviation occurs towards the ulna and the little finger.

#### 2.4.4 A Kinematic Model of the Wrist

The Standardization and Terminology Committee of the International Society of Biomechanics (ISB) has suggested a general standard for reporting of kinematic data for the hand and wrist (Werner and Buchholz, 1994). In the proposed model, the FEM axis of rotation is defined as being fixed to the proximal bone and PSM fixed to the distal bone, while the RUD axis is the “floating axis” which is perpendicular to the other two. According to its originators, this model corresponds to clinical terminology. Adopting the convention that the DoFs of a kinematic chain are listed in order from proximal to distal, the ISB proposal can be denoted a FEM–RUD–PSM configuration.

This model is tailored for application to pairs of adjacent bones as well as to “global wrist motion”. In biomechanics literature, global wrist motion is frequently taken as motion of the metacarpals with respect to the radius. Palmer et al. (1985) used a triaxial goniometer to measure FEM, RUD and PSM between the distal radius and the metacarpals in healthy subjects during the performance of 52 standardized tasks. Their model was similar to the FEM–RUD–PSM configuration of Werner and Buchholz (1994) and Werner (2001). Their reported average range of carpal PSM motion (one subject only) was  $6.9^\circ$ , which is more than an order of magnitude smaller than the PSM range of approx.  $150^\circ$  exhibited when forearm rotation is included (van der Heijden and Hillen, 1996, Linscheid, 1986). The results of Moore et al. (1993) even imply that the wrist (i.e. the RCJ and the ICJ) has only two DoFs, suggesting that the PSM components observed by Palmer et al. (1985) might be due to misalignment of the goniometer with the anatomical axes of rotation or movements of the instrumentation with respect to the bones. In either case, the preponderance of the PSM potential of the human forearm and wrist can be attributed to the radioulnar articulation. In agreement with this obser-

vation, kinematic models comprising both forearm and wrist function published by Raikova (1992), Lemay and Crago (1996) and Barker et al. (1996) place the PSM axis proximal to the other two.

Several qualitatively different results have been published with respect to the positions of the FEM and RUD axes of rotation. There seems, however, to be a convergence towards the view that both these axes pass through the proximal part of the capitate, the FEM axis being slightly proximal to the RUD axis (Youn et al., 1978, Ohshima et al., 1994). Such a FEM–RUD configuration is also supported by the hypothesized wrist joint mechanism of Moore et al. (1993), and is used by numerous authors for studying or modelling movements of the carpal (Jackson et al., 1994) or the metacarpals (Ruy et al., 1991, O'Driscoll et al., 1992, Raikova, 1992, Salvia et al., 1994, Lemay and Crago, 1996, Salvia et al., 2000) with respect to the radius.

Supported by the above discussion, the following PSM–FEM–RUD configuration is used in this thesis, cf. Figure 2.6. The PSM axis is assumed fixed to the forearm (ulna) and parallel to the forearm's long axis. The RUD axis is fixed to the metacarpals and perpendicular to the plane defined by the second and third metacarpal. The FEM axis is the floating axis, i.e. perpendicular to the other two. In Figure 2.6 the three axes of rotation are drawn as intersecting in a common point; this does not strictly correspond to anatomical realities, but as the model and its subsequent utilization is of a purely rotational nature this fact does not have any implications in this thesis. The directions of the coordinate axes are chosen so as to comply as much as possible with ISB recommendations (Werner and Buchholz, 1994).  $S_u$  is the coordinate frame fixed to the ulna, with the  $x_u$  axis directed anteriorly and the  $y_u$  axis directed proximally.  $S'_u$  is a frame which orientation is identical to that of  $S_u$ , but translated so that its origin coincides with those of the subsequent ones.  $S_1$  and  $S_2$  are the intermediate coordinate frames resulting from subsequent rotations of  $S'_u$  about the  $y'_u$  and  $x_1$  axes, corresponding to PSM and FEM, respectively, and  $S_w$  is the final coordinate frame defining the wrist orientation after the RUD component is applied by rotating  $S_2$  about the  $z_2$  axis.

Other models imply other parameterizations, which is why data reported by different research groups often must be mapped onto the same parameter space before direct comparisons of their results can be made.

The “floating axis” concept is attributed to Grood and Suntay (1983), whose model included both rotational and translational kinematics. The rotational part of this model, of which the wrist model of Figure 2.6 is an example, resembles what is known in robotics as a spherical wrist: an open kinematic chain with revolute joints whose axes of rotation intersect at a common point. Spherical wrists are treated by researchers such as Spong and Vidyasagar (1989), who give suggestions for coordinate frame assignments and present the resulting forward and

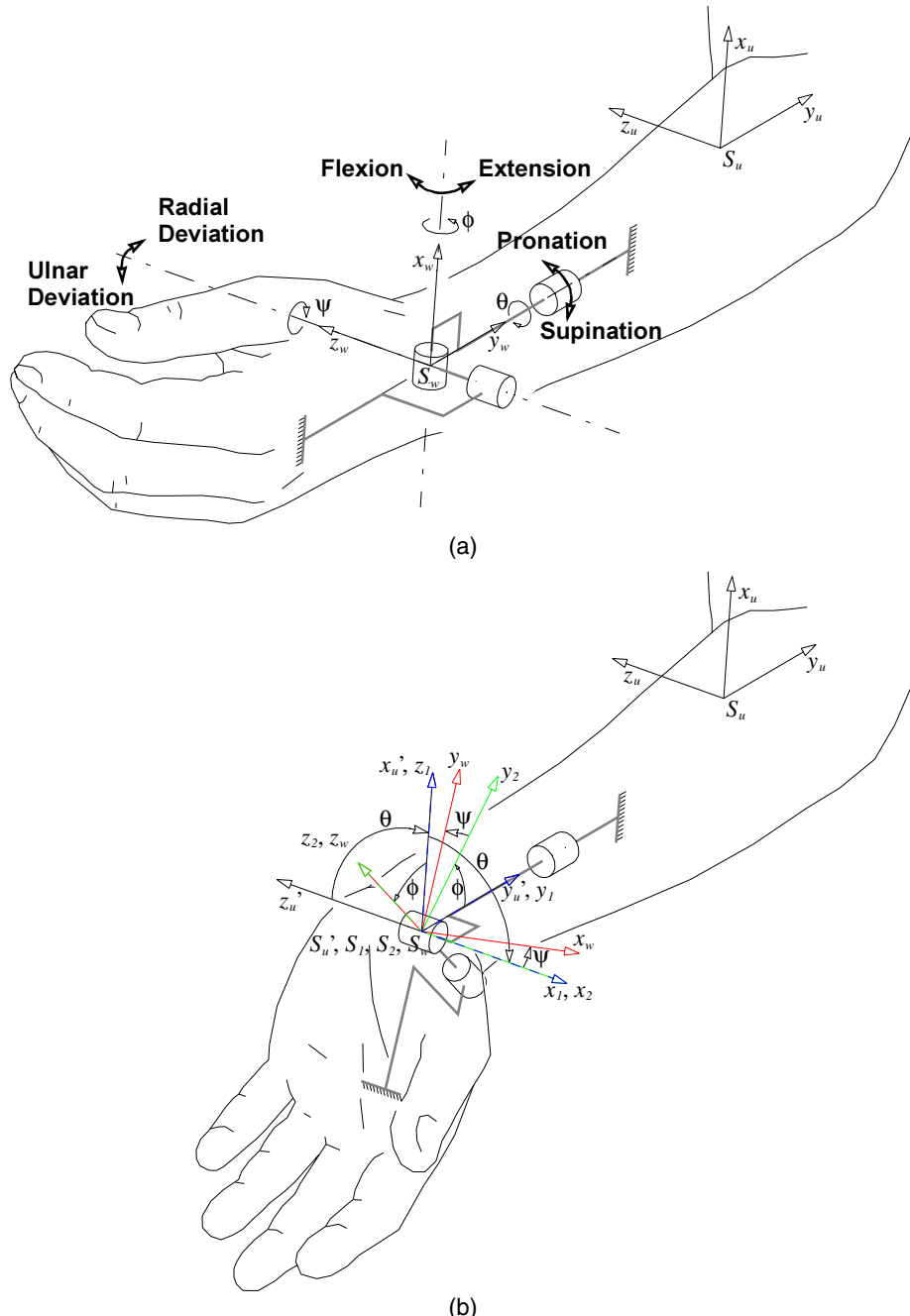


**Figure 2.6:** Kinematic model and clinical angles of the wrist. The model solely comprises orientational kinematics. In the posture shown in Figure 2.6(a), the clinical angles are all zero. Figure 2.6(b) shows the wrist in a somewhat extreme posture, with  $90^\circ$  supination  $\theta$ , approx.  $40^\circ$  of extension  $\phi$  and a slight radial deviation  $\psi$ .

inverse kinematic equations. The frame assignment convention adopted here, however, differs slightly from theirs, so the (inverse) kinematic equations corresponding to Figure 2.6 must be developed separately.

### **Forward Kinematics:**

#### **Computing the Rotation Matrix from Clinical Angles**

With reference to Figure 2.6, the orientation of the  $S_w$  frame with respect to  $S_u$  given the PSM, FEM and RUD angles, can be expressed by the matrix equation

$$\begin{aligned} R_w^u &= R_{y, \theta} R_{x, \phi} R_{z, \psi} \\ &= \begin{bmatrix} c_\theta c_\psi + s_\theta s_\phi s_\psi & -c_\theta s_\psi + s_\theta s_\phi c_\psi & s_\theta c_\phi \\ c_\phi s_\psi & c_\phi c_\psi & -s_\phi \\ -s_\theta c_\psi + c_\theta s_\phi s_\psi & s_\theta s_\psi + c_\theta s_\phi c_\psi & c_\theta c_\phi \end{bmatrix} \end{aligned} \quad (2.2)$$

where  $R_{y, \theta} R_{x, \phi} R_{z, \psi}$  represents a rotation through the angle  $\theta$  about the proximal y-axis followed by a rotation through the angle  $\phi$  about the current (i.e. rotated) x-axis and subsequent rotation through the angle  $\psi$  about the final z-axis; and where  $c_t = \cos t$  and  $s_t = \sin t$ .

### **Inverse Kinematics:**

#### **Computing Clinical Angles from the Rotation Matrix**

Generally, the inverse kinematics problem at hand does not have a unique solution; different sets of the angles ( $\theta, \phi, \psi$ ) yield the same matrix in (2.2). However, some of these mathematical solutions can be excluded by applying known range limitations for the clinical angles.

If we let  $R_w^u = \{r_{ij}\}$ , from (2.2) we can readily express the RUD angle as

$$\tan \psi = \frac{r_{21}}{r_{22}}. \quad (2.3)$$

Technically, due to the periodicity of the tangent function, (2.3) always has two valid solutions within the range  $[-180^\circ, 180^\circ]$ . The wrist RUD angle as defined in the present model lies safely within the range  $[-90^\circ, 90^\circ]$ , with  $-42.9^\circ$  (ulnar) and  $21.1^\circ$  (radial) as the mean extremes (Ruy et al., 1991). The RUD angle can therefore be unambiguously calculated as

$$\psi = \text{atan} \frac{r_{21}}{r_{22}}. \quad (2.4)$$

The cosine of the FEM angle can be calculated as

$$\cos\phi = \pm\sqrt{r_{21}^2 + r_{22}^2}. \quad (2.5)$$

Ruy et al. (1991) reported the mean extreme FEM angles as  $-68.4^\circ$  (flexion) to  $69.3^\circ$  (extension), which is in favour of selecting the positive solution in (2.5). Furthermore, it justifies the assumption that  $\phi \neq \pm 90^\circ$ ; in other words, the singular configuration characterized by the PSM and RUD axes being coincident, will not occur. Thus the FEM angle can be computed as

$$\phi = \text{atan} \frac{-r_{23}}{\sqrt{r_{21}^2 + r_{22}^2}}. \quad (2.6)$$

Finally, the PSM angle can be computed as

$$\psi = \text{atan} \frac{r_{13}}{r_{33}}. \quad (2.7)$$

Thus, given the rotation matrix  $R_u^w$ , the clinical angles can be computed by means of Equations (2.4), (2.6) and (2.7).

## 2.5 Modes of Operation

Napier (1956) divided the movements of the hand into two main groups, namely *prehensile movements* – in which an object is seized and held partly or wholly within the compass of the hand; and *non-prehensile movements* – in which no grasping or seizing is involved but by which objects can be manipulated by pushing or lifting motions. In this section these and related concepts are discussed in order to get a grasp of the vast variety of operational modes of the distal upper limb, the limb's general applicability and some of the consequences of upper limb amputation.

### 2.5.1 Non-prehensile Movements

The non-prehensile mode of operation is very simple in that it mainly involves a single point or surface of contact between the limb and the environment. Consequently, the same functional outcome can often be accomplished by employing several different parts of the limb. For example, a push-button may be operated by the thumb or a by single finger, by the palm, or even by the wrist, forearm or elbow – or any other body part that is mechanically compatible with the button's

size, position, force of opposition and other relevant properties. Because of this multitude of possible implementations and their low dexterity requirements, non-prehensile movements will be granted little attention in the rest of this thesis.

### 2.5.2 Prehensile Movements

#### *Power vs. Precision*

Several investigators have studied different hand postures and classified these with respect to the type of action they are applicable to, or the type of objects they are suited for holding and manipulating. Napier (1956) rejected earlier classifications and introduced the simple but effective and generally accepted division of prehensile movements into *power grips* and *precision grips*. Here, a power grip is what is usually applied when holding a hammer or a large screwdriver, while precision grip is the more delicate class of prehensile postures usually used for manipulating light and small objects. Landsmeer and Long (1965) studied EMG signal patterns and divided the observed movements into 12 different classes according to the contributing muscles. Long et al. (1970) in particular noted characteristic changes in muscle recruitment patterns as the hand changed from free motion to power or precision grip, respectively. Hazelton et al. (1975) noted that of the two major nerves that control hand function, the ulnar nerve controls the fingers involved in the power grip (the little, ring and long finger), while the radial nerve predominantly innervates muscles associated with precision grip (thumb, index and long finger).

#### *Virtual Fingers and Oppositional Forces*

Prehension always involves application of at least two forces in opposition to each other against the object's surface. Arbib et al. (1985) observed that similar grasping actions involve different numbers of fingers, depending on the size of the object being grasped. On this basis they introduced the notion of a *virtual finger* (*VF*), which in the words of MacKenzie and Iberall (1994) is "...an abstract representation, a functional unit, for a collection of individual fingers and hand surfaces applying an oppositional force". Thus, a particular prehensile situation can be categorized by the type of *opposition* used, that is which part(s) or side(s) of the palm, thumb and/or finger(s) are utilized for applying the functional forces, and by the specific *VFs* employed. Three types of opposition were defined, namely *palm*, *pad* and *side opposition*; the former two crudely correspond to power grip and precision grip, respectively, as discussed above. Side opposition, which covers the grip types used such as for turning a key or holding a cigarette, can be regarded as something between the other two types. Iberall and Fagg (1996) also noted that even the types and distribution of mechanoreceptors and

mechanical properties of the skin in different areas of the hand are tailored for power grip or precision grip, or both, according to the opposition types these areas implement.

### ***The Picture is More Complex***

It should be noted that in many contexts, such as when evaluating hand function, the bimodal classification scheme of Napier becomes too simple. Therefore, in order to better span the vast “opposition space” of the human hand, some investigators have introduced more detailed grip classification schemes. Examples include the standardized hand function tests by Jebsen et al. (1969) and Sollerman and Ejeskär (1995), which both comprise activities believed to be representative for the most common basic grip types used in everyday life.

## **Chapter 3**

# **Upper-limb Prostheses**

### **3.1 A Brief Introduction**

A *prosthesis* is an artificially supplied device designed and applied to alleviate the loss of a set of normal body functions. The requirements that need to be met by different types of prosthetic components are as diverse as the functions which they are meant to mimic. Consequently, a comprehensive treatment of different organ prostheses is beyond the scope of this thesis. With the previous chapter's description of the healthy upper limb as a backcloth, the present chapter outlines the "anatomy" of upper-limb prostheses in terms of typical mechanical structures, power supply, control system and properties in general.

The present part of this thesis is entitled *The Distal Upper Limb and its "Replacement"*. The use of quotation marks is deliberate; though the fundamental purpose of an upper-limb prosthesis is to replace or restore *some* of the lost functionality, a prosthesis will always exhibit inferior performance compared to the real limb in virtually all respects except – ironically – its replaceability. Even the often severely impaired function of an arm which is replanted after traumatic amputation may produce a functionally superior result compared with amputation and application of a prosthesis (Graham et al., 1998). This calls for a high degree of humility on the side of anyone trying to improve the functional quality of prosthetic components.

### **3.2 Principal Functions Impaired by Transradial Amputation**

All the "roles" of the upper limb represent challenges relevant for a prosthesis to meet.

The high level of dexterity of the wrist and hand makes them suitable for a wide spectre of tasks that changes with age and context. For the toddler a primary function may be its very existence as a visible object that can be influenced by the baby's will; this is claimed to play an important role in the child's initial motor learning (van der Meer et al., 1995). In this situation the hand's mechanical properties are presumably of minor importance. Later in early childhood the limb constitutes a part of the locomotion system in the crawling mode, its basic function being to lift the trunk off the floor and move it around. All along the hand serves as a tool for exploring the environment, an ability which is actively employed even by adults.

With growing age the locomotion aspect of the limb becomes less important and the hand's other applications become evident. A relatively passive but important functional property is its *cosmetic appearance*. The "normal" human body has certain outer characteristics, two fully developed and relatively symmetric upper limbs being among the most visible, and deviations from this "norm" may have significant social implications. Not only the envelope of the limb but also its colour, texture, temperature and mechanical properties are relevant in his context.

A more active role of the limb is that which is associated with non-prehensile movements, as a means for *support* or *exertion of force*. In this kind of situations the entire distal upper limb can be said to constitute a single virtual finger.

Still more active is the role as a general *prehensor* and *manipulator*, as discussed in Section 2.5.2.

Finally, the upper limb plays a role in human communication both at a conscious and at a subconscious level as a means for descriptive gesticulation and signalling.

### 3.3 Principal "Anatomy" of Upper-limb Prostheses

For reasons such as robustness, energy consumption, cost, cosmesis and weight limitations, the functionality implemented in the prosthesis must be restricted to the few functions most imperative for the prospective user in the intended context. Moreover, a prosthesis introduces additional challenges which are not associated with a healthy limb. As a consequence there are a vast number of different solutions available, some which are tailored to a single task and others which are more general-purpose tools. In the following, the fundamental functions and properties that a prosthesis may or must exhibit are briefly discussed.

**Suspension** A prosthesis must be attached to the user’s body in a manner which facilitates the use of the device. A minimum requirement is that the suspension supports the weight of the prosthesis itself; it should also support the weight of any object being carried and counteract the prosthesis’ contact forces with the environment.

**Control Interface** In case the prosthesis offers any kind of active function, it must include an interface through which the user’s motor intent can be relayed to the device. We define the control interface to also include any so-called *sensory feedback*, i.e. the relaying of prosthesis state information (i.e. positions, velocities, forces and the like) back to the user.

**Power Supply** Any function of the prosthesis that requires energy of any kind implies the need for a power source within the prosthesis or an interface through which energy can be delivered to the device during operation.

**Control System** This function represents or implements the relation between the user’s control input and the actual behaviour of the prosthesis. This may or may not be implemented in a separate physical unit. The logical behaviour of the control system can be denoted the *control principle* of the prosthesis.

**Actuators** The purpose of actuators is to transform energy from the form initially provided to the mechanical energy involved in implementing the intended or commanded motion or force pattern.

**Functional Surfaces** These are the surfaces by which the motion and/or force pattern generated by the actuators is relayed to the environment. A prosthetic component providing a grip or prehension is usually referred to as a *terminal device*; the functional surfaces then include the opposing finger or pincher surfaces used for holding and manipulating objects, any other outer surface used for mechanical interaction with the environment, as well as any visible surface relevant to communication or social settings. For intermediate components such as a wrist joint, the functional surfaces comprise the points of attachment to the forearm socket and to the terminal device (for transmitting forces and movements between these segments), and – to a lesser degree – the physical properties of its outer surface.

Surfaces directly involved in suspending the prosthesis in the residual limb are treated under the separate functional category *Suspension* (cf. separate paragraph above) because of their ubiquitousness and high degree of specialization.

**Kinematic Constraints** The set of obtainable postures of a prosthesis is constrained by the number joints, their ranges of motion and the geometry of the mechanical links interconnecting them. These are the kinematic constraints. The functional surfaces of the prosthesis are positioned and

oriented in space by the positioning of each of the device's movable joints, so the kinematic constraints fundamentally influence the versatility of the prosthesis.

In anthropomorphic devices there is a relatively simple relationship between the joints and links of the prosthesis and the joints and bones of the human limb. Other devices may employ joints and geometry not found in a healthy hand and thus may transcend some kinematic constraints exhibited by the normal human limb.

### 3.4 Overview of Prosthetic Solutions

This section gives a brief description of several types of prostheses for transradial amputees. The literature describing and documenting the available options is rich; the reader is generally referred to Atkins and Meier III (1989) and Bowler and Michael (1992), which comprise chapters by some of the most knowledgeable specialists in the international orthopaedic-technical community. For more recent advances other references are given in the text below.

#### 3.4.1 The Residual Limb as a “Prosthesis”

The simplest prosthesis, and not the least popular one, is none at all. Some even maintain that discarding prostheses altogether is the soundest approach to mastering the loss of a limb, as it prevents the amputee from becoming dependent upon an artificial device which might cease to function or might not always be available. In any case, the residual limb provides the senses related to touch in a way not obtainable in a prosthesis, and the joint functions that possibly remain intact are under direct neural control. Transradial amputees often have a good elbow flexion which can be utilized for shaping the limb like a hook, enabling activities like carrying a bag, picking up certain objects (cf. Figure 3.1, where the stump is used for picking up the prosthesis harness), and even windsurfing and other sporting activities that require predominantly non-prehensile actions. Application of a prosthetic terminal device inevitably isolates the residual limb from the environment which it is meant to interact with, severely impairing the sense of touch and introducing some kind of motion control scheme often inherently foreign to the CNS.

Management of the residual limb from the moment of amputation on is among the most challenging in the context of prosthetics. Phantom sensation, including pain, is known to outdo the physical limb loss as a problem in some cases, and painful neuroma may develop at the distal end of damaged nerves. Severe dermatological problems and reduced temperature regulation are not uncommon. While these issues are not treated any further in this thesis, it should be noted that these kinds of problems may eliminate the use of a prosthesis altogether, and represent

immense research challenges involving numerous areas of physical medicine as well as psychology. Interestingly, the active use of a prosthesis is reported to reduce the problems associated with phantom sensation (Weiss et al., 1999).

### 3.4.2 Cosmetic Prostheses

For the user prioritizing natural appearance or not tolerating the extra weight and mental load implied by using an active device, a *cosmetic prosthesis* is the alternative. This is a completely passive unit, and its functional surface consists primarily of its artificial skin. Being relatively light, the prosthesis can be suspended in a more discreet way than its actively functional counterparts. Since it contains virtually no mechanical structures dictating geometry, its envelope can be made very similar to that of a healthy limb, and surface texture and compliance can be optimized for cosmesis without considering properties like grip friction.

The kinematic constraints of a cosmetic device are at best identical to those of the residual limb except for the elongation implied by the prosthesis. Despite its passive nature, Fraser (1998) demonstrated that even cosmetic prostheses are actively used in the performance of non-prehensile tasks. Recent cosmetic improvements include the use of contralateral finger casts to create a hand with individually adapted geometry (Leow et al., 1999).

### 3.4.3 The Krukenberg Procedure

The Krukenberg prosthesis is formed by surgically separating radius and ulna (cf. Figure 2.2) to allow the bones to be pulled apart or forced together, forming a large active grasping organ. The same person has the option of being fitted with other kinds of prostheses as well. The natural control, intact proprioceptive paths and intrinsic sense of touch yields a superior prosthesis in many respects, but the extremely non-human appearance makes it a controversial procedure. In bilateral transradial amputees who are also blind, the Krukenberg solution is considered to be among the best as these subjects have no visual feedback and thus need the sensory system naturally provided in the residual limb. The absence of vision in these persons also reduces the importance of cosmesis (Atkins and Meier III, 1989, Stavdahl, 1995).

### 3.4.4 Body-powered Prostheses

A *body-powered prosthesis*<sup>†</sup> is so named because its active function relies on mechanical energy from the user's body. Figure 3.1 shows a user with a typical transradial prosthesis with a body-powered split-hook. The harness serves multi-

---

<sup>†</sup>. The term *conventional prosthesis* is considered to be synonymous with a body-powered device. However, others use *conventional* to denote any established technique or device, as opposed to novel ones. The latter convention is used in this thesis.

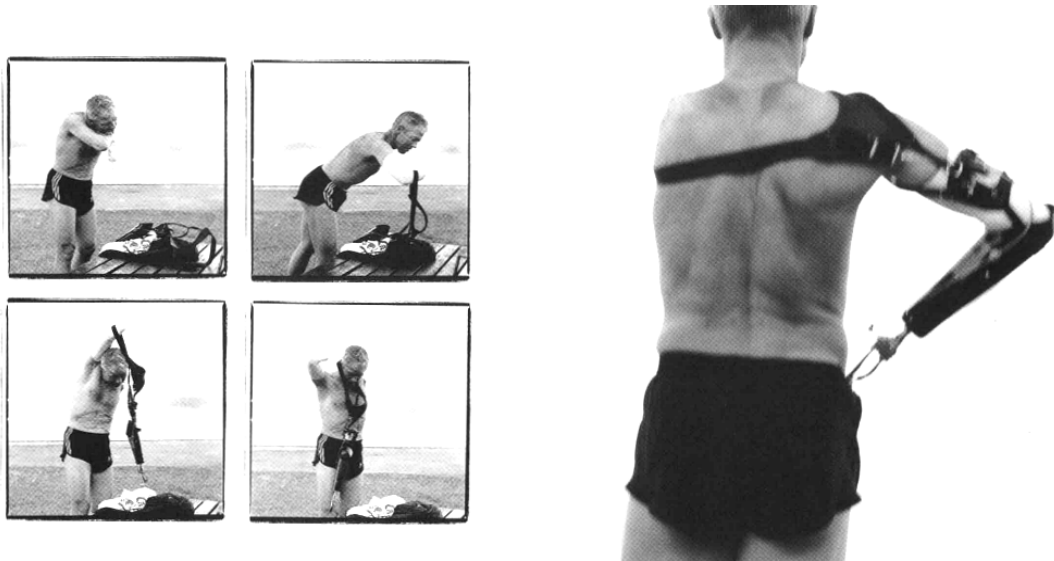


**Figure 3.1:** Transradial amputee with a body-powered split-hook. Left: donning of an elastic stocking and subsequently the prosthesis harness; right: harness with cable for actuating the hook. The pictures show Cato Zahl-Pedersen, bilateral upper-limb amputee and several times paralympics champion. Zahl-Pedersen also was head of the expedition “Unarmed to the South Pole”, which reached the South Pole by ski in 1994.

Photo courtesy of MOMENTUM, ©Dag E. Thorenfeldt. From Momentum (2001).

ple functions: aside from suspending the prosthesis it also relays body movements to the device, so that the split-hook can be opened or closed by shrugging the shoulder. Thus, the harness simultaneously plays the roles of suspension, power transmission and control interface. In this case the “control system” is implicitly given by the mechanical construction of the device. The user in the picture has a forequarter amputation<sup>†</sup> on the contralateral side where he uses no prosthesis. Thus contralateral shoulder motion can be used for controlling the prosthesis, leaving the ipsilateral shoulder free to position and orient the residual arm with the prosthesis.

### 3.4.5 Externally Powered Devices

As indicated by the title, these devices involve some sort of energy source external to the user’s body. The first attempts to make externally powered prostheses involved pneumatic and electric actuators, while today electric motors are predominant in commercially available devices. For decades battery capacity has

---

<sup>†</sup>. The whole arm as well as parts of the shoulder and trunk are absent.

represented a major drawback in electric prostheses (Atkins et al., 1996), but recent advances in battery technology have significantly reduced and virtually solved this problem (Stavdahl et al., 1997b).

Current off-the-shelf electric terminal devices still span a narrow range of functions, typically involving only a simple precision grip and optionally a single wrist function (usually prosupination). As for outer appearance, electric terminal devices come in virtually all “flavours”, from antropomorphic hands with five fingers and artificial skin to electrically actuated split-hook types in numerous shapes and sizes optimized for different tasks.

In order to better mimic the functions of a real hand, significant research effort has been devoted to adding multiple independent motions (DoFs) to the prosthesis. Alderson (1952) patented an ingenious but impractically complex electromechanical device that comprised a precision-type grip, flexion/extension and prosupination at the wrist as well as elbow flexion/extension (Figure 3.2). A

FIG. 4.

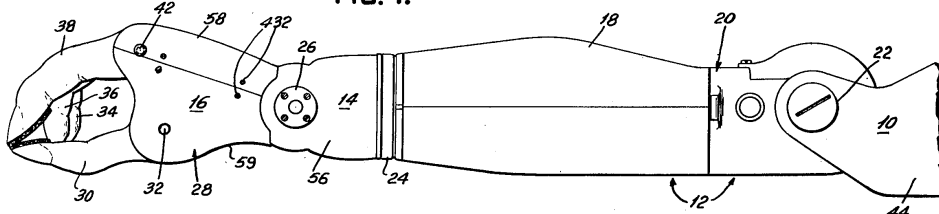


FIG. 5.

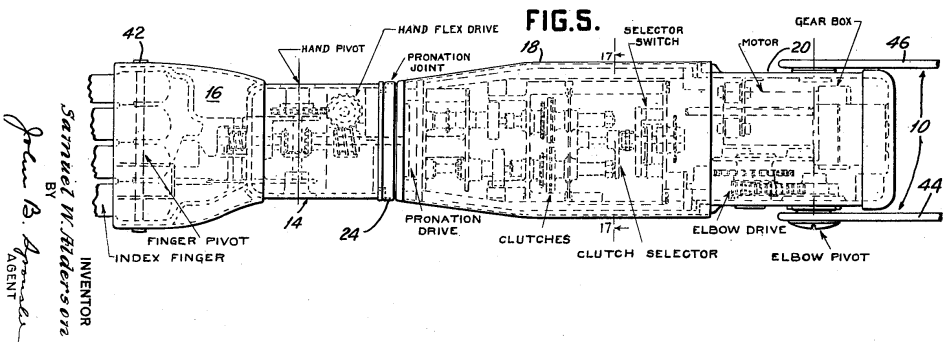


Figure 3.2: Joints and internal structure of the so-called IBM arm (Alderson, 1952).

later attempt was made in Sweden with the so-called SVEN hand which comprised as many as six DoFs (Herberts et al., 1978a, 1978b).

Independent control of multiple joints often requires too much concentration; an alternative option is to move the point of input of the operator up the control hierarchy and leave the details to a computer. The *Southampton Adaptive Manipulation Scheme (SAMS)* is of this form, and prostheses controlled according

to this scheme are commonly referred to as *Southampton hands*. Originally developed at Southampton University, UK in the 1960's, the ideas have propagated to Oxford and have been the core of one of the most comprehensive lines of hand prosthesis research from a scientific point of view; see for example (Kyberd et al., 88, Kyberd, 1990, Chappell and Kyberd, 1991, Kyberd et al., 1994, Light and Chappell, 2000). The most extensive Southampton hand to date has six degrees of freedom and is able to perform both the precision and power grips as well as allowing the thumb to oppose the side of the index finger.

One of the most recent advances is the Edinburgh Modular Arm System, which offers a flexible menagerie of grip, elbow and even shoulder functions (Gow et al., 2001). A novel German hand with hydraulically actuated MCP, PIP and DIP joints is reported to yield a 50 % weight reduction compared to previous hands (Schulz et al., 2001).

### 3.4.6 Suspension

Traditional suspension techniques for transradial prostheses include a harness or frame entwining the upper arm or trunk, a method often employed in body-powered or hybrid devices (Figure 3.1); and a laminated plastic socket that fits closely around the residual limb and embraces most of the elbow. The socket tends to reduce the angular excursion of the elbow. A more recent but very popular development is the use of an elastic silicone liner which is rolled onto the stump and held in place by the resulting vacuum. These solutions differ significantly as to what extent they limit residual elbow and forearm function, weight bearing capacity and user comfort in general.

The concept of *osseointegration* (direct skeletal attachment) of prostheses via percutaneous metal fixtures is a well established technique in dental and facial prostheses as well as for some implanted prosthetic joints. The application of osseointegration in transradial prostheses was first reported by Branemark et al. at the 8th World Congress of the International Society of Prosthetics and Orthotics, Melbourne, Australia, 1995<sup>†</sup>, and was met with sceptical anticipation. Some of the method's important implications have recently been documented. These include its superior capacity for communicating haptics-related sensation, the so-called *osseoperception* (Jacobs et al., 2000), when compared to traditional prosthesis suspensions, and its surprisingly low susceptibility to cause skin infections in the penetrated area (Holgers and Branemark, 2001). The technique is also superior in that it preserves virtually all intact functions of the residual limb, such as elbow flexion/extension and forearm pronation/supination. There is even reason to believe that the user's tolerance with respect to the prosthesis' weight is higher in osseointegrated prostheses than in conventionally suspended devices, because the weight is carried by the skeleton and not by soft tissue. However there is rea-

<sup>†</sup>. No written material was included in the conference proceedings.

son to believe that osseointegration will remain a rarely applied technique for still some time for the sole reason that it takes a surgical procedure to implement and therefore is linked to discomfort, danger of complications and possibly association with a traumatic amputation.

The perhaps most recent advance in suspension technology involves an implanted titanium structure denoted an *endogenous suspension condyle* that changes the shape of the residual limb to allow stable suspension while minimally restricting the residual movability and minimizing the need for harnessing (Tønnevold, 2002). To date this procedure is only applied to transhumeral amputees, but preparations are being made for adapting the technique to other types of amputations.

### 3.4.7 Control Aspects

#### ***Body-Powered Control***

One of the major advantages of body-powered prostheses is the inherent integration of the control system in the suspension and control interface. This offers the user proprioceptive information about the state of the prosthesis: a body part is moved, this movement is mechanically relayed to the prosthesis, and any counteracting forces from the environment is inherently relayed back to the actuating body part via the mechanical linkage. This old and well proven principle has been subject to continuous improvements. Recent mechanical improvements include a lightweight body-powered prosthesis which permits full control of the terminal device regardless of the orientation of the shoulder and elbow joints (Cupo and Sheredos, 1998). Doshi et al. (1998) and de Visser and Herder (2000) similarly designed body-powered hands with emphasis on force distribution rather than movement characteristics and thus improved the force control capabilities of the device.

On the downside, a body-powered prosthesis always requires intact body movements to be harnessed and dedicated to the control of the prosthesis. When for example utilizing shoulder movements to control the grip of a terminal device, the user must move his/her shoulder in an unnatural manner and also avoid accidental shoulder motion when the terminal device is being used.

#### ***Sensory Feedback***

A large number of studies have been dedicated to providing state information feedback from the prosthesis to the user; Lundborg and Rosen (2001) gives a brief overview of the concept in a wide perspective including physiological, technical and psychological perspectives. Attempted feedback methods include electrical stimulation of the residual limb percutaneously (Shannon, 1979) and via implanted circuits (Lovely et al., 1985), as well as vibrotactile stimulation (Shan-

non, 1976). Despite the research efforts, none of these methods are employed in today's commercial prostheses, and there seems to be a consensus that the EPP principle treated in the next paragraph is the most viable option to date.

### ***Extended Physiological Proprioception – EPP***

Simpson (1973, 1974) generalized the inherent control advantages of body-powered prostheses to externally powered devices by introducing the principle of *Extended Physiological Proprioception*, or *EPP*. In EPP control, the force exerted on the prosthesis by one of the user's body parts commands the force exerted by the prosthesis on the environment, while the excursion of the prosthesis is reflected by an “unbeatable servo” to the controlling body part. Except for the (ideally negligibly fast) dynamics of the electronic servo system, this principle keeps the advantages of a body-powered interface while allowing amplification of the commanded force by use of externally supplied energy.

### ***Myoelectric Control***

Reiter (1948) introduced the use of the EMG signal as a control interface for powered prostheses. Since then, EMG-based control has become one of the most popular alternatives and has been subject to substantial research and improvements. So-called *digital control*<sup>†</sup>, in which the prosthesis actuator is switched ON as the EMG amplitude exceeded a preset threshold, was predominant until a decade ago. Use of two antagonistic muscle groups permitted control of the prosthetic joint in two opposite directions; if only one EMG site was available, the rate of change of the EMG amplitude could be used for choosing the direction. Later so-called *proportional control* was introduced; here, the speed or force of the prosthesis is proportional to some parameter of the EMG signal, typically the amplitude. Interestingly, the proportional EMG processing technique known as MyoPulse was described some two decades before the introduction of proportional control in commercial prostheses (Isidori and Nicolo, 1966) (the MyoPulse is also described by Philipson (1985)). Today, proportional EMG systems are common, and sometimes integrated with force or slip sensors to facilitate more advanced control schemes.

### ***Other Control Concepts***

Several other options exist that include the EPP principle in a varying degree. One principal solution includes a harness equipped with strain gauges (e.g. the Pro-Control<sup>‡</sup> system) or a spring mechanism in combination with a linear position transducer, which allows control of the terminal device position (i.e. joint angle)

---

<sup>†</sup>. The term *digital* refers to the ON/OFF characteristic of the control scheme; the actual control system was typically implemented by means of analog electronics.

<sup>‡</sup>. Motion Control, Inc., 2401 South 1070 West, Suite B, Salt Lake City, Utah, 84119-1555, USA

and/or grip force in relation to the stress and strain applied to the harness by the shoulder complex. So-called *touchpads*, resistive pressure sensors operated by an intact joint function, also offers a proportional control channel utilized in several commercial and experimental systems.

Experimental solutions also include EMG-based direct position control (Stavdahl et al., 1995); a system mimicing the stretch reflex of human muscle (Okuno et al., 1996); the Southampton Adaptive Manipulation Scheme (cf. Section 3.4.5) and other approaches seemingly derived from it (Tura et al., 1998); use of statistical pattern recognition techniques, (Almström, 1977, Herberts et al., 1978b), artificial neural networks (Bergantz and Barad, 1988, Kelly et al., 1990a, Kelly et al., 1990b, Hudgins et al., 1992, Kuruganti et al., 1995) and genetic algorithms (Farry et al., 1997) in order to classify myoelectric signal patterns according to the intended movement; use of tunnel cineplasties (“exteriorized tendons”) as a mechanical interface to the forearm motors (Childress et al., 1993, Weir et al., 2001); estimation of muscle contraction from ultrasound pulse-echo measurements (Stavdahl et al., 1997a); and pneumatic sensors placed between the prosthetic socket and the superficial forearm tendons (Abboudi et al., 1999). Recent advances related to the peripheral nervous system comprise neural interfaces (Haugland and Sinkjaer, 1999, Loeb et al., 2001) and even “sorting” of sensory fibres from motor fibres in one and the same nerve (Jerregard et al., 2001), suggesting radical future improvements in prosthesis control interface technology.

## 3.5 Elaboration of the Scope

The purpose of this section is to provide a justified definition and limitation of the scope of the present research.

### 3.5.1 The Focus: Kinematic Constraints

The overall goal of this work is to investigate whether the kinematic constraints of a typical powered 1-DoF wrist joint prosthesis are optimal with respect to the functional properties of the device.

The typical powered wrist unit offers a single rotational DoF resembling a pron-supination movement (“forearm rotation”). We adopt the follwing definition:

**Definition 3.1** *A prosthesis is kinematically functional to the degree to which it is able to mimic the postures taken on by a healthy limb during activities of daily living (ADLs).*

□

In terms of the classical hypothetico-deductive method, the purpose of the research then is to evaluate the null hypothesis

*A powered wrist prosthesis with an exclusive forearm rotation is at least as kinematically functional as a device with any other single axis of rotation*

against the alternative hypothesis

*For a powered one-DoF wrist prosthesis there exists at least one axis of rotation that is more kinematically functional than that corresponding to forearm rotation.*

### 3.5.2 The Unavoidable Restrictions

All the functions and properties of a prosthesis are candidates for improvement. Many functions and properties are also closely related or coupled, an example of which is the cosmetic consequences of changing the one-DoF wrist's axis of rotation. An oblique axis of rotation will cause an elliptic wrist cross-section (cf. Figure 3.3). If this oblique axis is in the sagittal plane of the hand, the resulting prosthesis will be geometrically more like a natural human wrist, which is indeed elliptic rather than circular in section and wider in the mediolateral than in the anteroposterior direction. This will yield a device that is cosmetically more acceptable. If the oblique axis lies in a coronal plane however, the long axis of the ellipse will be perpendicular to that of a normal wrist, causing a potential cosmetic problem.

To develop “*the* optimal prosthesis” (assuming for a moment that such a concept is meaningful) one would therefore have to optimize most or all aspects of the device simultaneously: suspension, control interface, control system, actuators, power supply, functional surfaces and kinematic properties. This is not only impossible because the optimization would be dauntingly complex to carry out, it is also meaningless because prosthesis users and applications are very different. Thus, it is necessary to limit the study to optimizing a few functions or properties for a small group of users and a for limited set of applications.

The following paragraphs briefly discuss the limitations imposed on the present work.

**Wrist Prostheses** Improved wrist function is rated among the most important future improvements by users of externally powered transradial prostheses (Atkins et al., 1996).

**Kinematics Only** Among the many functional properties of transradial prostheses, kinematics is one of the least studied issues, especially with respect to wrist function. In experimental systems offering active wrist motion, focus has often been on control rather than geometry (Herberts et al., 1978a).

It should be noted, however, that concentrating the study on kinematics excludes important factors like dynamic response and sensory feedback.

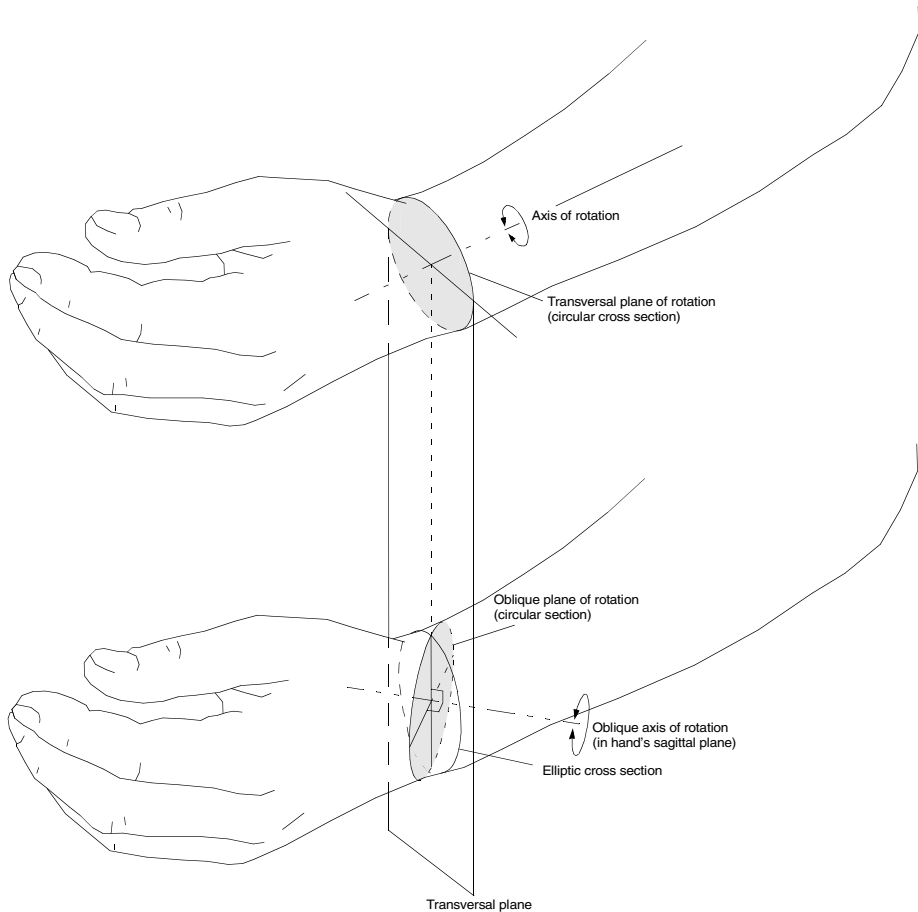


**Figure 3.3:** Consequence for wrist cross section of an oblique axis of rotation. An axis of rotation parallel to the forearm gives a circular wrist cross section (upper part of the figure) while an oblique axis in the hand's sagittal plane gives an elliptic cross-section more like a real wrist (lower part).

**Rotational Motion** Kinematically complex one-DoF structures like four-bar linkages (“polycentric joints”) do not necessarily have a fixed axis of rotation. Though potentially interesting in a wrist context, such solutions are not considered here. The following discussion is restricted to simple revolute motion because revolute joints constitute the simplest and thus the most viable option when considering the weight and space limitations of a prosthetic wrist unit. More importantly, in the present context the wrist joint can be approximated as a linkage of three consecutive revolute joints with a common point of coincidence. This is because the hand translations caused by rotation about the (realistically non-coincident) wrist axes is

negligible compared to the hand translations following elbow or shoulder rotation, and thus too small to represent any significant kinematic functionality of the wrist as far as the utilization of the hand is concerned.

**A single degree of freedom** The ever-present weight and space limitations applying to prosthetic devices call for maximally restricting the mechanical complexity of any such device, as does the wish to minimize the maintenance cost and maximize time between failure. Finally, the more DoFs exhibited by the device, the more complex the control system and the more mental load imposed on the user; a simple device is simpler to control.

The extreme restriction is that actually found in most prostheses, namely the zero-DoF wrist which offers a static orientation of the terminal device with respect to the forearm (not counting passive forearm rotation as a DoF in this context). Realizing that the healthy wrist exhibits three, the intermediate options are one or two DoFs. This study is focused on the simpler 1-DoF case, which would be the easiest to implement mechanically and the easiest to control. However, the data collected is equally relevant to a 2-DoF study, and the methods employed can easily be generalized to a 2-DoF case.

**Unilateral Transradial Amputees** Below-elbow amputees represent the largest group of potential users of active wrist prostheses. Focus is held on the unilateral case, because bilateral amputation is relatively rare and because these patients have a different set of concerns and needs as they do not have any intact limb that can take on the role as a dominant hand (Atkins et al., 1996).

**Activities of Daily Living** Prosthesis users employ their limb substitutes for virtually all thinkable tasks. To limit the scope of the study to a manageable level, it is restricted to the class of *Activities of Daily Living (ADL)*. This class is perceived to represent the most necessary and/or common tasks to any normal individual.

An important fact is that there is no generally accepted definition of ADL. Included in this study is a set of carefully selected “generic” activities which is believed to span a wide range of more specialized tasks relevant to Western culture and to the user group in question.

## Part II

# MATERIALS AND METHODS

*The more precisely a designer knows the specific needs of life, the more effectively he has restricted the movements of artificial fingers to those movements which are really indispensable, the more useful and solid his designs are. A real master reveals himself in restriction.*

*(Schlesinger, 1919)*<sup>†</sup>

---

<sup>†</sup>. As cited by Näder (1995).



## **Chapter 4**

# **Experimental Design**

*The experimental design described in this chapter was developed in close cooperation with several people, in particular Tordis Magne, OT, of the Department of Prosthetics and Orthotics, University Clinic of Trondheim and Assistant Professor Klara Jakobsen of the School of Health Education, Department of Occupational Therapy, Sør-Trøndelag University College. Also, several groups of students of the OT programme and of the Department of Engineering Cybernetics, Norwegian University of Science and Technology, have contributed during the preliminary phase (Ervik et al., 1996, Lindanger and Jøsang, 1997, Knutsen et al., 1997).*

*The significant contributions of these individuals and groups are acknowledged by the author.*

### **4.1 Introduction**

#### **4.1.1 Compensatory Movements**

Hand prostheses today differ from the healthy human hand to the extent that most available devices only allow for a simple simultaneous flexion or extension of the MCP joints of the fingers and thumb in a pinch-like grip with the thumb opposing the first and second digit. No afferent information is explicitly fed back to the user's central nervous system. Being so different from a healthy limb, there is no reason to expect that the need for wrist functionality when using a prosthetic terminal device is identical to that when using a healthy hand. Differences may be attributed to *compensatory movements*; movement components that differ from those typical and natural to a healthy limb and that are consciously or subconsciously employed in order to compensate for the missing functionality. This phenomenon is addressed in the literature. For instance, Carlsson and Tromby (1983) observed fatigue in the shoulders and upper trunk of subjects with immo-

bilized wrists, and attributed this to compensatory efforts to position the fingers. Similarly, O'Neill et al. (1988) briefly outlined an experiment to evaluate compensatory motion at the shoulder complex following elbow arthrodesis.

In the present context, a hand prosthesis can be regarded as a severely immobilized hand with virtually no afferent pathways. Thus, the inability of a typical hand prosthesis to adduct and abduct the thumb and fingers and flex the fingers independently possibly induces compensatory movements involving wrist movements, forearm prosupination, elbow flexion and/or shoulder rotation to obtain or approximate a desired orientation and position of the fingers. Likewise, the suspension of a forearm prosthesis is likely to influence the range of motion of the elbow, potentially inducing compensatory actions in other joints. An intact (i.e. unrestricted, fully mobilized) wrist in such a context is likely to take on significant portions of the total compensatory scheme.

#### 4.1.2 The Simulated Prosthesis

In order to unveil the actual need for wrist functionality associated with a prosthetic hand, the ideal situation would be to study the wrist utilization of subjects using such a device while at the same time using a wrist which is minimally restricted with respect to angular excursion and which can be unconsciously and intuitively controlled by the user.

The angular excursion of a healthy wrist is naturally restricted. To the extent that compensatory movements constitute a cosmetic problem in the form of unnatural-looking postures and movements, similar problems would appear in a prosthesis if excursion were to significantly exceed that of its healthy human equivalent. There are in fact indications that prosthesis users desire the ability to turn their prosthetic wrists  $360^\circ$  or more (Randström, 1996), but the exact reason for this is not known. One possible explanation is that it is related to the inferior performance of the prosthesis as a whole, so that the apparent need for excessive excursion in fact represents a class of compensatory movements in itself.

No conceivable prosthetic control system compares with the motor control system of a healthy body when it comes to intuitive control and sensory feedback. In the present study this benefit was decided to outweigh the drawbacks associated with limited angular excursion, and the healthy wrist was chosen as the “optimal” one for the experiment.

A theoretical option now would be to study the wrist utilization of subjects with partial hand amputations fitted with a terminal device similar to the REACH or the Prodigit hand (Gow et al., 1993, Gow et al., 2001), which offer a powered prehensile function while preserving natural wrist motion. However, the population of such users is extremely small and consequently collecting data would be impractically time consuming. Therefore the concept of a simulated prosthesis was introduced as follows.

**Definition 4.1** A Simulated Prosthesis is a healthy limb which freedom of movements and sensorimotor abilities are artificially and temporarily restricted or altered to resemble those of a real prosthesis.

□

By transforming healthy hands into simulated prostheses without restricting the wrist's freedom of motion, it is possible to conduct studies similar to those mentioned for the partial hand amputee population by employing healthy volunteers. This approach was chosen for the present study.

### 4.1.3 Restatement of the Purpose

The aim of the study now can be expressed as finding out how the human sensorimotor system utilizes wrist kinematics in order to facilitate the optimal (in the subjective sense) use of the (simulated) prosthesis. It is hypothesized that any compensatory movements of joints other than the wrist will be less articulated with a healthy wrist in place than in the case of a suboptimal prosthetic wrist, because the healthy wrist is capable of taking a larger share of the compensatory movements involved and in a virtually subconscious manner.

## 4.2 Materials and Methods

### 4.2.1 Brief Overview

The experiment involved instrumenting eight healthy subjects, instructing them to perform a set of ADLs and tracking their movements during performance. Subsequent data analysis aimed at extracting information about the functional kinematics and whether and how well it can be approximated by a prosthetic device with a restricted number of DoFs.

### 4.2.2 Selection and Performance of Activities

#### *Activity Selection Criteria*

Everyday activities of humans span an enormous range of movements, and presumably also vary considerably across the population, over time, in different social contexts etc. Obviously, a practical experiment cannot completely span this range. To make probable the general validity of the results, a pilot study was conducted in order to research different criteria for the selection of activities and for assessing technical aspects of the experiment (Ervik et al., 1996, Knutsen et al., 1997, Lindanger and Jøsang, 1997). Based on an evaluation of the results, the following criteria were decided upon for the selection of ADLs:

**Bilateral** Subjects with unilateral amputation are assumed to perform most unilateral activities using the healthy limb. Therefore the prosthesis does not play a significant role in these activities, so only activities that require use of both upper limbs were included.

**Culturally relevant** Only ADLs that are of cultural importance were considered.

In this context, “culturally important” implies ADLs that are frequently performed and/or of special importance in our (Norwegian) culture. As such, Norwegian culture was considered to be crudely representative for those of western-European and American industrialized societies.

**Low level of dexterity** Given that the prostheses considered only have a simple open/close function, activities that require a notable level of dextrous manipulation were not considered appropriate for inclusion in the study. Likewise, since the speed, mechanical output power and quality of control of limb replacements are likely to stay inferior to real limbs far into the future, activities during which the grasp configuration and thus the angles of finger and wrist joints change rapidly and frequently were left out.

**Basic activities** Most ADLs can be divided into simpler and more basic activities.

One tried to focus the study on such basic activities, because this potentially simplifies the interpretation of the results. Also, each basic activity may be part of several complex ones, and thus a large set of fundamentally different basic activities are likely to span a more general and complete range of movements than a small set of more complex activities.

**Compensatory movements** These movements are believed to contribute positively to the subjectively perceived overall utilization of the terminal device, because the human body seeks to minimize the “effort” - in the most general and subjective sense - needed for carrying out a given task.

Nonetheless, compensatory movements are claimed to occasionally cause long-term overload injury in otherwise healthy body parts, and thus are considered unwanted. Compensatory movements are undesired also from a social point of view as they make the subject deviate from a normal movement pattern. This calls for the inclusion in our study of activities known to frequently be accompanied by compensatory movements, in order to optimize the wrist prosthesis with respect to minimization of such movements.

### ***Activities Selected***

Of a total of 49 ADLs considered, 15 were chosen for inclusion in the experiment. A 16th control activity was included to be able to check the validity of certain central assumptions. The activities were subdivided into the four categories

- Personal (related to personal care and hygiene)

- Culinary (related to food preparation and feeding)
- Other (other household activities)
- Non-ADL (control activities)

The activities chosen were as follows, listed in the order in which they were carried out.

- 1. Donning/doffing<sup>†</sup> of a T-shirt (Personal).** Standing on his/her feet, the subject was instructed to put on and then take off a cotton T-shirt.
- 2. Buttoning/unbuttoning of a shirt (Personal).** Standing on his/her feet wearing a shirt with buttons, the subject was instructed to button and then unbutton it.
- 3. Donning/doffing of pants (Personal).** Standing on his/her feet wearing his/her own pants, the subject was instructed to slide the pants down the legs to the floor as if (s)he were going to take them off, then slide them back on. The activity included (un)buttoning or (un)zipping when relevant.
- 4. Zipping/unzipping of a zip-lock (Personal).** Standing on his/her feet wearing the upper part of a sweat suit, the subject was instructed to zip and then unzip the suit, including initial joining and final separation of the zipper's two parts.
- 5. Hanging clothes on a clothesline and taking them off the line (Other).** Standing on his/her feet, the subject was instructed to pick pieces of clothing (socks, shirts, T-shirts, sweaters) from a plastic tub and fasten them to a clothes line with clothes-pegs and then, when finished, picking them off the line and placing them into the tub. The line was approx. 1.7 m above the floor, and the subject was allowed to put the tub on a nearby table while carrying out the activity.
- 6. Slicing bread (Culinary).** Subject standing by a kitchen bench-height table, cutting a loaf of bread in slices approx. 2 cm thick by using a 20 cm bread knife.
- 7. Spreading butter on slices of bread (Culinary).** Subject sitting or standing by a table, spreading butter from a jar on slices of bread by using a kitchen knife.
- 8. Eating with knife and fork (Culinary).** Subject sitting by a table, cutting pieces from bread slices with a kitchen knife and eating these pieces.

---

<sup>†</sup>. Putting on and taking off.

- 9. Opening and closing milk carton (Culinary).** Subject sitting or standing by a table, releasing and bending back the two flaps of a Pure-Pak®† milk carton to open it; then closing it again by folding back the flaps. Carton initially unopened (i.e. opening flaps sealed).
- 10. Stirring in a pan (Culinary).** Subject standing by a cooker-height table, freely selecting one out of two relevant kitchen utensils, then stirring in the pan as if preparing a hot meal (e.g. a soup).
- 11. Pouring water from casserole with a lid (Culinary).** Subject standing by a cooker-height table, pouring water from the casserole into a tub as if pouring hot water from boiled or steamed potatoes or vegetables, using the lid for keeping the food in the casserole while pouring.
- 12. Cutting with scissors (Other).** Subject sitting with the activity “on the lap”, holding an A4-size 80 g/m<sup>2</sup> paper and cutting along a large circle printed on the sheet. The scissors were freely chosen from two available ones of different sizes.
- 13. Sweeping floor with a broom (Other).** Subject standing, gathering debris spread onto the floor into a heap by using a domestic brush.
- 14. Opening and closing containers with threaded lid/cap (Other).** Subject standing by a table, opening and then closing two types of containers: a thermally insulated coffee pot with a threaded lid and a large plastic cosmetics tube with a threaded cap.
- 15. Do the dishes by hand (Other).** Subject standing by a table, simulating washing dishes, cups, knives, forks and other kitchen utensils by using a hand-held washing-up brush.
- 16. Range-of-Motion (Non-ADL).** This activity was included in order to assess whether the set-up actually did restrict wrist movement. The subject was asked to move his/her wrist as far as possible in the direction of extension, then flexion, then radial deviation, ulnar deviation and finally pronation and supination, and the observed ROM was compared to results of similar studies reported by others.

#### 4.2.3 Choice and Design of Utensils

The instrumentation employed for measuring subjects' wrist movements was inherently sensitive to magnetic field distortion. Thus to minimize measurement errors, only plastic and wooden utensils were used, and a plastic vessel with lid played the role of a casserole. Scissors and the bread knife were custom-made for the experiment; the scissors had the plastic handles of a standard household scis-

---

†. Pure-Pak® is a registered trademark of Elopak a.s., P.O. Box 124, N-3431 Spikkestad, Norway.

sors with the stainless steel cutters replaced by hard plastic replicas. The knife comprised a fibreglass-enhanced epoxy blade and a wooden handle. Care was taken to resemble the geometry and mechanical properties of authentic utensils as closely as possible.

#### 4.2.4 Selection and Preparation of the Subjects

##### ***Selection Criteria***

Subjects were required to meet the following three criteria:

- 1. 18 years or older** to ensure a certain level of motor skills and experience with ADLs in general.
- 2. Right-handed** to simplify data collection and analysis by ensuring that all data would be directly comparable without the need for “mirroring” between right-handed and left-handed data sets. Also to ensure compatibility with utensils and other laboratory objects that were not symmetric and thus not equally suitable for right- and left-handed.
- 3. Healthy and without any known history of pathology related to motor function** in order to ensure a minimum of representativity with respect to the general population.

##### ***The Population***

The study comprised eight volunteers, including five female and three male. Ages ranged from 21 to 64 years, with an average of 38.4 years and a standard deviation of 15.9 years; two subjects were 60 years or older, four were in their thirties while two were between 20 and 30.

##### ***Preparation of Subjects***

Unilateral amputees normally use their prosthesis in a non-dominant way, regardless of which side was dominant prior to amputation. Healthy right-handed subjects are trained in using their left hands in a non-dominant fashion; therefore the left hand of each subject was selected for the simulated prosthesis (hereafter referred to simply as the *prosthesis* wherever the meaning is clear from context).

##### ***Hand***

A Plaster-of-Paris gauntlet-like socket was cast on each subject’s hand in a manner that maximally restricted adduction and abduction of the thumb and yet allowed free thumb flexion and extension (figure 4.1(a)). The socket was tightly fitted around the ulnar side of the hand i.e. the fifth metacarpal, in order to eliminate incurvation of the palm which would otherwise allow spherical grip postures.

After partial hardening, the socket was split open on the palmar side and carefully removed from the subject's hand. After complete hardening and drying, the proximal edge of the socket was trimmed to assure that it did not restrict wrist motion, and its remaining edges were adjusted as appropriate in each case. The split was widened by removing approx. 5 mm of the socket material to enable a tight fit. The socket was then firmly attached to the subject by fitting it on the hand and tightly taping it.

The subject's index, long, ring and little fingers were taped together to resemble a "super-finger" with a single, common degree of freedom. The tape covered a large portion of the fingers' palmar side in order to reduce their sense of touch. Another purpose of the tape was to reduce the friction between the fingers and objects being grasped to resemble the relatively low friction of a cosmetic glove ("prosthetic skin").

#### *Elbow and Forearm*

A second Plaster-of-Paris socket was cast on each subject's left elbow and forearm. This socket closely resembled a standard self-suspending socket used in myoelectric transradial prostheses. Care was taken to assure close fit around the epicondyles and the olecranon. When partially hardened, the socket was split open on the ventral side and carefully removed from the subject's arm. After complete hardening and drying the socket was trimmed to increase comfort and further mimic the case of a real prosthetic device. The split was widened by approx. 5 mm as in the case of the hand socket. A hole was carved at the location of the lateral epicondyle in order for the corresponding calibration mark to be visible (mark g in Figure 4.2). Subsequently the socket was reapplied to the subject's arm. A rectangular piece of thin cardboard was placed between the skin and the socket at the ventral side, bridging the socket split, so as to prevent pinching of the soft tissue; then tape was firmly wrapped around the socket to assure a close fit.

#### **4.2.5 Motion Measurement**

This section describes equipment and procedures employed to collect and assure the quality of the data. Numerous references are made to Figure 4.2, which illustrates several important aspects of the laboratory set-up. In particular, single and double letters in parentheses refer to the labels showed in the figure.



**Figure 4.1:** Plaster-of-Paris sockets. (a) hand socket for restriction of thumb abduction and incursion of the palm and for attachment of hand sensor, (b) elbow and forearm socket for restriction of elbow movement and for attachment of ulnar sensor. A hole was carved at the location of the lateral epicondyle (to the lower right in the picture) in order for the corresponding calibration mark to be visible (mark *g* in Figure 4.2).

### Instrumentation

A MotionStar magnetic tracking device<sup>†</sup> was used for recording wrist movements. Two MotionStar sensors were employed; a proximal *ulnar sensor* (*us*) that was firmly taped to the subject's elbow/forearm socket, and a distal *hand sensor* (*hs*) firmly taped to the hand socket.

### Sensor Calibration

#### Prior Techniques

Nelson et al. (1994) calibrated their electromagnetic motion tracker by manual measurements of the wrist orientation of each subject and correlating these data with readouts from the instrument, yielding nonlinear correction functions that were applied to subsequent sensor data before analysis took place. The procedure is reported to be very time consuming, and is only suitable for cancelling some of the static errors caused by soft tissue deformations; it cannot account for dynamic artifacts.

<sup>†</sup>. Ascension Technology Corporation, P.O. Box 527, Burlington, VT 05402, USA

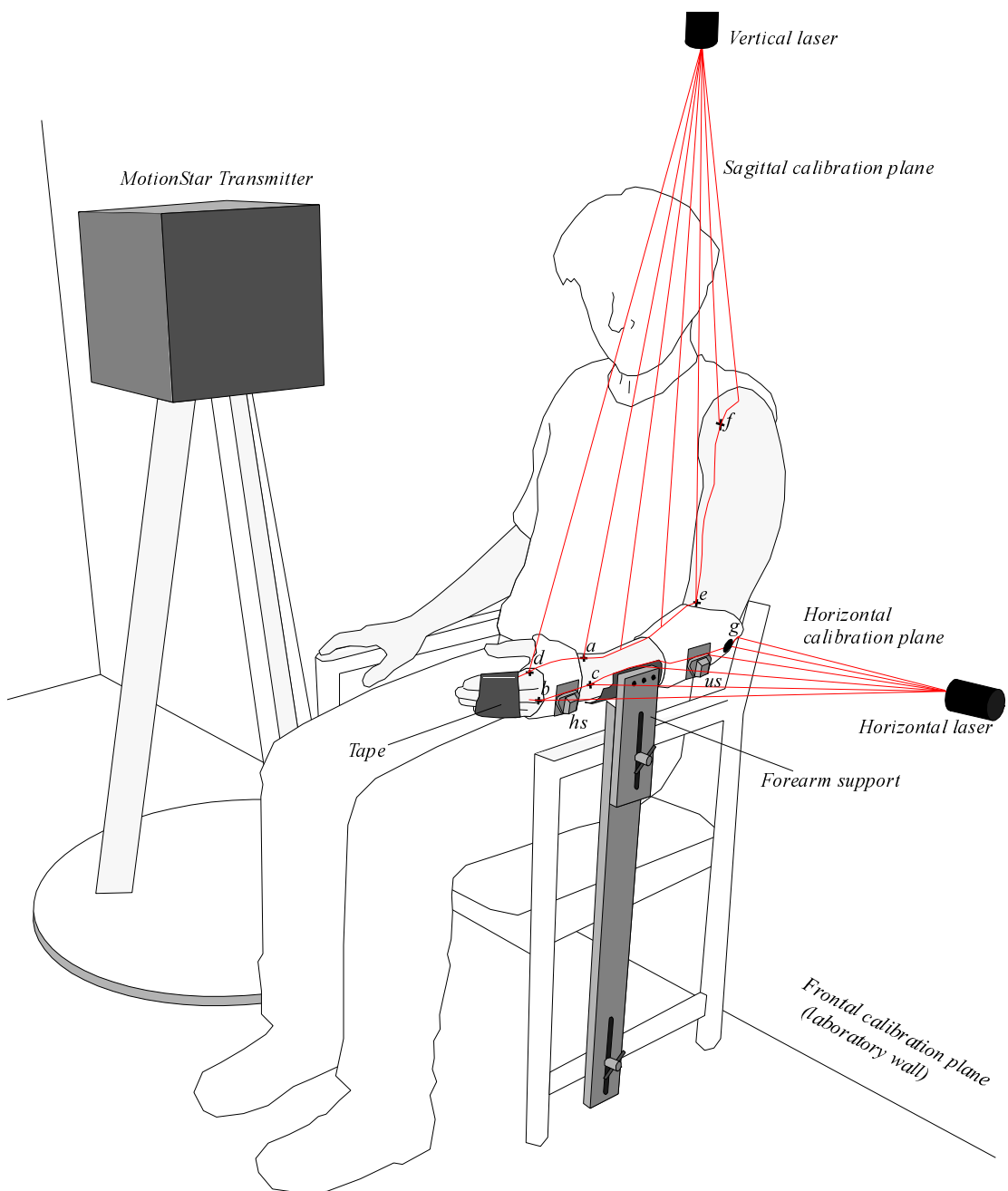


**Figure 4.2:** Calibration measurement set-up. Subject is depicted in the calibration posture, calibration marks indicated by crosses and named by single letters (details are given in the main text).

In the present case dynamic factors were believed to be dominant, and so it was decided not to employ this technique for the current experiment. Steps were instead taken to statically calibrate each sensor's orientation with respect to the corresponding body segment, and to investigate whether the sensors had moved relatively to these body segments during each experimental run.

#### *Measurement Set-Up*

A ceiling mounted vertical laser with a cylindrical lens provided a sagittal calibration plane, while a wall mounted horizontal laser provided a corresponding horizontal calibration plane. These planes were aligned with the  $yz$ - and the  $xy$ -planes, respectively, of the MotionStar transmitter. Before and after each run the subject was placed in the calibration posture depicted in Figure 4.2: upper arm straight down, elbow flexed  $90^\circ$ , forearm pointing forwards and thumb pointing upwards; this resembles the so-called neutral forearm rotation (Werner and Buchholz, 1994). The posture was adjusted until the subject's hand and forearm were aligned with the laser calibration planes and thus with the MotionStar transmitter's frame.

#### *Alignment of Body Segments*

To ensure proper alignment, an extended version of the palpation based method used by Salvia et al. (1994) was employed. Note that the calibration posture depicted in Figures 4.2 and 4.3 is different from the standard anatomical position; in the following, references to the sagittal, horizontal and frontal *calibration planes (CP)* refer to the two laser planes depicted in Figure 4.2 and the plane perpendicular to both these planes (laboratory wall), respectively. The frontal calibration plane is used here for explanation purposes only, and was not employed explicitly in the calibration procedure.

*Hand Alignment in the Sagittal Calibration Plane* The location of the radial styloid (a), the ulnar styloid and the dorsal side of the third metacarpal head (b) were found by palpation and marked with a felt tip pen. The position of the third metacarpal in the sagittal CP was taken as the position of the line connecting the head of the third metacarpal (b) and the midpoint (c) of the straight line between the radial and the ulnar styloid on the dorsal side of the wrist.

*Hand Alignment in the Horizontal Calibration Plane* The midpoint between the dorsal and the palmar surface of the second metacarpal head was marked (d), and the position of the third metacarpal in the horizontal CP was taken as that of the straight line connecting this point and the radial styloid (a).

*Forearm Alignment in the Horizontal Calibration Plane* The ventral midpoint between the medial and the lateral epicondyle was marked (*e*). The position of the ulna in the horizontal CP was taken as that of the straight line connecting this mark and the radial styloid (*a*). The rationale for using the radial instead of the ulnar styloid was as follows. The ulnar and the radial styloids and the long axis of the ulna itself crudely lie in the same vertical plane during calibration, and the two styloids are thus equivalent with respect to their positions in the horizontal CP. The radial styloid was chosen because it is exposed to the vertical laser during calibration, as opposed to the ulnar styloid which is occluded by the wrist itself.

*Forearm Alignment in the Frontal Calibration Plane* The position of the humeral head in the frontal plane was found by palpation and marked on the ventral side (*f*). The position of the humerus in the frontal CP, which determines the orientation of the ulna about its longitudinal axis when the elbow is flexed, was taken as that of the straight line connecting this point (*f*) and the midpoint between the medial and the lateral epicondyles (*e*).

*Forearm Alignment in the Sagittal Calibration Plane* The position of the ulna in the sagittal CP was taken as that of the straight line connecting the lateral epicondyle (*g*) and the midpoint (*c*) between the radial and the ulnar styloid.

Salvia et al. (1994) confirmed the validity and reliability of their alignment method for the hand and wrist by means of X-ray images. The landmarks used in the present study for alignment of the ulna were not used by Salvia et al. (1994). These were chosen primarily because they are easily palpable. Linscheid (1986) makes the following statement about the axis of rotation of the radioulnar joint:

*The axis of rotation itself moves in an arc from full supination to pronation due to a deflection of the ulna, which describes an arc of slight medial adduction flexion in supination through extension at the neutral position to abduction flexion at pronation.*

It is not stated what anatomical reference frame this description is based on, but it is assumed here that the attitude of the ulna is described with respect to the long axis of the forearm. Given this assumption, the quotation above directly confirms that the line *a–e* in Figure 4.2 and the prosupination axis of rotation both lie in the sagittal calibration plane when in the calibration posture (i.e. “neutral position”).

The axis of rotation of the radioulnar joints run close to the centres of their cylindrical parts (Linscheid, 1986). A visual inspection of the relevant skeletal anatomy reveals that marks *c* and *g* in Figure 4.2 are situated above this axis in the sagittal plane when in the calibration posture (see e.g. Linscheid (1986) and Stroyan and Wilk (1993) for details on the radioulnar joints).

### *Calibration Measurements*

A horizontal forearm support with adjustable height was mounted on a wooden chair and placed just below the line of intersection of the laser calibration planes. The subject was seated, and the subject's left forearm with calibration marks and instrumented sockets was placed upon the support. The support's height and the subject's general posture was adjusted until the marks (d), (a), (e) and (f) were in the sagittal CP and the marks (b), (c) and (g) were in the horizontal CP.

With the subject's hand and arm in this calibration posture, the MotionStar output was logged for three seconds at 20 Hz, yielding time series for each sensor's orientation. The sensors' mean orientations were calculated with respect to the reference frame. This procedure was repeated before and after each single ADL run. If any sensor was displaced 5° or more during the run, the entire run was discarded and reiterated.

### *Overall Procedure for Data Capture*

Before each new activity, the subject was given the opportunity to optionally and autonomously practice the activity in order to test alternative ways of performing it with the simulated prosthesis. Each experimental run comprised 20s of motion measurements at a rate of 20 Hz. Care was taken to start the sampling slightly (approx. 1 s) *after* the subject was given the signal to start performing, in order to reduce the influence of transient motion not directly related to the activity. The subject was instructed to continuously or repeatedly do (and undo, whenever relevant) the activity until the signal was given to stop performing. Each experimental run was subject to the calibration process detailed in the previous section. When all activities were performed and recorded once, the entire list of activities was run through a second time to yield two experimental runs per activity. This procedure yielded a total of 102 400 samples corresponding to approx. 1 h 25 min of movement; 1 h 20 min hereof was related to ADL while the remainder was related to the non-ADL control activity (*Range-of-Motion*).

### *Quantification of Measurement Precision*

#### *Sources of Error*

Electromagnetic motion trackers are known to be susceptible to interference from other electric equipment and metal objects in or near the workspace. Of special concern in the present case was the potential influence of computer equipment, fluorescent lights and the two lasers present. Even if care was taken to conduct the experiment in a building mostly made of wooden and plastic materials, there was uncertainty of whether there were any large metal structures hidden in the walls or floors of the laboratory. Furthermore, due to the way the MotionStar unit samples and calculates the orientation of the sensors with respect to the reference

magnetic field, absolute measurement errors increase as the velocity of the sensors increases. For these reasons a special experiment was designed and conducted to quantify the overall measurement precision obtainable with the present set-up. Only the relative orientation between two MotionStar sensors was to be considered in the main experiment; consequently, only the corresponding relative precision needed to be quantified.

#### *Measurement Set-Up*

Two MotionStar sensors were taped to a wooden beam approx. 50 cm apart, crudely corresponding to the distance between the wrist and elbow of an adult person. The sensors were placed on the same side of the beam and with the same orientation with respect to the beam. The orientation of each sensor was then sampled at 20 Hz for several 20 s runs. During the different runs, the instrumented beam was moved at different translational and rotational speeds ranging from zero to velocities exceeding those of natural human movements, spanning relevant parts of the laboratory workspace. Measurements were taken with the lasers turned off and then with the lasers turned on to reveal any laser-induced error contribution. The ceiling-mounted fluorescent lights and all computer equipment present was on during the whole experiment.

For each 20 s run, the orientation of one sensor with respect to the other was calculated for each time step, and the average relative orientation of the sensors during the run was computed. The maximum angular deviation of the instantaneous relative orientation from the run's average was recorded. Finally the angular standard deviation of the sensors' relative orientation was computed as the square root of the corresponding angular variance.

The firm attachment of the sensors to the beam and the stiffness of the beam itself justifies the assumption that the sensors did not move relatively to each other during each run. Thus, with perfectly noise-free measurements, the sampled relative orientation of the sensors would be constant, and consequently the relative angular standard deviation would amount to zero. In the presence of disturbances, however, the angular standard deviation would be finite and closely correlated with the amplitude of the measurement error induced by these disturbances.

#### **4.2.6 Coordinate Frames and Transformations**

Let  $S_o$  denote a reference coordinate frame which is fixed to the room (i.e. to the MotionStar transmitter), and let the coordinate axes of  $S_o$  be denoted  $x_o$ ,  $y_o$  and  $z_o$ . Let  $S_u$  and  $S_h$  be the coordinate frames fixed to the forearm (represented by the ulna) and hand (represented by the third metacarpal), and let the coordinate axes of these frames be denoted  $x_u$ ,  $y_u$ ,  $z_u$  and  $x_h$ ,  $y_h$ ,  $z_h$ , respectively. These were chosen according to Werner and Buchholz (1994), so that when the arm under investigation is in the calibration posture,  $y_u$  and  $y_h$  are pointing proximal

mally along the long axis of the forearm, the positive  $x_u$  and the negative  $z_h$  axes are pointing upwards and the remaining axes  $z_u$  and  $x_h$  are chosen so that  $S_u$  and  $S_h$  form Cartesian right-hand coordinate frames (Figure 4.3).

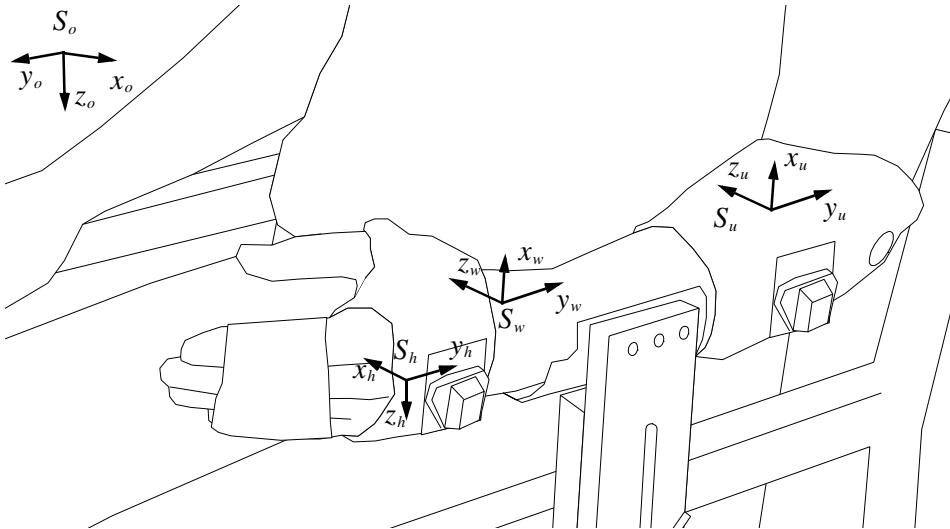


**Figure 4.3:** Orientation of body-fixed coordinate frames in calibration posture.

Let  $S_{us}$  and  $S_{hs}$  be the coordinate frames of the MotionStar sensors attached to the forearm and the hand, and let the orientations of  $S_{us}$  and  $S_{hs}$  with respect to  $S_o$  be defined by the rotation matrices  $R_o^{us}$  and  $R_o^{hs}$ , respectively.

Now let orientations measured with the arm in the calibration posture be denoted by a subscript  $0$ ; thus, the orientation of each of the MotionStar sensors with respect to  $S_o$  when in the calibration posture is represented by the rotation matrices  $R_{o,0}^{us}$  for the  $S_{us}$  frame and  $R_{o,0}^{hs}$  for the  $S_{hs}$  frame, respectively. These matrices were taken as the average of the orientation matrices measured during the calibration measurements before and after the experimental run in question.

Likewise, let the orientations of  $S_u$  and  $S_h$  in the calibration posture be represented by the rotation matrices  $R_{o,0}^u$  and  $R_{o,0}^h$ , respectively; these were assumed to be *constant over the entire experiment* and given by the geometry of the laboratory set-up. In our particular case, as illustrated in Figure 4.3, these matrices are given by

$$\begin{aligned} R_{o,0}^u &= R_{y,\pi/2}R_{x,\pi} \\ R_{o,0}^h &= R_{z,\pi} \end{aligned} \tag{4.1}$$

The orientations of the body-fixed coordinate frames with respect to the corresponding sensor-fixed frames can now be represented by the rotation matrices  $R_{us}^u$  and  $R_{hs}^h$  defined by

$$\begin{aligned} R_{us}^u &= (R_{o,0}^{us})^T R_{o,0}^u \\ R_{hs}^h &= (R_{o,0}^{hs})^T R_{o,0}^h \end{aligned} \quad . \quad (4.2)$$

These matrices were assumed to be *constant over an entire experimental run*. Now, at each time step  $t$ , the orientations of the  $S_u$  and  $S_h$  frames with respect to  $S_o$  are given by

$$\begin{aligned} R_{o,t}^u &= R_{o,t}^{us} R_{us}^u \\ R_{o,t}^h &= R_{o,t}^{hs} R_{hs}^h \end{aligned} \quad , \quad (4.3)$$

respectively, where  $R_{o,t}^{us}$  and  $R_{o,t}^{hs}$  represent the instantaneous orientations of the sensor-fixed coordinate frames with respect to the reference frame, in other words, the output from the MotionStar system.

Finally, the instantaneous global wrist orientation implicitly comprising prosupination, flexion/extension and radioulnar deviation angles at time step  $t$ , is given by the instantaneous relative orientation between the ulnar and the hand sensor, that is the rotation matrix

$$R_{u,t}^h = (R_{o,t}^u)^T R_{o,t}^h, \quad (4.4)$$

which written in expanded form becomes

$$R_{u,t}^h = (R_{o,t}^{us} R_{o,0}^{us T} R_{o,0}^u)^T R_{o,t}^{hs} R_{o,0}^{hs T} R_{o,0}^h. \quad (4.5)$$

The hand- and ulna-fixed coordinate frames are not parallel in the calibration posture. This is the natural choice for a neutral posture, that is a posture in which the clinical angles are all zero by definition, and so the wrist's orientation should be expressed relatively to this posture. Therefore let the instantaneous wrist orientation with respect to the calibration posture be denoted  $R_{u,t}^w$ , which is then given by

$$\begin{aligned}
 R_{u,t}^w &= (R_{o,t}^u)^T R_{o,t}^h R_h^w \\
 R_h^w &\stackrel{\Delta}{=} (R_{o,0}^h)^T R_{o,0}^u \equiv R_{z,-\pi} R_{y,\pi/2} R_{x,\pi} \\
 &= R_{y,\pi/2}
 \end{aligned} \tag{4.6}$$

where the final line trivially follows from inspection of Figure 4.3. Note that  $R_h^w$  can be thought of as the orientation with respect to  $S_h$  of a hand-fixed frame  $S_w$  which axes are parallel to those of  $S_u$  in the calibration posture.

### ***Range-of-Motion Calculation***

Every sample of the wrist orientation during performance of the range-of-motion (RoM) activity was converted to a triple of instantaneous clinical angles. The maximum negative and the maximum positive value of each angle were recorded for each experimental run, yielding the maximum pronation, supination, flexion, extension and ulnar and radial deviation angles, respectively. Subsequently the statistics of these quantities were computed in order to allow comparison with previous results.



# Chapter 5

## Rotational Foundations

This chapter lays a theoretical foundation for the succeeding chapter, which is focused on statistical analysis of rotational data. In the present chapter, essential properties of rotations are explored, and commonly used parameterizations of three-dimensional rotations are discussed. In the final sections, kinematic models of relevant wrist configurations are developed.

For a more complete exposition and proofs of the topics and statements covered in this chapter, the reader is referred to standard textbooks on robot modelling and control, for example Spong and Vidyasagar (1989). A more mathematically involved treatment is given by Samson et al. (1991).

### 5.1 Motivation

#### 5.1.1 Human Joints Rotate

In the context of the human body, a joint is a junction between two bones or groups of bones that permits relative motion between them. The joints of the human body span an impressive range with respect to size, complexity and kinematic properties: from the millimetre-sized joints linking the auditory ossicles to the decimetre-sized adult knee.

Despite this remarkable range, the aggregate function of every human joint is of an almost completely rotational nature. Numerous studies have documented translational movement components in several human joints, see for example van der Heijden and Hillen (1996) who reported transversal movement of the distal ulna with respect to the radius during prosupination. Such translations are believed to stem from a combination of rotational asymmetry and compliance of the articulated surfaces, net translational forces from muscles, tendons, ligaments and other nearby tissue, as well as from external forces acting via these structures.

Precise knowledge of such translations can be of crucial importance for understanding and preserving stable joint function after injuries and surgical procedures. In the present context, however, these translations are essentially negligible compared to the joints' rotational potential.

### 5.1.2 Conventional Methods are Not Applicable

From the previous paragraph it is obvious that the study of rotational movements is essential to the study of human motion. Several aspects of rotational data differ substantially from those of translational data. As an example, translations can simply be added vectorially to form their gross sum, while the net effect of a series of rotations generally has to be calculated in a non-linear and non-commutative fashion. Consequently, many conventional signal processing techniques and statistical methods do not translate into the rotational domain in a straightforward manner.

## 5.2 Terminology

We start by defining some important terms used in this chapter. Most symbols and notions introduced in the following paragraphs are illustrated in Figure 5.1. Rotations and their parameterizations will be thoroughly treated in Section 5.3.

### 5.2.1 A Rigid Body's Degrees of Freedom

A rigid body  $b$  has six mechanical DoFs. Of these, three are related to the body's linear displacement (i.e. its translation), and are easily represented by Cartesian coordinate triplets. The body's current set of translational coordinates ( $\mathbf{p}$  in Figure 5.1) defines the current *position* of the origin of a body-fixed coordinate frame  $S_b$  with respect to the origin of a given reference frame  $S_o$ . Often the coordinate vector is referred to as representing the body's current position, the body-fixed frame and the reference frame being implicit; so also in this text whenever it is clear from the context which frames the coordinates refer to.

The remaining three degrees of freedom are related to the body's angular displacement (i.e. its rotation). These may be represented by a  $3 \times 3$  rotation matrix, which may again be parameterized in numerous ways. The corresponding parameter vector can be regarded as the body's rotational coordinate vector, which, together with the semantics of the parameterization chosen, defines the current *orientation* of a body-fixed coordinate frame  $S_b$  with respect to the axes of a given reference frame  $S_o$ . The term *orientation* will thus be used to denote a parameterized representation of the orientation of a body-fixed frame whenever this is consistent with the context.

Often the rotational coordinates are referred to as representing the body's current orientation, the body-fixed frame and the reference frame being implicit; so also in this text whenever it is clear from the context which frames the rotational coordinates refer to.

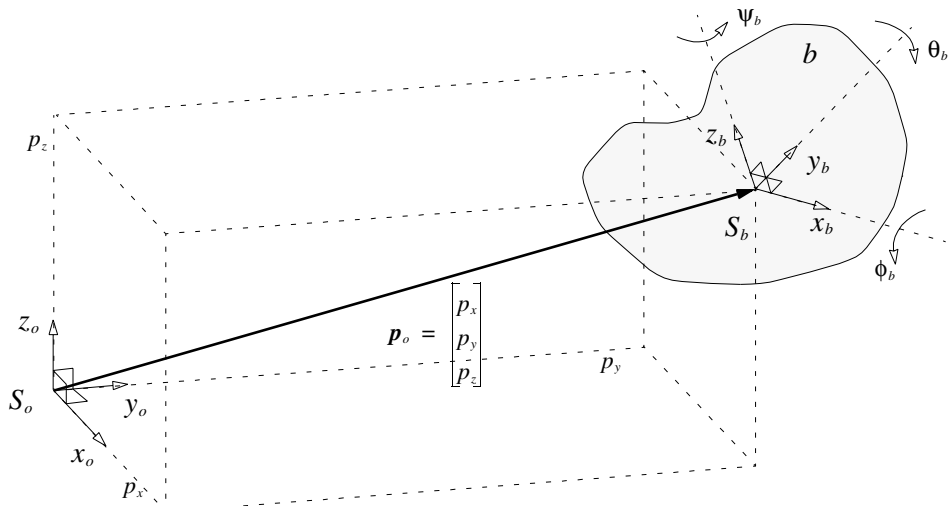


**Figure 5.1:** Illustration of a rigid body's six mechanical DoFs.

In Figure 5.1 the rotational DoFs of the rigid body  $b$  are illustrated by the three rotation angles  $\phi_b$ ,  $\theta_b$  and  $\psi_b$ , the corresponding rotations taken about the body-fixed  $x$ -,  $y$ - and  $z$ -axes, respectively. In reality this is just one out of a multitude of possible rotation sequences, each giving rise to a separate parameterization of the body's orientation.

### 5.2.2 Orientation of a Joint

In this text, occasional references are made to the *orientation of a joint*, which we define to be the relative orientation of the coordinate frames fixed to each of the two body segments that are connected by the joint.

Unless otherwise explicitly stated, this relative orientation is expressed in terms of the more proximal of the frames in question. This means for example that the wrist orientation will generally express the orientation of a hand-fixed frame with respect to a forearm-fixed frame, rather than the opposite.

To illustrate this, Figure 5.2 depicts a section of a slightly flexed finger with the proximal phalange labelled  $pp$  and the middle phalange labelled  $mp$ . The coordinate frames fixed to these bones are denoted  $S_p$  and  $S_m$ , respectively (note that the origin of each of these frames is located outside the bone to which it is fixed). Thus, the orientation of the proximal interphalangeal (PIP) joint is defined as the

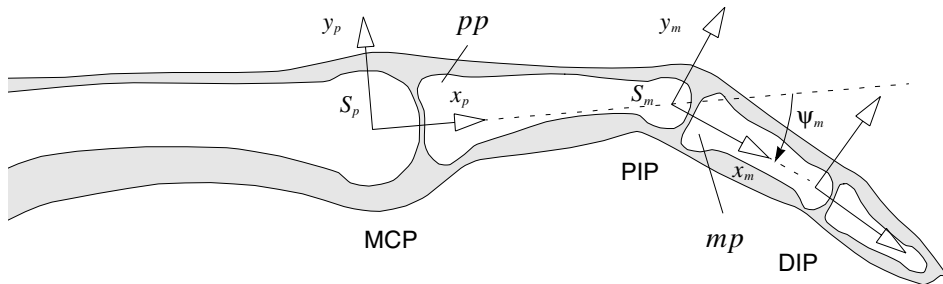


**Figure 5.2:** Orientation of a joint, exemplified by the proximal interphalangeal (PIP) joint. Since the  $xy$ -planes of  $S_p$  and  $S_m$  are parallel and both are perpendicular to the PIP joint axis of rotation, only the scalar angle  $\psi_m$  needs to be specified for the joint's orientation to be defined.

orientation of  $S_m$  with respect to  $S_p$ . In this particular case both frames'  $z$ -axes, which are perpendicular to the image plane, are also parallel to the PIP joint's axis of rotation. Therefore the joint's orientation is uniquely defined by the single angle  $\psi_m$  between the two frames'  $x$ - (or equivalently between the  $y$ -) axes. For this reason joint orientation is frequently referred to as *joint angle* for simple revolute joints.

### 5.2.3 Parallelity of Coordinate Frames

A set of coordinate frames are said to be *parallel* if and only if their  $x$ -,  $y$ - and  $z$ -axes, respectively, are parallel. The same set of frames are said to be *coincident* if and only if they are parallel and share a common origin.

### 5.2.4 Orientation vs. Rotation

The terms *orientation* and *rotation* will be used somewhat synonymously since the orientation of a coordinate frame is uniquely defined by the rotation that the frame must undergo in order for it to be parallel to the reference frame – or vice versa.

### 5.2.5 Orientation, Attitude and Posture

These three terms are closely related, but are used with slightly different meanings in this text. Before giving a detailed definition, it should be noted that several other related terms are used in the literature, apparently with poor consensus. For example, Woltring (1994) stated that “orientation”, as used in photogrammetry, includes translational position; this again corresponds to the term “pose” as used in biomechanics. To resolve this discrepancy, Woltring chose to define “attitude” as describing rotational (angular) position only. In this text, however, the following interpretations apply.

*Orientation* denotes, as just stated, the angular displacement of a rigid body or a joint. At least three parameters, corresponding to three angular DoFs, must be specified in order for an orientation to be completely specified.

Now consider a vector  $v \in \mathbb{R}^3$ , which defines a directed line in space. Because a rotation of  $v$  about itself leaves the vector unchanged, the vector only has two rotational DoFs. Consequently, given  $\|v\|$ , only two parameters need to be specified for the orientation of  $v$  to be uniquely defined, such as its azimuth and elevation angles with respect to some reference frame. The orientation of a vector, a line or an axis of rotation is therefore referred to by a special term: *attitude*.

A *kinematic chain* is a set of rigid bodies, commonly referred to as *links*, which are connected by joints. A finger and a hand are both examples of kinematic chains. As each joint (or, equivalently, each link) is associated with a separate orientation, the overall angular configuration of a kinematic chain is referred to by the special term *posture*. Thus, for a posture to be completely defined, the orientations of all joints (links) involved must be specified. Note, however, that when discussing the angular displacement of a single rigid body or joint, the term *orientation* is used even if the body (joint) in question is a member of a kinematic chain.

## 5.3 The Rotation Matrix Space: SO(3)

The set of all  $3 \times 3$  rotation matrices, that is all orthogonal  $3 \times 3$  matrices  $R$  with  $|R| = +1$ , is referred to as the *special orthogonal group of order 3* and is denoted  $\text{SO}(3)$ . A most central property of this group is that the inverse of any of its elements equals its transpose:

$$R \in \text{SO}(3) \Rightarrow R^{-1} = R^T \Leftrightarrow R^T R = I \quad (5.1)$$

$\text{SO}(3)$  is a subgroup of  $\text{GO}(3)$ , the *general orthogonal group of order 3*, which also includes the rotoinversion matrices: the orthogonal  $3 \times 3$  matrices  $R$  with  $|R| = -1$ .

### 5.3.1 Topology

For small angles of rotation,  $\text{SO}(3)$  is homeomorphic (topologically equivalent) to Euclidean 3-space  $\mathbb{R}^3$ . Globally, however, basic properties like Pythagoras' theorem are not valid. A fundamental difference between  $\text{SO}(3)$  and  $\mathbb{R}^3$  is that while the three linear dimensions of the latter extend infinitely from the origin, each of the three "angular dimensions" of  $\text{SO}(3)$  is inherently cyclic modulo  $2\pi$ : whenever a physical or mathematical object is rotated an angle of  $2\pi$  about any fixed axis, the orientation of the rotated object is identical to that of the original (unrotated) one. The essential implication is that in  $\text{SO}(3)$ , all "straight lines" (in

terms of rotations about a single, fixed axis) are in fact circles; if you travel in any direction, you will end up where you started after having travelled a rotational distance of  $2\pi$ .

While the Euclidean 3-space  $\mathbb{R}^3$  is easy to picture as the span of three linearly independent base vectors, the topology of  $\text{SO}(3)$  is more difficult to visualize. One of its three dimensions can be illustrated by cutting a piece of length  $2\pi$  out of the real line and attaching its two ends, as in Figure 5.3a.

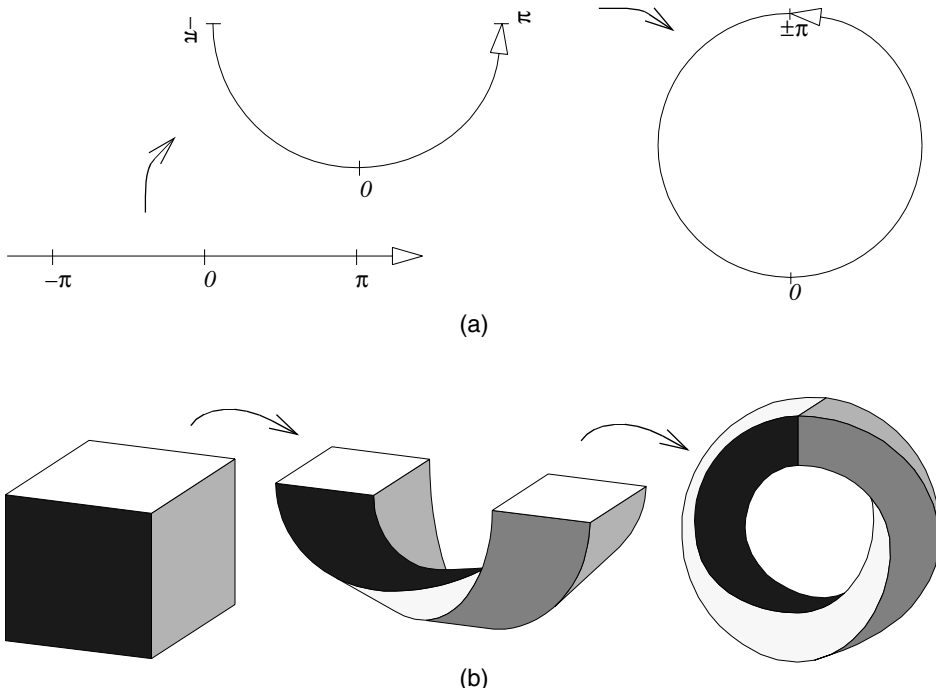


**Figure 5.3:** The topology of rotation spaces. (a) illustrates a single rotational dimension as a circle with circumference  $2\pi$ , while (b) shows the first of three steps needed to transform a cube into an object with topology equivalent to that of  $\text{SO}(3)$ .

An extension of this picture to two dimensions can be thought of as the surface resulting from the following process: Start out with a square piece of paper, grasp two opposite sides, twist the sheet half a turn and glue the two sides together to get a Möbius band. Then hold the other two sides and repeat the process. In three dimensions the starting point would be a cube which three pairs of opposite side planes would be glued together after having been twisted half a turn. Figure 5.3b illustrates the result of the first of these three twist-and-glue steps, the final two of which cannot be carried out unless the cube is made of a solid material that can unrestrictedly pass through itself, that is a non-physical situation. Also, just as the

closed circle in Figure 5.3a does not have any end point, the twisted-and-glued cube corresponding to SO(3) does not have any outer surface; clearly another non-physical feature.

### 5.3.2 Parameterizations of SO(3): Special Phenomena

#### *Singularities*

Euler's Rotation Theorem states that any rotation may be described by only three parameters. It has been shown that every such three-parameter representation of SO(3) exhibits at least one *representation singularity*. For illustration, consider a three-axial gimbal structure, in which case the rotation angles about the structure's three axes constitute a three-parameter representation of the gimbal's overall rotation. This representation exhibits a singularity, commonly referred to as the *gimbal-lock* effect, whenever two of the three axes of rotation become parallel. In this configuration there are infinitely many sets of rotation angles that give the same overall result with respect to orientation, because any rotation about one of the parallel axes can be compensated by an opposite rotation about the other. Also, in this configuration a finite rotational velocity in certain directions requires infinite angular velocity about some of the gimbal axes. In particular, for a passive gimbal structure certain rotations are mechanically impossible in this configuration (thus the designation *gimbal-lock*).

#### *Non-Uniqueness*

Another obscure property shared by most popular parameterizations of SO(3) is referred to in biomechanics literature as *Codman's Paradox* (Woltring, 1994): generally there are two or more sets of parameters that represent one and the same orientation. As is the case for singularities, this non-uniqueness introduces insurmountable complications in conjunction with even the simplest arithmetic operations: which of the parameter values should be used for the computation?

#### *Overrepresentations*

To avoid representation singularities, four or more parameters must be employed. In light of Euler's Rotation Theorem, such parameterizations are referred to as being *overrepresentations*. Euler parameters, often and somewhat erroneously referred to as quaternions, constitute an important four-parameter representation frequently applied in robotics and vessel control. However, even Euler parameters suffer from drawbacks like non-uniqueness of representation.

### 5.3.3 Properties of the Full Matrix Representation

A full  $3 \times 3$  rotation matrix may be considered a trivial nine-parameter representation of itself. Not only is this a severe overrepresentation; it is truly redundant since any two rows or columns uniquely define the third. However, the full matrix representation also has some important advantages:

**Uniqueness** An arbitrary rotation can be represented by one and only one rotation matrix. There are no singularities or multiple representations.

**Geometric Interpretation** The rows of a rotation matrix can be regarded as the (transposed) unit base vectors of the coordinate frame which orientation is represented by the matrix, expressed in terms of the reference frame. Therefore the matrix can easily and directly be visualized as an orthonormal vector triplet as exemplified in Figure 5.4.

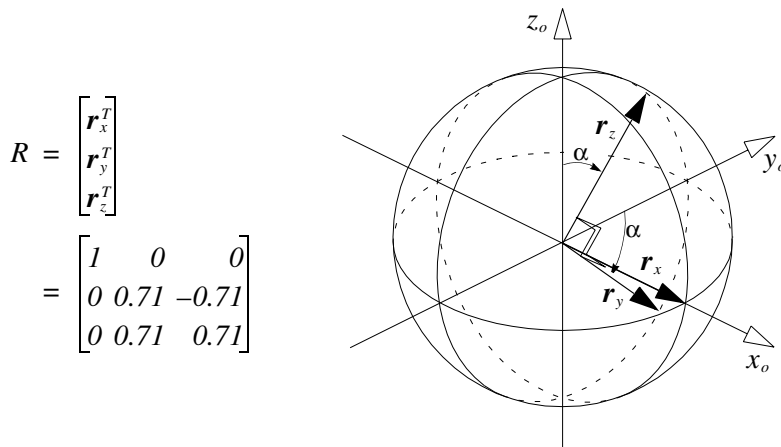


**Figure 5.4:** A rotation matrix and its geometric interpretation. The given matrix corresponds to a rotation of the coordinate frame through an angle  $\alpha = -\pi/4$  about the  $x_o$ -axis ( $\cos(-\pi/4) = 0.71$ ).

**Isotropy and Linearity** From the geometric interpretation above it follows that no axis or angle of rotation is treated any different from others. The matrix literally instantiates the rotated coordinate frame, eliminating the non-linear relationships exhibited in other representations between the parameters and the rotation or orientation they represent.

### 5.3.4 Angle/Axis Parameterization

The orientation corresponding to any matrix  $R \in \text{SO}(3)$  can be generated by a single rotation about a suitable axis by a suitable angle. We write

$$R = R_{k, \theta} \quad (5.2)$$

where  $\mathbf{k}$  is the unit vector defining the axis of rotation,  $\theta$  is the angle of rotation about  $\mathbf{k}$ , and the direction of rotation is given by the right-hand rule. This is known as the *angle/axis parameterization* of SO(3). Each of the nine elements of the matrix in (5.2) turns out to be a quite simple function of  $\theta$  and the components of  $\mathbf{k}$  (Spong and Vidyasagar, 1989):

$$R_{k, \theta} = \begin{bmatrix} (k_x^2 v_\theta + c_\theta) & (k_x k_y v_\theta - k_z s_\theta) & (k_x k_z v_\theta + k_y s_\theta) \\ (k_x k_y v_\theta + k_z s_\theta) & (k_y^2 v_\theta + c_\theta) & (k_y k_z v_\theta - k_x s_\theta) \\ (k_x k_z v_\theta - k_y s_\theta) & (k_y k_z v_\theta + k_x s_\theta) & (k_z^2 v_\theta + c_\theta) \end{bmatrix} \quad (5.3)$$

$$v_\theta = 1 - c_\theta, \quad c_\theta = \cos \theta, \quad s_\theta = \sin \theta$$

$$\mathbf{k} = [k_x \ k_y \ k_z]^T$$

Given a rotation matrix, the axis and the angle of rotation are not uniquely defined, as a change of signs of both  $\mathbf{k}$  and  $\theta$  will leave the matrix unchanged. In the context of this thesis, by convention we will choose  $\theta \in [0, \pi]$  which yields a uniquely defined  $\mathbf{k}$  except at  $\theta = \pi$  and  $\theta = 0$ ; in the first case  $\mathbf{k}$  is defined except for its sign, in the latter case *any* unit vector  $\mathbf{k}$  yields the same result, thus  $\mathbf{k}$  is completely undefined.

If  $\mathbf{k}$  is parallel to one of the coordinate axes, the matrix of (5.3) degenerates to the “elementary” rotation matrices well known from basic linear algebra. These matrices will be referred to as  $R_{x, \phi}$ ,  $R_{y, \theta}$  and  $R_{z, \psi}$  for rotation of angles  $\phi$ ,  $\theta$  and  $\psi$  about the  $x$ -,  $y$ - and  $z$ -axis, respectively, with the second index as the “free” (and only) variable.

### 5.3.5 Metric on SO(3); Rotational Distance

A metric of the geodesic distance between any two elements of SO(3) can be defined as follows. Let  $S_1$  and  $S_2$  denote two coordinate frames whose orientations are given by  $R_1$  and  $R_2$ , respectively,  $R_1, R_2 \in \text{SO}(3)$ . The *geodesic distance* between  $R_1$  and  $R_2$  then is defined to be the minimum angle by which any of the two frames must be rotated, about a suitable fixed axis, in order to make the two frames parallel. As can be readily verified from (5.3), this distance can be calculated as

$$\begin{aligned} \angle(R_1, R_2) &= \arccos \frac{\text{tr}(R_1 R_2^T) - 1}{2} \\ &= 2 \arccos \frac{\sqrt{1 + \text{tr}(R_1 R_2^T)}}{2} \end{aligned} \quad (5.4)$$

where  $tr$  is the *Trace* operator. As can readily be verified, by substituting  $R_{k,\theta} = R_1 R_2^T$  in (5.3), this metric corresponds to the angle  $\theta$  in that equation.

### 5.3.6 Equivalent Axis of Rotation

Equation (5.3) can similarly be used for calculating the equivalent axis of rotation for any given rotation matrix  $R = \{r_{ij}\}$  as

$$\mathbf{k} = \frac{1}{2\sin\theta} \begin{bmatrix} r_{32} - r_{23} \\ r_{13} - r_{31} \\ r_{21} - r_{12} \end{bmatrix}. \quad (5.5)$$

### 5.3.7 Euler Angles

The term “Euler (or Eulerian) angles” covers a total of 12 different parameterizations of SO(3). Any rotation can be implemented by a series of three consecutive rotations about three axes where the first and the third axes are orthogonal to the second. The Euler angles are the three angles of rotation about the respective axes, and are typically denoted by the symbols  $\phi$ ,  $\theta$  and  $\psi$ . By a proper choice of coordinate frames any Euler angle sequence can be performed as rotations about the coordinate axes, and the 12 Euler angle variants arise from the different possible sequences of these axes:  $xyx$ ,  $xyz$ ,  $xzx$ ,  $xzy$ ,  $yxy$ ,  $yxz$ ,  $yzx$ ,  $yzy$ ,  $zxy$ ,  $zxz$ ,  $zyx$  and  $zyz$ .

Some authors refer to “Cardan (or Cardanic) angles” whenever the three axes of rotation are all different (e.g.  $xyz$ ) and reserve the term “Euler angles” for those cases where the first and third axes are identical (e.g.  $yxy$ ). In this thesis, however, all 12 cases will be referred to as Euler angles.

Each element of a rotation matrix parameterized by Euler angles is a function of the sines and cosines of the three angles in question.

### 5.3.8 The Orientation Vector

A close relative of the axis/angle parameterization is the *orientation vector* representation; see Woltring (1994) for a brief theoretical and historical treatment<sup>†</sup>.

Consider the vector

$$\boldsymbol{\theta} \stackrel{\Delta}{=} \mathbf{k}\theta \quad (5.6)$$

---

<sup>†</sup>. Woltring (1994) refers to this as the “attitude vector”. The present the term “orientation vector” is introduced to comply with pertinent robotics literature and the definitions of Section 5.2.

by which it immediately follows that

$$\begin{aligned} \theta \parallel k \\ |\theta| = \theta \end{aligned} \quad (5.7)$$

A rotation matrix parameterized by an orientation vector will be denoted by a bold subscript letter representing the vector without the angle of rotation indicated explicitly as a second index of the matrix. By convention,  $|\theta| \in [0, \pi]$  for any orientation vector  $\theta$ . At  $|\theta| = \pi$  there is a representation singularity; here,  $\theta$  and  $-\theta$  represent one and the same rotation matrix.

In this thesis, the orientation vector representation will mainly be used for visualization purposes as it has a straightforward physical interpretation: Its direction defines the axis of rotation, its length defines the rotation angle.

### 5.3.9 Euler Parameter Representation

The Euler parameter vector has four elements and can be calculated from the angle/axis representation as

$$\begin{aligned} \mathbf{q} &= \begin{bmatrix} q_0 \\ q_1 \\ q_2 \\ q_3 \end{bmatrix} = \begin{bmatrix} \eta \\ \boldsymbol{\epsilon} \end{bmatrix} \\ \eta &= \cos \frac{\theta}{2} \\ \boldsymbol{\epsilon} &= \sin \frac{\theta}{2} \mathbf{k} \end{aligned} \quad (5.8)$$

It follows that  $|\mathbf{q}| = 1$ . Given an Euler parameter vector  $\mathbf{q} = [q_0 \ q_1 \ q_2 \ q_3]^T$ , the equivalent rotation matrix can be calculated in several different ways, e.g. by the following formula:

$$R_q = \begin{bmatrix} (2q_0^2 + 2q_1^2 - 1) & (2q_1q_3 + 2q_0q_3) & (2q_1q_3 - 2q_0q_2) \\ (2q_1q_2 - 2q_0q_3) & (2q_0^2 + 2q_2^2 - 1) & (2q_2q_3 + 2q_0q_1) \\ (2q_1q_3 + 2q_0q_2) & (2q_2q_3 - 2q_0q_1) & (2q_0^2 + 2q_3^2 - 1) \end{bmatrix}. \quad (5.9)$$

Since all elements of  $R_q$  are quadratic in the elements of  $\mathbf{q}$ , it follows that the sign of  $\mathbf{q}$  carries no information. Thus,  $\mathbf{q}$  and  $-\mathbf{q}$  represent one and the same orientation; SO(3) is doubly represented in Euler parameter space.

## 5.4 Kinematics of the Restricted Wrist

In this section the consequences of limiting rotation motion to less than three DoFs are explained. General kinematic models for a one- and a two-DoF kinematic chain are established and their properties briefly discussed. The non-linearity and generally complex topology of corresponding parameter spaces are illustrated graphically. Finally the process of finding optimal parameter values is considered.

### 5.4.1 Introduction

A wrist joint with less than three DoFs will impose restrictions on the range of wrist orientations obtainable as compared to a healthy human wrist. Although the discussions and results presented in this section apply to a wider range of systems, the terminology is chosen in order to easily relate the text to the wrist application.

An articulated chain with three mechanical degrees of freedom (that is three independent joint functions) spans  $\text{SO}(3)$  in its entirety under certain conditions. The healthy human wrist does not comply with these conditions because its angular excursion is severely limited by mechanical constraints. Nevertheless, the functional range of a healthy wrist spans a continuous three-dimensional subspace of  $\text{SO}(3)$ . We will denote this subspace by the symbol  $W_F$ . Thus, the task of replacing a healthy wrist by a kinematically optimal prosthesis with less than three DoFs (cf. Section 3.5) can be expressed as that of approximating  $W_F$  by a fewer-dimensional subspace of  $\text{SO}(3)$ .

### 5.4.2 Model of the Single-Degree-of-Freedom Wrist

Figure 5.5 depicts  $\text{SO}(3)$  as a 2-D surface for convenience. Each point on the surface corresponds to a rotation matrix. The shaded region  $W_F$  may be thought of as representing the functional range of a human wrist. The symbol  $I$  in the upper right corner represents the identity matrix, corresponding to neutral orientation (i.e. no rotation at all); it is the “zero element” of  $\text{SO}(3)$ .

If the axis of rotation  $\mathbf{k}$  is kept constant, the axis/angle parameterization  $R_{k,\theta}$  spans a 1-D subspace of  $\text{SO}(3)$ , corresponding to a line in Figure 5.5, which is insufficient for representing the range of motion of a general single-DoF wrist device. In mechanical terms, this is because the axis of rotation,  $\mathbf{k}$ , does not necessarily have the same attitude with respect to the hand-fixed coordinate frame as to the forearm-fixed frame. The difference can be captured by introducing a constant *orientational offset matrix*  $R_b$ , a rotation matrix uniquely defined by a parameter vector  $\mathbf{b}$ . In more theoretical terms,  $R_{k,\theta}$  spans only one of the three dimensions of  $\text{SO}(3)$ ; the matrix  $R_b$  serves to offset the solution in the remaining

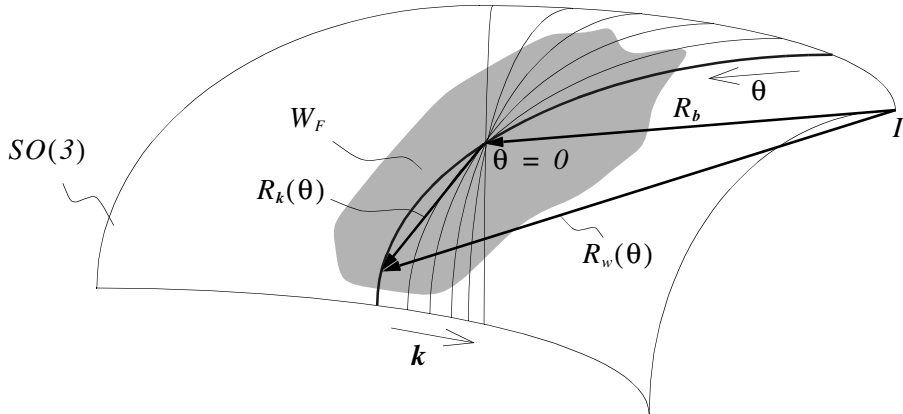


**Figure 5.5:** Illustration of  $SO(3)$  and a fewer-dimensional subspace.

dimensions, cf. Figure 5.5, so that the resulting range of motion (the bold curved line in the figure) approximates  $W_F$  as closely as possible. Thus, a single-DoF device can be modelled as follows:

$$R_w(\theta; \mathbf{k}, \mathbf{b}) = R_{k,\theta} R_b \quad (5.10)$$

where  $R_w$  is the overall wrist orientation,  $\mathbf{k}$  is the unit vector defining the fixed axis of rotation,  $\theta$  is the joint rotation angle and  $\mathbf{b}$  is the orientation offset vector.

In Figure 5.6, two actual one-dimensional subspaces of  $SO(3)$  are depicted in the orientation vector space. Each curve is generated by calculating the equivalent orientation vector for a rotation matrix given by (5.10) for a fixed set of vectors  $\mathbf{b}, \mathbf{k}$  (indicated below each graph) and for  $\theta$  in the range  $(-\pi, \pi)$ . The solid ball of radius  $\pi$ , which can be regarded as a visualization of  $SO(3)$  in its entirety, is indicated by a spherical cloud of dots. The figures are projected onto the planes  $x = -6$ ,  $y = -6$  and  $z = -6$ , respectively, in order to facilitate a three-dimensional interpretation of the graphs. The sole purpose of Figure 5.6 is to visualize the one-dimensional nature of the model of Equation (5.10), and the dependence of the corresponding one-dimensional space on parameters  $\mathbf{k}$  and  $\mathbf{b}$ .

With  $\mathbf{b} = \mathbf{0}$  (i.e. no offset) (a), the subspace degenerates to a straight line parallel to  $\mathbf{k}$  through the origin. In (b), with  $\mathbf{b} \neq \mathbf{0}$ , the parameter vectors  $\mathbf{b}$  and  $\mathbf{k}$  are shown to illustrate the connection with Figure 5.5 ( $R_b$  in Figure 5.5 corresponds to the orientation represented by  $\mathbf{b}$  in Figure 5.6).

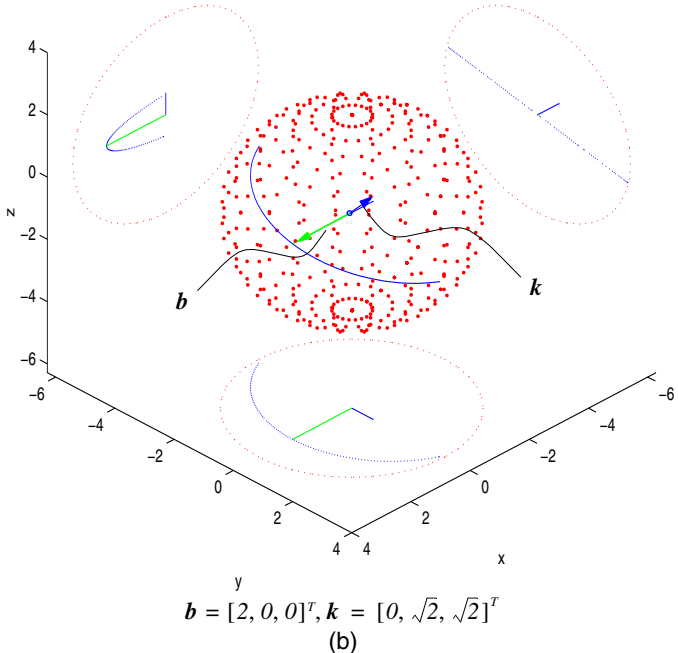
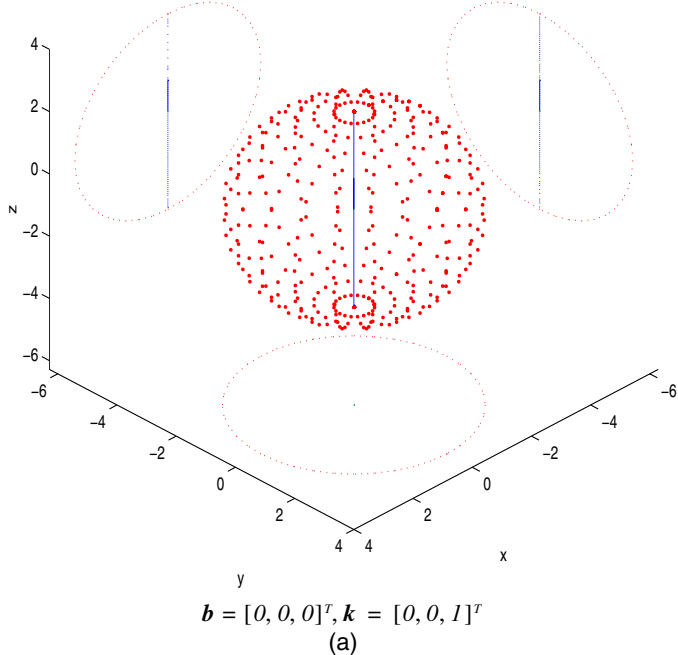


**Figure 5.6:** Actual one-dimensional subspaces of  $\text{SO}(3)$  with different rotation offsets and axes.

### 5.4.3 Model of the Two-Degree-of-Freedom Wrist

Following a similar argumentation, the kinematics of a two-DoF device can be modelled as

$$R_w(\theta_1, \theta_2; \mathbf{k}_1, \mathbf{k}_2, \mathbf{b}) = R_{k_2, \theta_2} R_{k_1, \theta_1} R_b \quad (5.11)$$

where  $(\mathbf{k}_1, \mathbf{k}_2)$  and  $(\theta_1, \theta_2)$  are the axes and angles of rotation, respectively, of the two rotational joints, and  $\mathbf{b}$  is the orientation offset vector. Figure 5.7 illustrates the physical meaning of the model parameters for one possible choice of  $\mathbf{b}, \mathbf{k}_1, \mathbf{k}_2$  in which the axes of rotation and the orientation offset vector are chosen to coincide with the clinical axes of rotation (cf. Figure 2.6). In the depicted case, the interlinked cylindrical objects coaxial with  $\mathbf{k}_1$  and  $\mathbf{k}_2$ , respectively, represent the possibility of rotational movement about the corresponding axes. The constant rotational offset consists of a rotation about the offset vector  $\mathbf{b}$ , which in this case coincides with the prosupination axis (the offset angle, which by convention is equal to  $|\mathbf{b}|$ , is indicated by the symbol  $\beta$  in the figure)<sup>†</sup>.

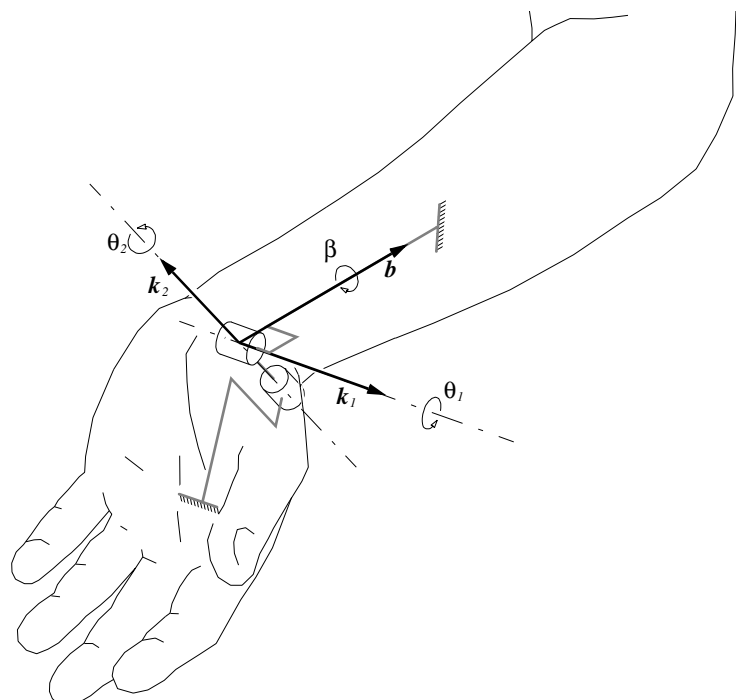


**Figure 5.7:** Physical meaning of the 2-DoF model parameters

<sup>†</sup>. Figure 5.7 actually corresponds to a slightly different model in which the offset is the more proximal of the three rotations, that is of the form  $R'_w(\cdot) = R_b R_{k_1, \theta_1} R_{k_2, \theta_2}$ . This model is equivalent to Equation (5.11) in that one can be transformed into the other by properly rotating each parameter vector.

Different choices of the model parameters  $\mathbf{b}, \mathbf{k}_1, \mathbf{k}_2$  imply different sets of obtainable wrist orientations. Figure 5.8 illustrates six different two-dimensional subspaces of  $\text{SO}(3)$  corresponding to (5.11) with six different parameter sets. Each surface is generated by calculating the equivalent orientation vector for a rotation matrix given by (5.11) for a fixed set of vectors  $\mathbf{b}, \mathbf{k}_1, \mathbf{k}_2$  (the values of which are indicated below each graph) and for  $\theta_1, \theta_2 \in (-\pi, \pi)$ . The solid ball of radius  $\pi$ , which corresponds to the entire  $\text{SO}(3)$ , is indicated by a cloud of dots. The figures are projected onto the planes  $x = -6$ ,  $y = -6$  and  $z = -6$ , respectively, in order to facilitate a three-dimensional interpretation of the graphs. Again, the sole purpose of Figure 5.8 is to visualize the two-dimensional nature of the model of Equation (5.11), and the relatively complex dependence of the corresponding two-dimensional space on parameters  $\mathbf{b}, \mathbf{k}_1, \mathbf{k}_2$ . Note that in Figure 5.8c the resulting surface passes through itself.

#### 5.4.4 On the Uniqueness of Solutions

Based on the previous definitions, designing an optimal wrist device now can be expressed as the task of choosing an optimal value for the rotational offset and optimal attitudes for the axis (or axes) of rotation.

Wrist prostheses typically can be rotated by any number of revolutions<sup>†</sup>. The “neutral point” of a joint, where the rotation angle is zero by definition, therefore can be chosen arbitrarily without functionally affecting the device. Thus, for the model of (5.10) and for any constant  $\theta_0 \in \mathbb{R}$  and  $R_{\bar{b}} \in \text{SO}(3)$  such that  $R_{\bar{b}} = R_{k, \theta_0} R_b$ , all solutions of the form

$$\begin{aligned} R_w(\theta) &= R_{k, \theta} R_{\bar{b}} \\ &= R_{k, \theta} R_{k, \theta_0} R_b \\ &= R_{k, \theta + \theta_0} R_b \end{aligned} \tag{5.12}$$

are equivalent, because the factor  $R_{k, \theta_0}$  of  $R_{\bar{b}}$  represents nothing but a constant offset of the joint’s “neutral point”. This implies that restrictions must be laid on the choice of the parameter vector  $\mathbf{b}$  in (5.10) for it to be uniquely defined.

From a practical point of view, however, all possible solutions would be equivalent; the only difference between them would be the different offsets on the joint rotation angle  $\theta$  (cf. (5.12)), which will not influence the kinematic workspace of the device if the joint angle is allowed to vary without restriction. Consequently, unless uniqueness of solution is a prerequisite for the success of the method employed to find the optimal parameter vector, no restrictions need to be laid on the choice of  $\mathbf{b}$  in (5.10).

---

<sup>†</sup>. Refers to pronation/supination type devices. Pure flexion/extension and radioulnar deviation excursion is physically restricted by the hand and forearm, in prostheses as in healthy limbs.

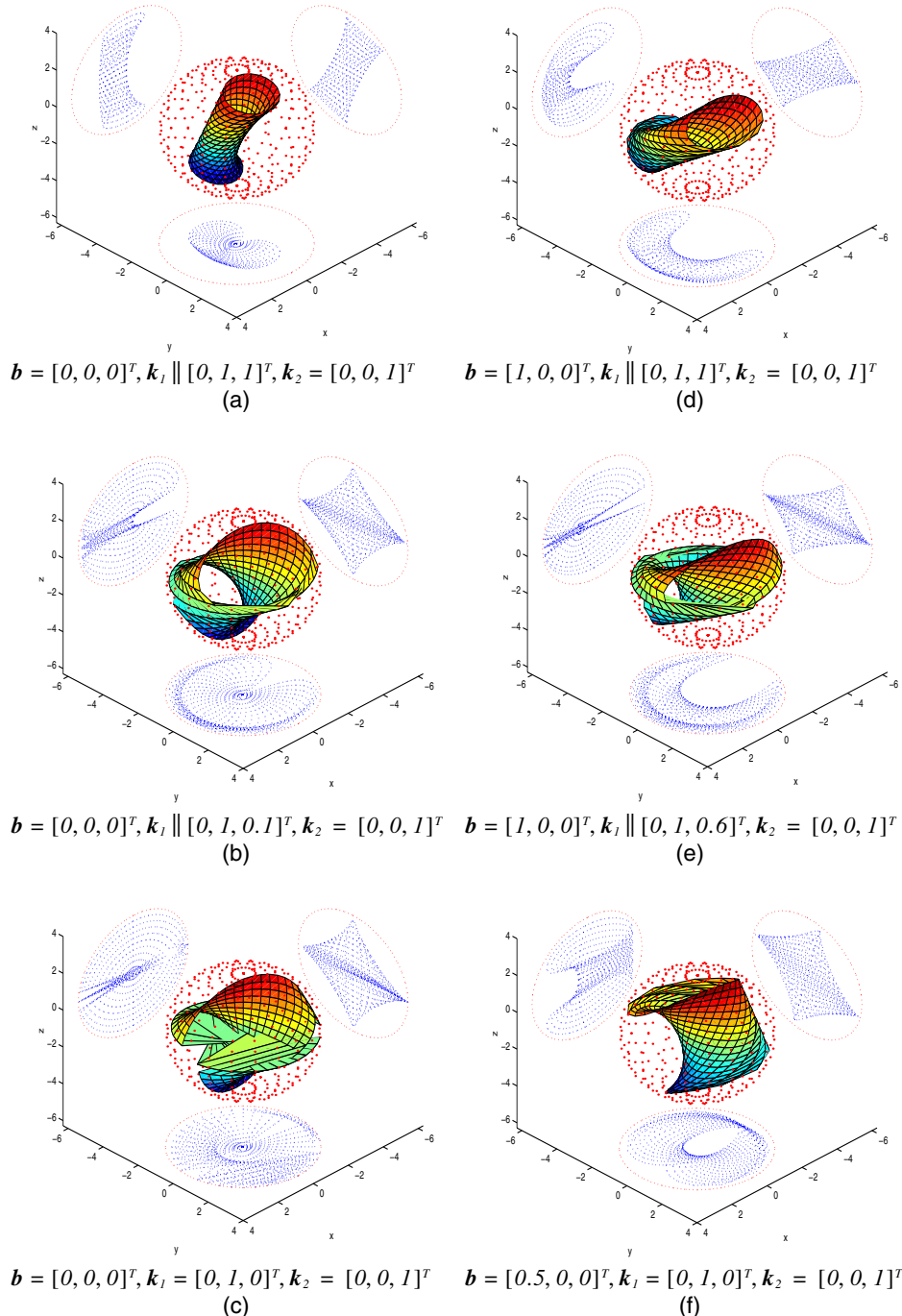


**Figure 5.8:** Actual two-dimensional subspaces of  $\text{SO}(3)$  with different rotation offsets and axes.



## Chapter 6

# Orientation Statistics

The contributions of this chapter are related to geometric interpretations of different approaches to orientation statistics, that is statistics on  $\text{SO}(3)$  or the related parameter spaces discussed in the previous chapter. After a review of prior research relevant to the subject, a few popular approaches are shown to be unsuitable for general application.

An established average operator for finite groups is generalized to cover finite samples on infinite groups. A general and optimal average operator for  $\text{SO}(3)$ , the *cosine average*, is gradually developed from here and thoroughly discussed from a geometric viewpoint. The operator is equivalent to theoretical results previously reported by others. A new concept, the *definity*, is presented as a measure of how far a given data set is from being degenerate and thus not having a definite average orientation. Simulations illustrate the robustness of the cosine average compared to more naive approaches.

A simple measure of the dispersion of rotational data, denoted cosine variance, is also presented. An appendix provides a discussion of possible generalizations and related applications of the results.

*Large portions of this chapter have been accepted for publication  
(Stavdahl et al., 2002).*

### 6.1 Previous Research

#### 6.1.1 Parameterizations Frequently Used in Biomechanics

The choice of representation for body or joint orientations and rotations has occupied the biomechanics society for more than two decades, and several publications have been dedicated to the subject (Chao, 1980, Grood and Suntay, 1983, Andrews, 1984, Woltring, 1994, Wu and Cavanagh, 1995, Sheehan and

Mitiguy, 1999). One popular so-called “joint coordinate system”, often attributed to Chao (1980) and Grood and Suntay (1983), in effect resembles an Euler angles convention. It has been adopted by the biomechanics community to the point where it is recommended by the Standardization Committees of the International Society of Biomechanics (ISB) (Wu and Cavanagh, 1995). This model has been opposed on the basis of singularities and poor metric properties, the latter which can cause the individual Euler angles to be much higher than the total rotation in question (Woltring, 1994). Therefore, averaging of Euler angles is given minor attention in the remainder of this thesis.

To alleviate these metric problems, Andrews (1984) suggested using the Euler parameter representation, while Woltring (1994) proposed to use the closely related orientation vector mentioned in Chapter 5. However, all these as well as the full rotation matrix representation may yield meaningless results if averaged arithmetically. This calls for a different approach to statistics that accounts for the special topology of three-dimensional rotations.

### 6.1.2 Orientation Statistics

In biomechanics, statistics have been applied to rotational data for example in conjunction with movement estimation from noisy marker position data (Woltring et al., 1985, Veldpaus et al., 1988). The reported results apply to differential (small) rotations, justifying certain simplifications that were actively exploited by the respective investigators. Other studies, for example those related to the human wrist, have focused on joint range of motion in the well-known clinical angles. The reported results include averaged extreme values for the clinical angles across a test population (Brumfield et al., 1966, Sarrafian et al., 1977, Ruy et al., 1991), average arcs of motion for each clinical angle (Palmer et al., 1985) and the “centroid” of motion in terms of the average flexion/extension angle and adduction/abduction angle (Youm et al., 1978). Such practice is acceptable when the clinical angles are viewed separately as such. However, pairs or triplets of average angles do not give a representative value for the joint’s overall average orientation; clinical angles resemble the Chao/Grood and Suntay convention (Chao, 1980, Grood and Suntay, 1983), and thus suffer from the metric defects previously mentioned. Use of Euler parameters has been suggested for interpolating orientation data in animation applications (Ariel et al., 2000). Rancourt et al. (2000) applied rotation statistics for the analysis of variations in static postures, but the specific methods used rely on the assumption of closely spaced data. However, there seems to have been little or no tradition in biomechanics and orthopaedics to consider the average of arbitrary sets of three-dimensional orientations.

Krieger Lassen et al. (1994) have concisely reviewed theoretical literature relevant to orientation statistics. Important results are related to the Bingham and the matrix Fisher probability distributions, which are equivalent but related to quaternion vectors and rotation matrices, respectively. Significant contributions

are due to Downs (1972), Prentice (1986), Khatri and Mardia (1977), Bingham et al. (1992) and Wood (1993). Krieger Lassen et al. (1994) applied this theory by estimating average crystal orientation from data obtained in an electron microscope. Others who reported the same application calculated the average orientation as the normalized sum of individual Euler parameter vectors (Humbert et al., 1996, Humphreys et al., 2001). This approach is computationally trivial; however, as will become apparent in the next section, it may lead to absurdities.

## 6.2 The Problem of Averaging Orientations

Let  $\{R_i\}_{i=1}^n$  be a set of rotation matrices. The aim of this section is to define an operator which calculates the single rotation matrix which best represents the whole set, that is the “average rotation” of the set, as well as operators related to the dispersion of the data about this average.

For an average quantity to be justifiable, it must satisfy certain criteria. For example, for trivial data sets it must yield the expected result; the average must be independent of the order of the data elements; and for a given data set it must provide a unique average value or an explanation of why a unique average cannot be found.

### 6.2.1 Arithmetic Attempts and their Shortcomings

Initially we note that taking the pure arithmetic mean of a set of rotation matrices generally does not represent a viable option, because it yields a result which is not a rotation matrix. This is readily illustrated by the following simple example:

$$\frac{1}{2}(R_{z,\pi/2} + R_{z,-\pi/2}) = \frac{1}{2}\left(\begin{bmatrix} 0 & -1 & 0 \\ 1 & 0 & 0 \\ 0 & 0 & 1 \end{bmatrix} + \begin{bmatrix} 0 & 1 & 0 \\ -1 & 0 & 0 \\ 0 & 0 & 1 \end{bmatrix}\right) = \begin{bmatrix} 0 & 0 & 0 \\ 0 & 0 & 0 \\ 0 & 0 & 1 \end{bmatrix} \notin SO(3). \quad (6.1)$$

It will now be shown how two techniques used in the literature, namely the arithmetic average of orientation vectors and normalized arithmetic average of Euler parameter vectors, respectively, may fall short in trivial cases. Without loss of generality we will assume rotations about the  $x$ -axis (i.e.  $k = [1, 0, 0]^T$ ), so that the two representations can be represented completely in the  $(\theta_x, \theta_y)$  and the  $(q_0, q_1)$  planes, respectively. These planes are illustrated in Figure 6.1a and b, respectively. As the angle of rotation  $\theta$  sweeps through the interval  $[0, 2\pi]$  the orientation vector  $\theta$  goes through the path defined by the bold arrows labelled 1, 2 and 3, in that order. The dashed arrow 2 represents the sign shift occurring at  $\theta = \pi$ , i.e. the representation singularity of the orientation vector representation. In contrast, the plain Euler parameter representation has no intrin-

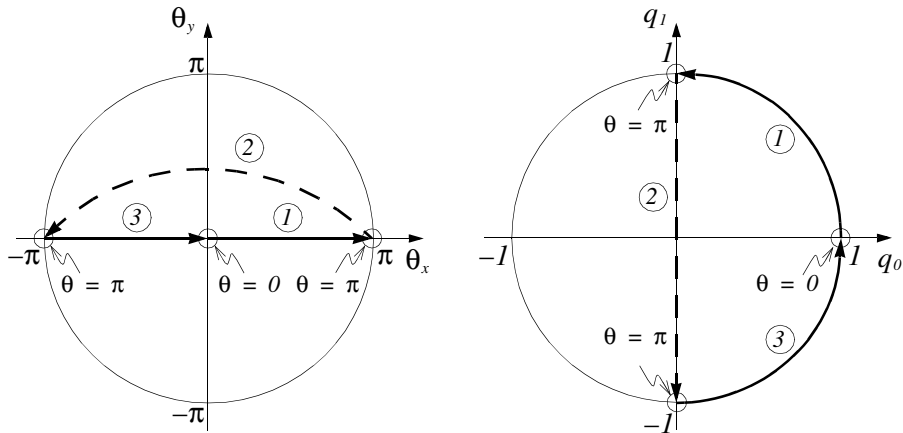


**Figure 6.1:** Sign shifts of the orientation vector and the Euler parameter vector. The figures show the trajectories of the first two elements of the orientation vector (a) and the Euler parameter vector (b), respectively, when the angle of rotation is gradually changed from 0 to  $2\pi$ . Rotations performed about the  $x$ -axis.

sic singularity. When averaging Euler parameters, however, their double representation of  $SO(3)$  introduces a dilemma: which sign should be used for the averaging? A common convention is to choose the sign so that  $q_0 \geq 0$  (Humbert et al., 1998), which is the case in Figure 6.1b where the labelled arrows correspond to those in the left-hand figure. As indicated by arrow 2, the sign convention has introduced a representation singularity very similar to that of the orientation vector.

We now quickly review a trivial case in which the data set contains only two elements corresponding to  $\theta_1 = (\pi - \delta\theta)$  and  $\theta_2 = (\pi + \delta\theta)$ , where  $\delta\theta \ll \pi$  and  $\mathbf{k} = [1, 0, 0]^T$  as before. It is then reasonable to expect the average of the rotations defined by  $(\mathbf{k}, \theta_1)$  and  $(\mathbf{k}, \theta_2)$  to be that corresponding to  $(\mathbf{k}, \pi)$ , that is a rotation through the angle  $\pi$  about the  $x$ -axis. The arithmetic average of the corresponding orientation vectors, however, is the null vector, which implies  $\theta = 0$ , i.e. no rotation at all. Normalizing the average of the corresponding Euler parameter vectors yields  $q_0 = 1$  and  $q_1 = q_2 = q_3 = 0$ , also implying a zero angle of rotation. Data sets similar to that considered here may appear as subsets of larger data sets if the data is dispersed and/or if the reference frame is chosen such that the data appear with angles of rotation in the vicinity of  $\pi$ . The consequence is potential bias of the estimated average. This is a very serious drawback that calls for extreme caution if applying these techniques.

### 6.2.2 The Least Squares Average

Diaconis (1988) briefly suggests the following definition, reproduced here using that author's notation and choice of words:

**Definition 6.1** Let  $P$  be a probability on a finite group  $G$ , and let  $\rho$  be a metric on  $G$ . Define

$$f(s) = \sum_t P(t)(\rho(s, t)) \quad (6.2)$$

where  $s, t \in G$ . The group element  $\eta$  is then said to be a  $\rho$ -median of  $P$  if  $\eta$  minimizes  $f(s)$ . The number  $f(\eta)$  is called the  $\rho$ -spread of  $P$ . Substitution of  $\rho^2$  for  $\rho$  in the formula for  $f(s)$  yields a  $\rho$ -mean.

□

Definition 6.1 can be generalized to cover finite samples (subsets) of any (finite or infinite) group that is a metric space, which is the case for  $\text{SO}(3)$ . Set  $G = \{R_i\}_{i=1}^n$ ,  $R_i \in \text{SO}(3)$ , and let the sum in (6.2) be taken over all elements of  $G$ . Now  $P(t) = 1/n$ . Finally, if the metric  $\angle(R_i, \bar{R})$  of (5.4) is substituted for  $\rho(s, t)$ , the *mean* variant of (6.2) gives rise to the following definition:

### Definition 6.2 Least Squares Average

Given a set  $\{R_i\}_{i=1}^n$ ,  $R_i \in \text{SO}(3)$ , the least squares average of  $\{R_i\}$  is denoted  $\bar{R}_{LS}$  and defined as

$$\begin{aligned} \bar{R}_{LS}\{R_i\} &\stackrel{\Delta}{=} \arg(\min_{\bar{R} \in \text{SO}(3)} J_{LS}(\bar{R}; \{R_i\})) \\ J_{LS}(\bar{R}; \{R_i\}) &\stackrel{\Delta}{=} \frac{1}{n} \sum_{i=1}^n \angle(R_i, \bar{R})^2 \end{aligned} \quad (6.3)$$

where  $\arg(\min_{\bar{R}} J_{LS}(\bar{R}))$  yields the argument  $\bar{R}$  that minimizes  $J_{LS}$  rather than the minimum of  $J_{LS}$  itself.

□

### Existence and Uniqueness of the Least Squares Average

The function  $J_{LS}(\bar{R}; \{R_i\})$  in (6.3) is a continuous function on a closed, bounded set, and thus must have at least one minimum.

The uniqueness of this minimum, however, depends highly on the sample  $\{R_i\}$ . This can be conceptually explained by means of a one-dimensional example. The upper left pane of Figure 6.2b depicts two individual functions of the form  $f_i(\theta) = ((\theta - \theta_i) \bmod 2\pi)^2$ ,  $i = 1, 2$  for arbitrary but constant offsets  $\theta_i$ , where *bmod* is the *modulo* operator. The following observations are noted:

1. Each function  $f_i(\theta)$  resembles a parabola in the interval  $\langle \theta_i - \pi, \theta_i + \pi \rangle$  with its global minimum at  $\theta = \theta_i$ .

2. Each function exhibits a maximum at the point where  
 $(\theta - \theta_i) \bmod 2\pi = \pi$ , at which point its first derivative is discontinuous.

As shown in the lower left pane of Figure 6.2b, the sum of these functions has two minima. Moreover, the first derivative of the summed functions is discontinuous at the same points as that of the individual functions.

Applying similar arguments to Equation (6.3), the following holds:

1. The  $i$ 'th of the summed elements of (6.3) defines a mapping  
 $\angle(R_i, \bar{R})^2 : \text{SO}(3) \rightarrow \mathbb{R}$  which resembles a hyperparaboloid (at least in the neighbourhood of  $R_i$ ) parameterized by means of  $\bar{R}$ . This hypersurface exhibits a global minimum at  $\bar{R} = R_i$ .
2. The same function takes on its maximum value at all locations where  
 $\angle(R_i, \bar{R}) = \pi$ . At these locations the first derivative of  $\angle(R_i, \bar{R})^2$  with respect to  $\bar{R}$  is discontinuous.

If we also introduce the  $j$ 'th element of (6.3), this element defines a hypersurface identical to that of the  $i$ 'th element, but with its global minimum displaced a certain distance  $\angle(R_i, R_j)$  away from that of the other. When superimposing one of these surfaces onto the other, the uniqueness of the minimum is generally lost. Generalization to summation of  $n$  functions is straightforward. The picture is further complicated by the projective properties of  $\text{SO}(3)$ , which causes the hyperparaboloid-like surfaces to be warped together in a way impossible to visualize. The discontinuity of the first derivative, the likely existence of local minima and the complexity of the surface definition itself effectively eliminates analytic solutions and even the use of traditional numeric optimization techniques.

### 6.2.3 A Class of Average Operators for Samples on Groups

It is now proposed to further generalize Definition 6.2 to a class of average operators for samples on groups as follows:

**Definition 6.3 Sample Average on a Group** Let  $\Gamma = \{\gamma_i\}_{i=1}^n$  be a discrete sample on (i.e. a finite subset of) a group  $G$ , and let  $\rho$  be a metric on  $G$ . Furthermore, let  $h$  be a lower bounded scalar function which is monotonously increasing throughout the range of  $\rho$ . Define

$$J(s; \Gamma) = \sum_{i=1}^n P(\gamma_i) h(\rho(s, \gamma_i)) \quad (6.4)$$

where  $s \in G$ . The group element  $\eta$  is then said to be a candidate sample average of  $\Gamma$  if  $\eta$  minimizes  $J(s; \Gamma)$ .  $\square$

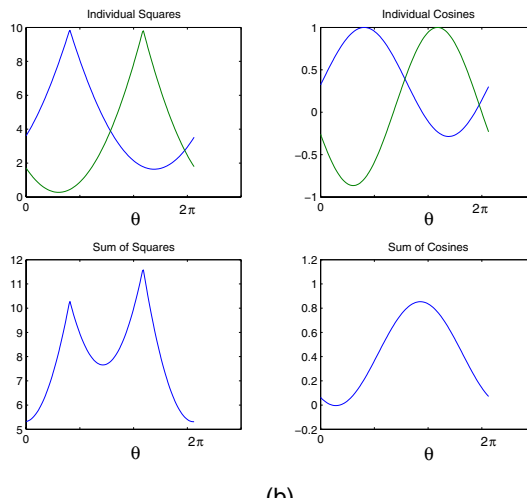
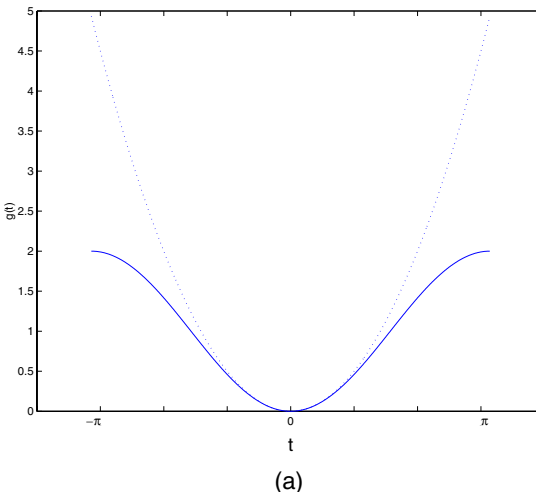


**Figure 6.2:** Comparison between the square and the cosine function. Figure a shows  $g(t) = I - \cos t$  (solid line) and  $g(t) = t^2/2$  (dotted).

Figure b illustrates the possibility for multiple minima when a number of square functions (upper left) are added (lower left); when the corresponding cosines (upper right) are summed, the result is another cosine (lower right) which displays a unique minimum in the “circular” domain  $[0, 2\pi]$ .

The figures are made by first randomly picking  $R_1 \in \text{SO}(3)$ , then generating a one-dimensional subspace  $\Pi \subset \text{SO}(3)$  parameterized by a rotation angle  $\theta$  (the free variable) and a random but fixed unit vector  $k$ . For each  $\theta$  in the interval  $[0, 2\pi]$ , the squares and the cosines, respectively, of the angular distance  $\angle(R(\theta; k), R_1)$  are calculated and plotted in the upper figures. The procedure is then repeated for a second randomly picked  $R_2 \in \text{SO}(3)$ , giving rise to the two graphs in each figure. The lower figures show the sums of the pairs of graphs above.

**Remark 6.1** The existence of a minimum for  $J$  is guaranteed by Definition 6.3; however, uniqueness of this minimum is not; it depends on the metric properties of the group in question, the distribution of the sample and the choice of  $h$ . Hence the use of the term candidate sample average.

□

**Remark 6.2** Definition 6.3 yields a candidate sample average which is an element of the group  $G$ , but which is not necessarily an element of the sample  $\Gamma$ . This is consistent with the definition of arithmetic average of samples on  $\mathbb{R}^n$ .

□

**Remark 6.3** Definition 6.3 is extremely general. As should be expected, and as already illustrated in section 6.2.2 with  $h(\cdot) = (\cdot)^2$ , the qualitative and quantitative properties of the resulting average operator depends highly on the choice of the function  $h$ , which thus should be carefully selected and verified in each case. A proof of the relevance and appropriateness of Definition 6.3 for subsets of groups in general is beyond the scope of this thesis.

□

### 6.3 The Cosine Average

In this section Definition 6.3 is instantiated in the form of an operator tailored specifically for samples on  $\text{SO}(3)$ . Figure 6.2a depicts a cosine and a parabola with identical shape in the neighbourhood of their common minimum ( $t = 0$ ). The major difference between the two functions (and the one most important in the present context) is that while the parabola takes off into a steep slope at  $|t| = \pi$ , the cosine function levels off and has a zero derivative at these points.

This feature makes the cosine an interesting candidate for the  $h$  function in (6.4), potentially eliminating many complications associated with the square function. The equation  $h(\rho(R_i, \bar{R})) = 1 - \cos(\angle(R_i, \bar{R}))$  is now selected, which gives rise to the following definition:

#### Definition 6.4 Cosine Average

Given a general sample  $\{R_i\}_{i=1}^n$ ,  $R_i \in \text{SO}(3)$ , the cosine average (CA) of  $\{R_i\}$  is denoted  $\bar{R}_{\text{cos}}$  and defined as

$$\begin{aligned}\bar{R}_{\text{cos}}\{R_i\} &\stackrel{\Delta}{=} \arg(\min_{\bar{R} \in \text{SO}(3)} J_{\text{cos}}(\bar{R}; \{R_i\})) \\ J_{\text{cos}}(\bar{R}; \{R_i\}) &\stackrel{\Delta}{=} \frac{1}{n} \sum_{i=1}^n (1 - \cos(\angle(R_i, \bar{R})))\end{aligned}\tag{6.5}$$

whenever the solution is unique; if not, the cosine average is indefinite.

□

Equation (6.5) can be simplified by substituting (5.4), which yields

$$\begin{aligned} R_{\cos}\{R_i\} &= \arg(\max_{\bar{R} \in SO(3)} J_{tr}(R; \{R_i\})) \\ J_{tr}(\bar{R}; \{R_i\}) &\stackrel{\Delta}{=} \sum_{i=1}^n \text{tr}(R_i \bar{R}^T) \\ &= \text{tr}(R_\Sigma \bar{R}^T) \end{aligned} \quad (6.6)$$

where  $R_\Sigma$  is the sum of all the elements of  $\{R_i\}$  (cf. (6.33)) (note the change from  $\min$  in (6.5) to  $\max$  in (6.6)). This is exactly the maximum likelihood estimate of the mean orientation of a matrix Fisher distribution (Downs, 1972). It follows from Krieger Lassen et al. (1994) and Stephens (1979) that if  $\mathbf{r}_{ij}^T$  and  $\tilde{\mathbf{r}}_j^T$  are the  $j$ 'th row of  $R_i$  and  $\bar{R}$ , respectively, we have

$$\sum_{i=1}^n \sum_{j=1}^3 |\mathbf{r}_{ij} - \tilde{\mathbf{r}}_j|^2 = 6n - 2\text{tr}(R_\Sigma \bar{R}^T) \quad (6.7)$$

Thus, the CA can also be regarded as the least squares projection of  $R_\Sigma$  on  $SO(3)$ .

### 6.3.1 Geometric Interpretation

Recall from (6.6) that the CA is found by maximizing the functional

$$J'_{\cos}(\bar{R}; R_\Sigma) = \text{tr}(R_\Sigma \bar{R}^T) \quad (6.8)$$

with respect to  $\bar{R}$ . If we define

$$R_i \stackrel{\Delta}{=} \begin{bmatrix} \mathbf{r}_{i1}^T \\ \mathbf{r}_{i2}^T \\ \mathbf{r}_{i3}^T \end{bmatrix} \quad \bar{R} \stackrel{\Delta}{=} \begin{bmatrix} \tilde{\mathbf{r}}_1^T \\ \tilde{\mathbf{r}}_2^T \\ \tilde{\mathbf{r}}_3^T \end{bmatrix}, \quad (6.9)$$

Equation (6.8) can be written as the sum of the scalar products of the corresponding rows of  $R_\Sigma$  and  $\bar{R}$  as follows:

$$\text{tr}(R_\Sigma \bar{R}^T) = \sum_{i=1}^n (\mathbf{r}_{i1} \cdot \tilde{\mathbf{r}}_1 + \mathbf{r}_{i2} \cdot \tilde{\mathbf{r}}_2 + \mathbf{r}_{i3} \cdot \tilde{\mathbf{r}}_3). \quad (6.10)$$

As mentioned in Section 5.3, the rows of a rotation matrix are unit vectors defining the coordinate axes of the frame whose orientation is represented by the matrix; hence any rotation matrix can be said to be the matrix representation of a

coordinate frame's orientation. The trace in (6.6) thus is the sum of all the direction cosines (of the coordinate axes) of all the frames represented by the sample  $\{R_i\}$  with respect to (the corresponding axes of) the frame represented by  $\bar{R}$ . In plain and informal language, the CA represents the coordinate frame which axes point "as much as possible" in the same directions as those of the sample  $\{R_i\}$ . Figure 6.3 illustrates the vectors of (6.9) and the geometric interpretation of the scalar products of (6.10).

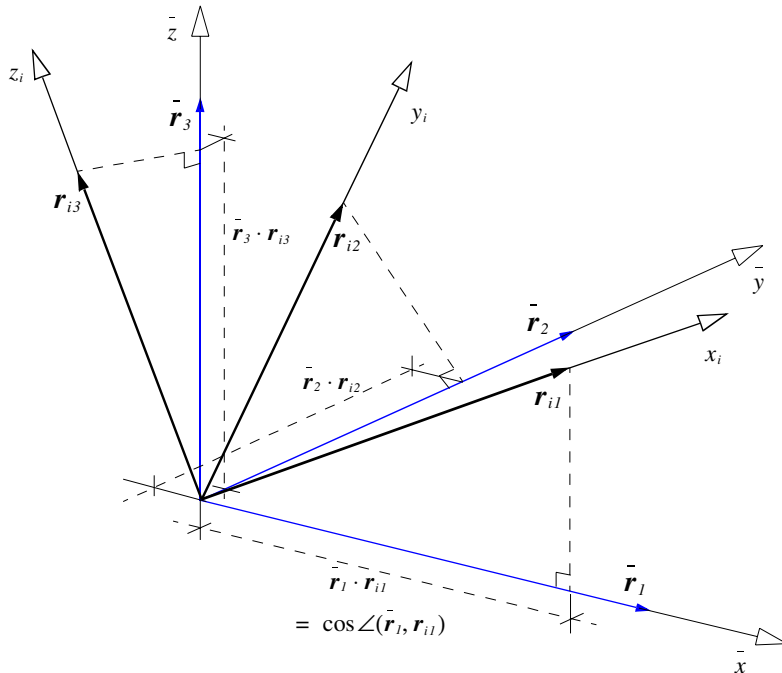


**Figure 6.3:** Geometric interpretation of the cosine average. Since all vectors in question have unit length, the scalar product reduces to a "direction cosine": the length of the projection of one vector onto the other. The cosine average is the orthogonal vector triple  $\bar{R} = [\bar{r}_1 \bar{r}_2 \bar{r}_3]^T \in \text{SO}(3)$  that maximizes the sum of all these projections for a given sample  $\{R_i\}_{i=1}^n, R_i \in \text{SO}(3)$ .

### 6.3.2 Existence

The function  $J_{cos}(\bar{R}; \{R_i\})$  in (6.5) is a continuous function on a closed, bounded set, and thus must have at least one minimum.

### 6.3.3 Uniqueness Properties

For a theoretical treatment of this problem the reader is directed to the original publications (Downs, 1972, Prentice, 1986, Khatri and Mardia, 1977, Stephens, 1979). This and the following section are built on these publications, but give a thorough geometric interpretation and a less stringent presentation of their results.

For the discussion to follow we recall that we can always apply a singular value decomposition to  $R_\Sigma$ , yielding

$$R_\Sigma = USV^T \quad (6.11)$$

where  $U$  and  $V$  are orthogonal (but not necessarily rotation) matrices, and  $S = \text{diag}(\sigma_1, \sigma_2, \sigma_3)$ , where  $\sigma_1 \geq \sigma_2 \geq \sigma_3 \geq 0$  are the singular values of  $R_\Sigma$ . We can then write

$$\text{tr}(R_\Sigma \bar{R}^T) = \text{tr}(S \tilde{R}^T) \quad (6.12)$$

with  $\tilde{R}^T = V^T \bar{R}^T U$ . Now let

$$\begin{aligned} S &= \text{diag}(\sigma_1, \sigma_2, \sigma_3) \stackrel{\Delta}{=} [\sigma_1 \ \sigma_2 \ \sigma_3]^T \\ \tilde{R} &\stackrel{\Delta}{=} [\tilde{r}_1 \ \tilde{r}_2 \ \tilde{r}_3]^T \end{aligned} \quad (6.13)$$

Here, the rows  $\{\sigma_j^T\}$  of  $S$  are orthogonal since  $S$  is diagonal, and so are the rows  $\{\tilde{r}_j^T\}$  of  $\tilde{R}$  because this is an orthogonal matrix. Consequently, without loss of generality the CA problem can be discussed in terms of fitting one orthogonal vector triplet (the rows of  $\tilde{R}$ ) to another (namely the rows of  $S$ ).

We will now discuss the different uniqueness modes one at a time:

1.  $\text{rank}(S) = 3$  and  $\det(R_\Sigma) > 0$ :  $\tilde{R}$  resembles a right-handed orthonormal coordinate frame. In this case the CA is uniquely defined; the rows of  $\tilde{R}$  are parallel to and point in the same directions as those of  $S$  (Figure 6.4a).
2.  $\text{rank}(S) = 2$ : The information contained in the sample  $\{R_i\}$  is related to two coordinate axes only, while the information pertaining to the third axis is cancelled out (Figure 6.4b). The CA is uniquely defined; the first two vectors of  $\tilde{R}$  are parallel to and point in the same directions as the corresponding vectors of  $S$ , while the third is determined by the right-hand rule.

3.  $\text{rank}(S) = 1$ : In this case only the first vector  $\tilde{\mathbf{r}}_1$  of  $\tilde{R}$  is determined by the data. The remaining vectors are restricted to forming an orthonormal right-handed triplet with  $\tilde{\mathbf{r}}_1$ , but their orientation in the plane normal to  $\sigma_1$  is undetermined (Figure 6.4c). Consequently there are infinitely many solutions, so the CA is indefinite.
4.  $\text{rank}(S) = 0$ : This is the totally degenerate case. The data set is distributed in  $\text{SO}(3)$  in such a way that all elements of  $R_\Sigma$  (and those of  $\tilde{R}$ ) are zero, and consequently any rotation matrix is equally representative for the data set; the CA is indefinite.
5.  $\text{rank}(S) = 3$  and  $\det(R_\Sigma) < 0$ :  $R_\Sigma$ , and thus  $\tilde{R}$ , resembles a left-handed (though generally not orthonormal) coordinate frame. In this case the uniqueness can be derived from the two smallest singular values of  $R_\Sigma$  as follows:
- $\sigma_2 \neq \sigma_3$ : The vector  $\sigma_3$  corresponding to the singular value  $\sigma_3$  is distinctly shorter than the other two. To obtain a right-handed case, we change the sign of  $\tilde{\mathbf{r}}_3$ , which corresponds to the shorter vector  $\sigma_3$ , before calculating the solution (Stephens, 1979). Figure 6.4d illustrates the geometry of this case. Once the sign is changed the problem becomes equivalent to that of case 1 above, and it can be easily shown that the solution found in this manner is indeed that which maximizes the expression in Equation (6.12).
  - $\sigma_2 = \sigma_3$ : This situation is illustrated in Figure 6.4e. The dominant axis  $\sigma_1$  of the data set is associated with the larger singular value  $\sigma_1$ , thus  $\tilde{\mathbf{r}}_1$  is aligned with it. The remaining two axes of  $S$  are of equal length. The geometry of this case ensures that we will always have  $\tilde{\mathbf{r}}_2^T \sigma_2 + \tilde{\mathbf{r}}_3^T \sigma_3 = 0$  (i.e. the second and third diagonal elements will not contribute to the value of the expression in Equation (6.12)), so the attitude of the last two vectors of  $\tilde{R}$  in the plane normal to the dominant axis is undetermined. Consequently there are infinitely many solutions corresponding to the infinite number of possible values of the angle  $\alpha$  in Figure 6.4e, so the CA is indefinite.

### 6.3.4 Calculation Formulae

From the preceding discussion we can derive a simple formula for calculating the CA. Since  $S$  is diagonal with nonnegative elements, then if  $\det(R_\Sigma) > 0$ , (and thus  $\det(\tilde{R}) > 0$ ), the trace in Equation (6.12) is maximized when  $R = I$ . This immediately yields

$$\bar{R}_{\cos}\{R_i\} = UV^T \quad (6.14)$$

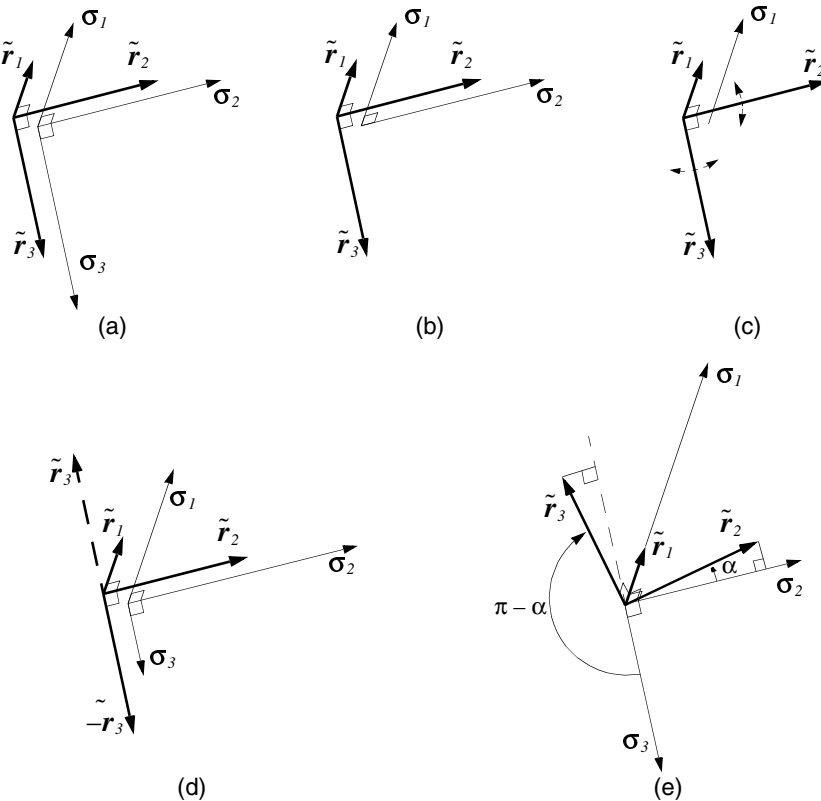


**Figure 6.4:** Uniqueness modes of the cosine average: geometric interpretations.

where  $V$  and  $U$  are as in (6.11). Equation (6.14) also yields the correct result when  $\text{rank}(S) = 2$ .

If  $\det(R_\Sigma) < 0$  and  $\sigma_2 \neq \sigma_3$ , the previously mentioned sign shift must be carried out. This can be accomplished by setting  $R_\Sigma^- = USJV^T$  where  $J = \text{diag}(1, 1, -1)$  and  $S, U$  and  $V$  are as before, and then calculating the CA from  $R_\Sigma^-$  instead of  $R_\Sigma$ . This yields

$$\bar{R}_{\cos}\{R_i\} = UJV^T. \quad (6.15)$$

### 6.3.5 Definity

Whenever the CA is not uniquely defined (i.e. it is indefinite), this is so because the data set exhibits perfect rotational symmetry. Obviously the data can be arbitrarily close to being rotationally symmetric without actually being so. When using the CA for analysing for example biomechanical data, we need a measure

of how far the CA is from being indefinite in order to correctly interpret the results. A simple measure is proposed, the *definity*, which is denoted by the symbol *Def* and which can be calculated as

$$\text{Def}(\mathbf{R}_n) \stackrel{\Delta}{=} \begin{cases} \frac{\sigma_2 + \text{sgn} \det(R_\Sigma) \sigma_3}{2\sigma_1}, & \sigma_1 \neq 0 \\ 0, & \sigma_1 = 0 \end{cases} \quad (6.16)$$

where  $\mathbf{R}_n = \{R_i\}_{i=1}^n$ ,  $R_\Sigma = \sum_{i=1}^n R_i$  and  $\sigma_i$  is the  $i$ 'th singular value of  $R_\Sigma$ . As can be readily verified, the definity takes on the value 1 if all elements  $R_i$  of the data set are identical (i.e. the most definite case possible), and becomes zero whenever the CA is indefinite; in all intermediate cases the definity takes on intermediate values.

It should be noted that even if the definity of  $\mathbf{R}_n$  with respect to the CA is close to or equal to zero, this does not indicate that  $\mathbf{R}_n$  is homogeneously distributed on  $\text{SO}(3)$ ; it may still exhibit a predominant axis of rotation. A homogenous distribution of  $\mathbf{R}_n$  would result in all singular values of  $R_\Sigma$  being zero.

In a practical setting in which  $\mathbf{R}_n$  is the result of real-world processes, including measurement errors and round-off errors, the situation  $\text{Def}(\mathbf{R}_n) = 0$  is not likely to occur. Thus, depending on the accuracy of the data, a tolerance  $\tau > 0$  should be established in each case, and the data set should be interpreted as being indefinite with respect to the CA if  $\text{Def}(\mathbf{R}_n) < \tau$ .

### 6.3.6 $\text{SO}(3)$ is Distributive over the Cosine Average Operation

The following property, which is typically associated with linear operators, also holds the CA:

**Theorem 6.1** Let  $Q, R_i \in \text{SO}(3)$ . Then,

$$\bar{R}_{\cos}\{QR_i\} = Q\bar{R}_{\cos}\{R_i\} \quad (6.17)$$

□

**Proof:** Substitution of Equation (6.6) and exploiting that the trace of a product of square matrices is independent of the order of the multiplication, yields

$$\begin{aligned} \bar{R}_{\cos}\{QR_i\} &= \arg(\max_{\bar{R} \in \text{SO}(3)} \text{tr}(\bar{R}^T QR_\Sigma)) \\ &= \arg(\max_{\bar{R} \in \text{SO}(3)} \text{tr}((Q^T \bar{R})^T R_\Sigma)) \end{aligned} \quad (6.18)$$

We substitute  $\bar{R} = Q\tilde{R}$  to get

$$\begin{aligned}\arg(\max_{(Q\tilde{R}) \in SO(3)} \text{tr}((Q^T Q \tilde{R})^T R_\Sigma)) &= Q \arg(\max_{\tilde{R} \in SO(3)} \text{tr}(\tilde{R}^T R_\Sigma)) \\ &= Q \bar{R}_{\cos}\{R_i\}\end{aligned}\quad (6.19)$$

□

The following immediate implication of Theorem 6.1 perhaps is the most desirable of all the CA operator's properties:

**Corollary 6.1.1** *For any given set of three-dimensional rotational data, the rotation or orientation implied by the cosine average is independent of the choice of reference coordinate frame for the data.*

□

## 6.4 Comparative Assessment of Cosine Average Performance

### 6.4.1 Application to Simulated Data

In this section we compare the CA with the values obtained by averaging the parameters of several different representations, namely Euler parameter (quaternion) vectors, Euler angle triples and orientation vectors. We also include separate averaging of angle and axis of rotation, the latter in the form of unit vectors  $k_i$ . For the Euler parameters we choose the sign so that the first element  $q_0$  of each vector is nonnegative. Also, the arithmetic mean of the Euler parameter vectors and that of the axis of rotation vectors are normalized to obtain results in the valid ranges.

We somewhat arbitrarily use the Euler angles  $\psi$ ,  $\theta$  and  $\phi$ , taken about the reference  $x$ -,  $y$ - and  $z$ -axis, respectively. The angles are calculated such that  $\phi \in [-\pi, \pi]$ ,  $\theta \in [-\pi/2, \pi/2]$  and  $\psi \in [-\pi, \pi]$ .

We will calculate the average of the set  $\{R_i\}_{i=1}^n$  with

$$R_i = R_{k, \alpha_i} R_o \stackrel{\Delta}{=} R_{k_i, \beta_i} \quad (6.20)$$

where the axis of rotation  $k$  and the “rotational offset”  $R_o$  are fixed, while  $\alpha$  takes on values in the interval  $[0, 2\pi]$ . This model spans a one-dimensional subspace of  $SO(3)$ . We let  $\alpha_i \sim N(\mu, \sigma^2)$  with given fixed expectation and variance. Intuitively we then expect that

$$\lim_{n \rightarrow \infty} \bar{R} = R_{k, \mu} R_0 \stackrel{\Delta}{=} R_{k_{exp}, \beta_{exp}}. \quad (6.21)$$

Several data sets were generated and the average orientation estimated using the different techniques. The parameter values chosen were:  $k = [1, 2, -5]/\sqrt{30}$ ,  $R_0 = R_{k_0, \theta_0}$  with  $k_0 = [1, 1, 1]/\sqrt{3}$ ,  $\theta_0 = 60^\circ$  and  $\mu = 70^\circ$ . The angular difference between the estimated average orientations and the expected value  $R_{k_{exp}, \beta_{exp}}$ , in other words the estimation error, was recorded for different values of the standard deviation  $\sigma$  and different sample sizes  $n$ . Figure 6.5 shows the average estimation error resulting from 50 different data sets with  $\sigma = 25^\circ$  (a) and  $\sigma = 60^\circ$  (b).

To obtain a conservative result with respect to the qualities of the CA,  $360^\circ$  was added to or subtracted from  $\psi_i$  for certain values of  $\theta$  to make  $\psi(\theta)$  a smooth function. Similar techniques were applied to the axis/angle and the orientation vector data prior to averaging.

In the figure legends “CosAv” denotes the cosine average, “Quat.” denotes quaternion (Euler parameter) averaging, “Orient” denotes orientation vector averaging, “k-Angle” denotes separate axis and angle averaging and “Euler” denotes Euler angle averaging.

In the present example the CA and the Euler parameter based estimates were virtually indistinguishable in quality for  $\sigma = 25^\circ$  (less than 1.5% difference, Figure 6.5a), while the CA was superior when the angular spread of the data was increased to  $60^\circ$  (Figure 6.5b). Of the other estimators, only the average orientation vector was comparable to the former two, and only when the spreading of the data was kept low. Furthermore, the CA converges towards the expected value as the data sets become larger, even as the data spreading is increased; this is not the case for any of the other estimators tested. The estimates based on average Euler angles display inferior performance in all scenarios investigated and is useless for most practical purposes.

#### 6.4.2 A Real-World Case

To illustrate the relevance and applicability of the cosine statistics they were applied to authentic data from an experiment involving eight right-handed healthy subjects. Full details about this experiment are given in Chapter 4; here, only a short description is given.

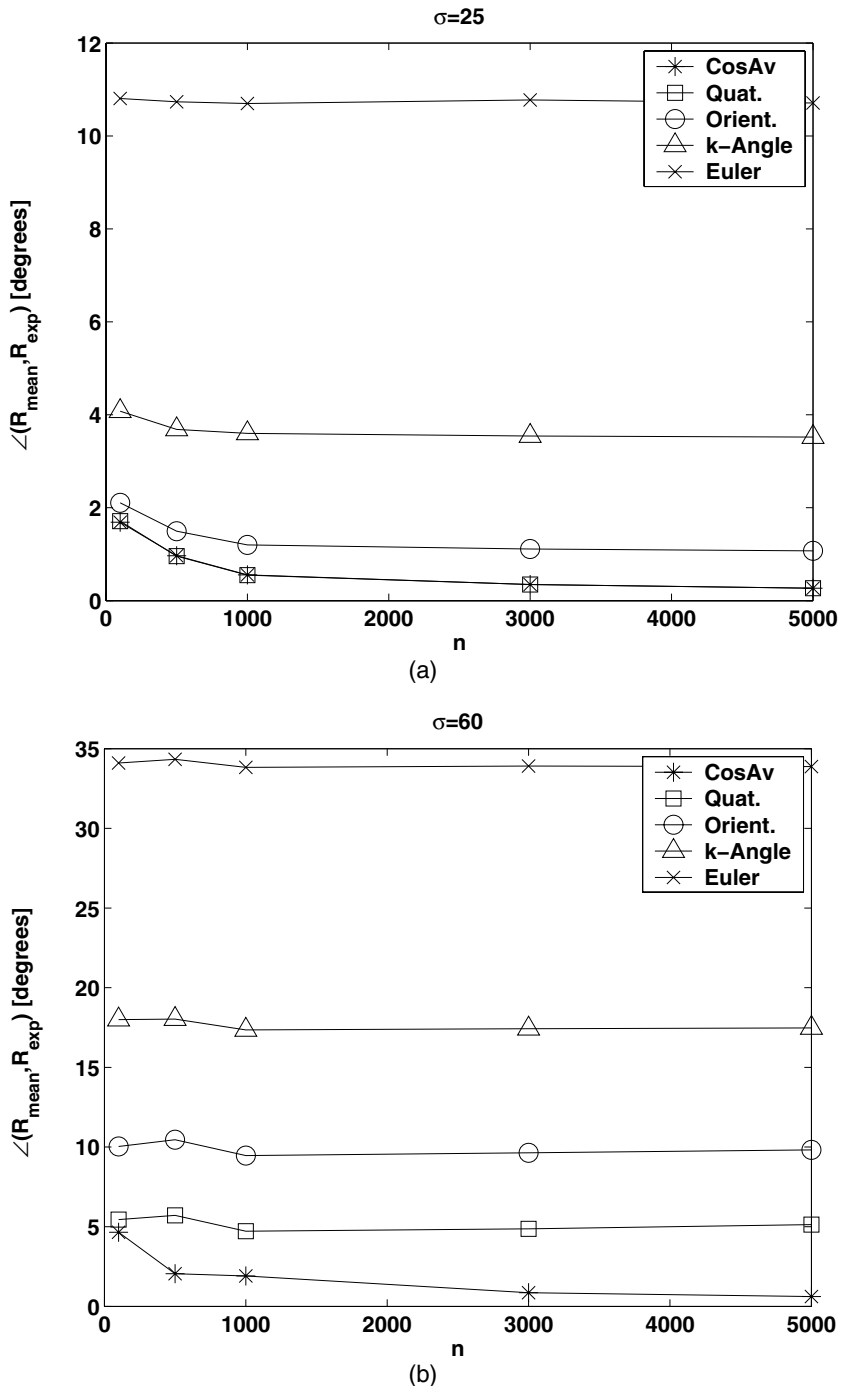


**Figure 6.5:** Comparison of different average operations. Estimation error with different sample sizes  $n$  (horizontal axes) for  $\sigma = 25^\circ$  (a) and  $\sigma = 60^\circ$  (b).

### **Experimental Set-Up**

A custom-made plaster of Paris gauntlet was firmly applied to the left hand and a socket made of the same material was applied to the left proximal forearm of each subject, and the four fingers were taped together to form a single unit. The purpose of these structures was to restrict the forearm, wrist and hand movements to those obtainable with a typical prosthetic terminal device.

Four body-fixed coordinate frames were defined as indicated in Figure 6.6: a proximal frame  $S_u$  fixed to the ulna, and three hand-fixed frames  $S_h$ ,  $S_{h'}$  and  $S_w$ , the latter which was parallel to the  $S_u$  frame when the limb was in the calibration posture of Figure 6.6. A motion capture system was employed to record the orientation of each socket during the performance of 15 predefined ADL. Subsequently the data were transformed to yield the hand fixed frames' orientations with respect to  $S_u$ .

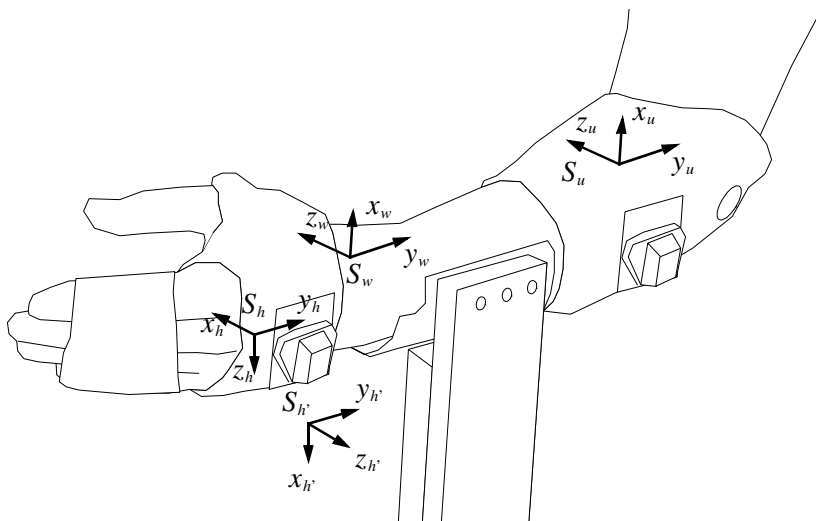


**Figure 6.6:** Forearm and hand: instrumentation and coordinate frame definitions.

The average wrist orientation was estimated by using the CA operator, by averaging individual Euler angles, by averaging orientation vectors and finally by means of the normalized average Euler parameter vector. The calculations were carried out twice, first by letting  $S_h$  represent the hand orientation and then by choosing  $S_h$  as the hand-fixed frame, to investigate the respective techniques' robustness with respect to this kind of choice. The results were all changed into rotation matrix form and transformed to express the orientation of the  $S_w$  frame with respect to  $S_u$ , a representation where all the clinical angles are zero when the overall angle of rotation is zero (i.e. in the calibration posture of Figure 6.6).

### Results

Table 6.1 displays two sets of data separated by slash symbols: quantities based on choosing  $S_h$  as the hand-fixed frame to the left, those obtained when choosing  $S_{h'}$  as the hand-fixed frame to the right of the separators.

**Table 6.1:** Average orientation estimates: Deviation from the CA and implied clinical angles. Calculations performed for two different hand reference coordinate frames, the results of which are separated by slash symbols in the table;  $S_h$  to the left and  $S_{h'}$  to the right of the separators (cf. Figure 6.6). All quantities in  $^\circ$ .

	Deviation from CA	Pronation	Extension	Ulnar deviation
Cosine average	—	3.3	7.3	4.9
Euler parameters	0.3 / 159	3.1 / 165	7.2 / 17.6	4.9 / 17.6
Orientation vectors	2.1 / 172	1.3 / 176	7.4 / 5.0	4.2 / 6.1
Euler angles	104 / 147	-24.5 / 132	-23.9 / -27	-88.6 / 64

The leftmost numeric column of Table 6.1 shows the angular deviation of the other average estimates from the CA. The results based on  $S_h$  as the hand-fixed frame are in general agreement with the simulation results in that the Euler parameter- and orientation vector-based estimates only deviates moderately from the CA while the Euler angle-based quantities show little agreement with the other. The orientation of  $S_{h'}$  was deliberately chosen with an approximate geodesic distance of  $\pi$  radians from  $S_u$  in the posture of Figure 6.6. This causes the Euler parameter vector representation and the orientation vector representation of the data set to frequently exhibit the sign shifts depicted in Figure 6.1 during movement. The results clearly illustrate the serious consequences of this discontinuity: the Euler parameter-based average estimate in this case deviates from the CA by as much as  $159^\circ$  and the corresponding pronation angle is  $165^\circ$ , which is in fact outside the pronation range of a healthy wrist. Figure 6.7b depicts this non-physical posture, whilst the posture in Figure 6.7a corresponds to the CA. The dashed line labelled  $Z_u$  indicates the axis of rotation of the humeroulnar joint (elbow flexion/extension) with the label on the medial side.

As implied by Corollary 6.1.1, the CA yielded exactly the same result before and after the change of the hand-fixed reference frame.

## 6.5 Variance and Standard Deviation of Orientations

In basic statistics, the average  $\bar{y}$ , the variance  $s^2$  and the standard deviation  $s$  of a sample  $Y = \{y_i\}_{i=1}^n$  are closely related by the following relations:

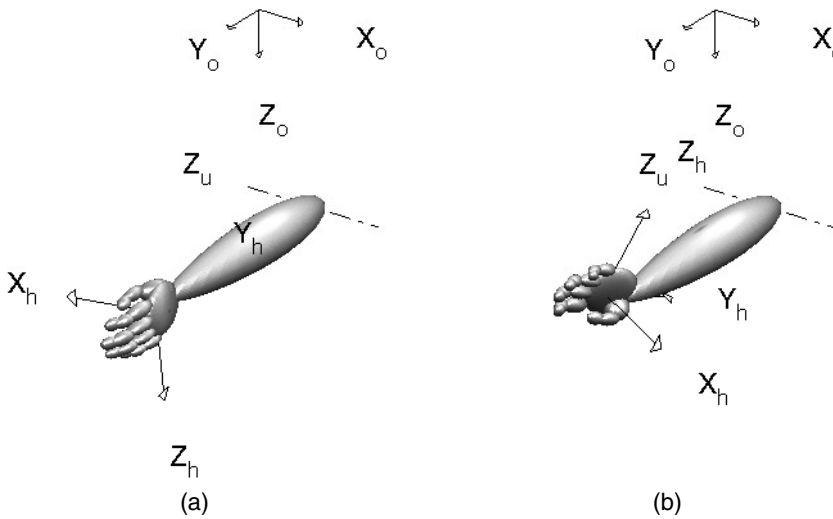


**Figure 6.7:** Comparison of average wrist orientation calculated using two different methods. Cosine average (a) and estimate based on Euler parameters and hand orientation represented by  $S_h$  (b).

$$\begin{aligned}\bar{y} &= \arg \left( \min_{\bar{y}} \left( \sum_{i=1}^n (y_i - \bar{y})^2 \right) \right) \\ &= \frac{1}{n} \sum_{i=1}^n y_i\end{aligned}\quad (6.22)$$

$$\begin{aligned}s^2 &= \frac{\sum_{i=1}^n (y_i - \bar{y})^2}{n-1} . \\ s &= +\sqrt{s^2}\end{aligned}\quad (6.23)$$

Note that the average is chosen so that the variance, which is defined by means of the former, is minimized.

When developing statistics for samples on  $\text{SO}(3)$  these or similar relations should be sought preserved. If we substitute  $\angle(R, \bar{R})$  for  $(y_i - \bar{y})$  in (6.22) it becomes the definition of the LSA of Section 6.2.2, and (6.23) can be reused for orientations in a straightforward way. This corresponds to the definition of variance for variables that take values on the unit circle (i.e. a one-dimensional rotation) by Levy (1939) (as cited by Diaconis (1988)). However, due to the potential compli-

cations associated with the LSA, the rest of this work will be based on the CA. The following definitions are adopted for the associated variance and standard deviation:

**Definition 6.5 Cosine Variance and Cosine Standard Deviation**

Let  $\mathbf{R}_n = \{R_i\}_{i=1}^n$ ,  $R_i \in \text{SO}(3)$ , be a sample with a definite cosine average  $\bar{R}_{cos}(\mathbf{R}_n)$ . The cosine variance of the sample is then denoted  $V_{cos}$  and defined as

$$V_{cos}(\mathbf{R}_n) \stackrel{\Delta}{=} \frac{\sum_{i=1}^n (1 - \cos \angle(R_i, \bar{R}_{cos}(\mathbf{R}_n)))}{2n} \quad (6.24)$$

Furthermore, the cosine standard deviation of the sample is denoted  $SD_{cos}$  and is defined as

$$SD_{cos}(\mathbf{R}_n) \stackrel{\Delta}{=} \sqrt{1 - 2V_{cos}(\mathbf{R}_n)} \quad (6.25)$$

□

Obviously, by definition the average of Equation (6.5) does in fact minimize the variance of (6.24).

Calculation of the concentration matrix for a sample assumed to be matrix Fisher distributed is known to be extremely complicated (Krieger Lassen et al., 1994). The much simpler cosine variance, however, can be found by Equation (6.24), or the following equivalent but simplified formula:

$$V_{cos}(\mathbf{R}_n) = \frac{3 - \frac{1}{n} \text{tr}(R_\Sigma \bar{R}_{cos}^T)}{4} \quad (6.26)$$

**Remark 6.4** Note that while the concentration parameters of a matrix Fisher distribution carry information about the three-dimensional rotational dispersion of the data, the cosine variance is a scalar and carries information about angular spread only. Therefore these two quantities are by no means equivalent.

□

**Remark 6.5** An alternative is to simply define the cosine variance and standard deviation as

$$V_c(\mathbf{R}_n) \stackrel{\Delta}{=} \frac{1}{n} \sum_{i=1}^n \cos \angle(R_i, \bar{R}_{LC}) \quad (6.27)$$

$$SD_c(\mathbf{R}_n) \stackrel{\Delta}{=} \sqrt{V_c(\mathbf{R}_n)}$$

However, this would yield a variance measure that tended to the value 1 for a sample in which the elements were all equal (i.e. with no variation), and that would gradually decrease as the spread of the sample were increased. This property would violate what is perceived as common sense. The slightly more complex definitions of (6.24) and (6.25) yields a cosine variance that assumes the value zero for non-dispersed data sets, and that has a theoretical maximum value of unity.

Note, however, that Definition 6.5 and Equation (6.27) yield identical values for the standard deviation.

□

### 6.5.1 Relative Cosine Variance

Just as the traditional variance of (6.23) is defined by means of a sum of squares, the cosine variance as defined in (6.24) is closely related to what may be called the sum of cosines, though in a linearly transformed fashion.

In Euclidean space, sums of squares are intimately related to distances via Pythagoras' theorem, and it is frequently used for example in the analysis of variations (ANOVA) for quantification of the “distance” or dispersion of a set of data from a certain point (Box et al., 1978). For assessing similar properties in SO(3) the plain sum of cosines is less suited due to the features discussed in Remark 6.5. Instead the following definition is adopted.

**Definition 6.6 Relative Cosine Variance**

The relative cosine variance of a sample  $\mathbf{R}_n = \{R_i\}_{i=1}^n$ ,  $R_i \in SO(3)$ , with respect to a given rotation matrix  $\Omega \in SO(3)$  is denoted  $V_{cos}^\Omega(\mathbf{R}_n)$  and defined as

$$\begin{aligned} V_{cos}^\Omega(\mathbf{R}_n) &\stackrel{\Delta}{=} \frac{\sum_{i=1}^n (1 - \cos \angle(R_i, \Omega))}{2n} \\ &= \frac{3 - \frac{1}{n} \text{tr}(R_\Sigma \Omega^T)}{4} \end{aligned} \quad (6.28)$$

□

Definition 6.6 is identical to the definition of the cosine variance except for the substitution of the matrix  $\Omega$  for the cosine average.

## 6.6 Kinematic Models Revisited: Estimating Optimal Parameters

### 6.6.1 The Maximum Cosine Estimate

As previously pointed out, the task of replacing a healthy wrist by an optimal prosthesis with less than three DoFs can be expressed as that of approximating the wrist's functional range  $W_F$  by a fewer-dimensional subspace of  $SO(3)$ . If we let  $R_w(t) \in W_F$  denote the actual orientation of the wrist at time  $t$ ,  $R_w(t)$  is a stochastic quantity with an unknown probability density  $P(R_w)$  which is likely to vary over time as well as across subjects and different manual activities. In a practical setting, our knowledge of  $P(R_w)$  is limited to that implied by a finite discrete sample  $\{R_i\}_{i=1}^n$  acquired for a specific set of subjects and activities. In this setting, the optimal prosthesis configuration can be found by assuming a kinematic model corresponding to the desired complexity of the device, such as the one- or two-DoF model in Section 5.4, and fitting this model to the sample  $\{R_i\}_{i=1}^n$  by selecting model parameter values that minimize some cost criterion. In classical parameter identification a least squares criterion is often employed. In light of the preceding sections of this chapter, estimation based on samples on  $SO(3)$  can more conveniently be based on maximizing a sum of cosines or, equivalently, a sum of matrix traces.

For the one-DoF model

$$R_w = R_{k,\theta} R_b, \quad (6.29)$$

five parameters must be estimated, namely the elements of the 3–vector  $\mathbf{b}$  and the direction of the unit 3-vector  $\mathbf{k}$ . The maximum cosines estimate now can be defined as

$$\begin{aligned} (\mathbf{b}, \mathbf{k})_{opt}\{R_i\} &= \arg(\max_{\mathbf{b}, \mathbf{k} \in \mathbb{R}^3, |\mathbf{k}|=1} J_{wl}(\mathbf{b}, \mathbf{k}; \{R_i\})) \\ J_{wl}(\mathbf{b}, \mathbf{k}; \{R_i\}) &\stackrel{\Delta}{=} \sum_{i=1}^n \max_{\theta_i}(\text{tr}(R_i(R_{k, \theta_i} R_b)^T)) \end{aligned} \quad (6.30)$$

where  $R_\Sigma = \sum_{i=1}^n R_i$ ,  $\mathbf{k}$  and  $\theta_i$  are the axis and the angle of rotation for the device,

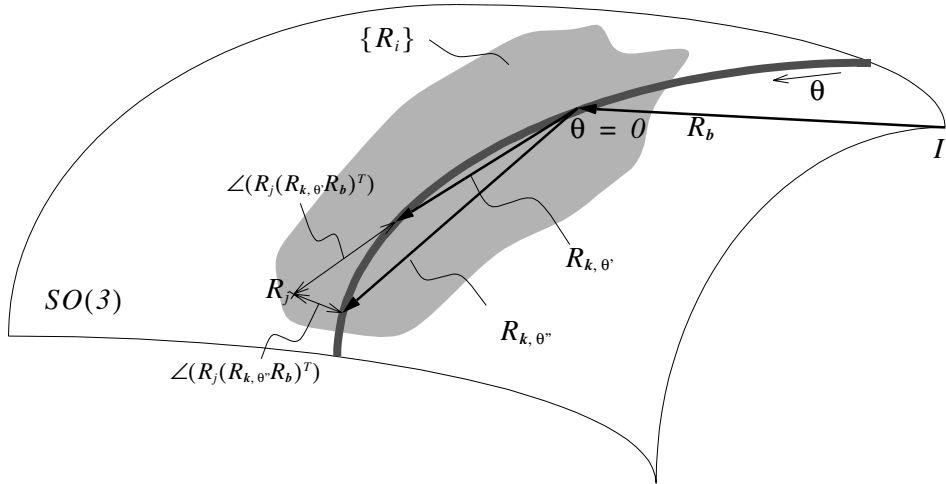


**Figure 6.8:** Distance from a point to a 1-DoF subspace on  $SO(3)$ . Since  $\theta = \theta''$  minimizes the distance from  $R_j$  to  $R_{k, \theta} R_b$ ,  $\angle(R_j(R_{k, \theta} R_b)^T)$  is the distance from  $R_j$  to the one-dimensional space spanned by  $R_{k, \theta} R_b$ ,  $\theta \in [0, \pi]$  (the bold curve).

respectively, and  $\mathbf{b}$  is the rotational offset vector. The rotation angle  $\theta_i$  is the free variable of the model, but with respect to the optimization  $\{\theta_i\}_{i=1}^n$  must be treated as a set of unknown discrete values that need to be estimated. The reason for this is as follows. Each element of the sum in (6.30) is the trace of a rotation matrix, so the element's maximum coincides with the minimum of the rotation angle of this matrix. In the current example this angle can be written as  $\angle(R_i, (R_{k, \theta_i} R_b))$ , and expresses the geodesic distance between  $R_i$  and the point  $R_{k, \theta_i} R_b$  in the device's available workspace. As illustrated in Figure 6.8, this geodesic distance may be different for different values for  $\theta_i$ ; thus, to maximize the sum in (6.30), each element needs to be maximized with respect to  $\theta_i$  in addition to  $\mathbf{k}$  and  $\mathbf{b}$ .

The angles  $\{\theta_i\}_{i=1}^n$  have relevance even aside from the process of estimating  $\mathbf{k}$  and  $\mathbf{b}$  in that they express how well the kinematic model of (6.29) fits the data set. For this reason  $\theta_i$  will be termed the  $i$ 'th *angular residual* or just *residual*.

By the definition of  $R_{k,\theta}$  in Equation (5.3), this matrix is linear with respect to the sine and the cosine of the angle  $\theta$ . Consequently, for any given  $\mathbf{k}$  and  $\mathbf{b}$ , the scalar expression  $tr(R_i(R_{k,\theta_i}R_b)^T)$  varies like the cosine of  $\theta_i$ , though generally offset with respect to angle, amplitude and mean. Hence it has either one unique or infinitely many maxima with respect to  $\theta_i$  in  $[0, 2\pi]$ .

### 6.6.2 Reparameterization

As already noted, for a complete determination of the single-DoF model in (6.29), the parameters of the  $R_{k,\theta}$  and the  $R_b$  matrix must be estimated. The unknown parameters can be represented in a five-dimensional parameter space since each rotation matrix requires only three parameters and  $\theta$  is left as a free variable. By the parameterization of (6.29), the six elements of  $\mathbf{k}$  and  $\mathbf{b}$  must be determined. In the following, however, we will remodel (6.29) as

$$R_w = R_{k,\theta} R_{b',\beta}, \quad (6.31)$$

i.e. we parameterize the orientation vector  $\mathbf{b}$  by means of the unit vector  $\mathbf{b}'$  and the scalar angle  $\beta$  such that  $\mathbf{b} = \beta\mathbf{b}'$ , yielding the seven-parameter vector  $[\mathbf{k}^T, \beta, (\mathbf{b}')^T]^T$ .

### 6.6.3 Assessment of a Numeric Solver

A MATLAB<sup>†</sup> script was written to numerically identify the parameters of the 1-DoF model for a given data set.

No real-world data set will perfectly fit the 1-DoF model. To get a crude picture of the robustness of the solution under various conditions, the script was applied to several simulated data sets of different size and with different but known levels of deviation from the model.

Each data set  $\{R_i\}_{i=1}^n$  was generated as

$$R_i = R_{n_p v_i} R_{k,\theta_i} R_{b',\beta} \quad (6.32)$$

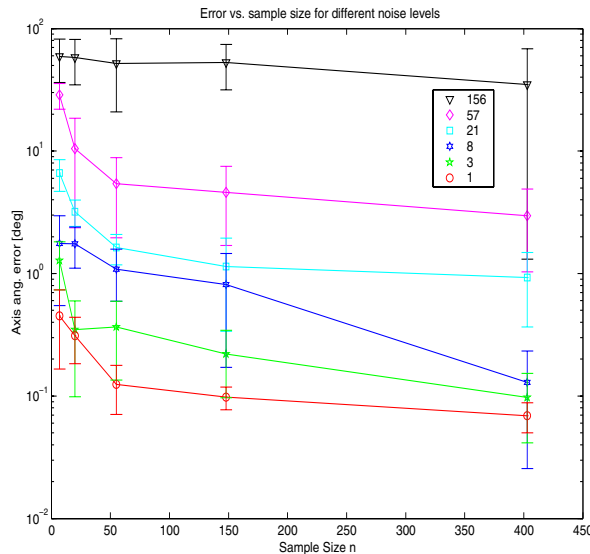
with a random unit vector  $\mathbf{b}' \in \mathbb{R}^3$ , a random offset angle  $\beta \sim N(0, \pi)$ , an axis of rotation represented by the random unit vector  $\mathbf{k} \in \mathbb{R}^3$ , and with a random angle of rotation  $\theta_i \sim N(0, \pi^2)$ . Noise was added by means of the matrix  $R_{n_p v_i}$ , deter-

<sup>†</sup>. The MathWorks, Inc., 3 Apple Hill Drive, Natick, MA 01760-2098, USA  
<http://www.mathworks.com/>

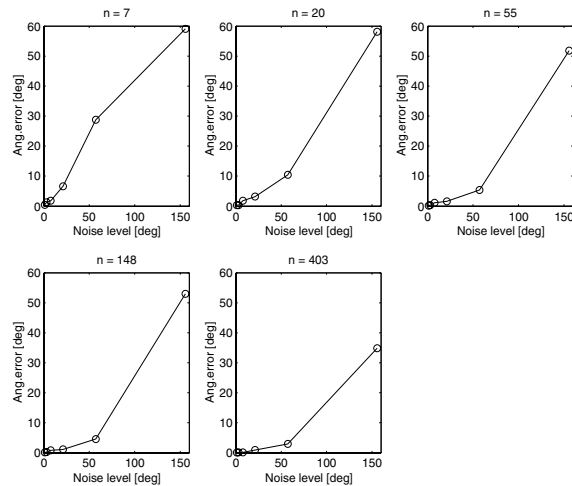
mined by the random unit vector  $\mathbf{n}_i \perp \mathbf{k}$  and the random angle of rotation  $v_i \sim N(0, \sigma^2)$ . The parameters  $\mathbf{k}$ ,  $\mathbf{b}^\dagger$  and  $\beta$  were fixed throughout each data set;  $\mathbf{n}_i$ ,  $v_i$  and  $\theta_i$  were randomly picked for each data point. For each data set, the axis of rotation  $\hat{\mathbf{k}}$  and the offset axis and angle  $\hat{\mathbf{b}}^\dagger$ ,  $\hat{\beta}$  were estimated, and the angular error of  $\hat{\mathbf{k}}$  with respect to  $\mathbf{k}$  (i.e. the angle between the estimated and the actual axis of rotation) was recorded. (The parameters related to the rotational offset were not recorded, as these are not uniquely defined and thus not of particular interest; cf. section 5.4.4). For each sample size  $n$  and each noise level  $\sigma$ , four data sets were generated and analysed, and the recorded estimation errors were averaged over these four runs. Figure 6.9 shows the resulting figures.

Both parts of the figure confirm the expected tendency that the estimation error increases with noise level. There is an amplitude difference of roughly two decades between the lower and the upper graph of Figure 6.9a; these graphs correspond to a noise standard deviation of  $1^\circ$  and  $156^\circ$ , respectively. Note that in the latter case the noise is exaggerated to the point that it is hardly relevant for the human wrist example. In practice the wrist's freedom of motion is limited to approx.  $90^\circ$  of rotation in any direction. Consequently, under no circumstances is the instantaneous deviation, let alone the overall standard deviation, of the actual wrist orientation from an optimally fit 1-DoF model likely to exceed this range. The second upper graph of Figure 6.9a, which corresponds to the noise level  $\sigma = 57^\circ$ , indicates an estimation error in the order of less than one degree as a conservative upper limit for samples of relevant size.

In Figure 6.9b all five subplots are markedly alike both qualitatively and quantitatively. The collective information of these plots is that except for irrelevantly small sample sizes (e.g.  $n = 7$ ), it is the degree of mismatch between the actual data and the 1-DoF model (i.e. the “noise level”) and not the sample size that determines the estimation error. This is the same phenomenon as the functions of Figure 6.9a being approximately constant for larger sample sizes.



(a)



(b)

**Figure 6.9:** Robustness of the 1-DoF model estimator. (a) The effect of sample size on the estimated axis of rotation's angular error with respect to the real axis  $k$ ; the legend shows the noise angle standard deviation  $\sigma$  for each graph. The vertical lines indicate standard deviations. (b) The effect of noise level  $\sigma$  on the same angular error for different sample sizes  $n$ . Note identical ordinate axes in all five subplots for direct comparability.

## 6.7 Appendix: Symmetry and Rotational Neutrality

This appendix explores certain geometric aspects of rotational data that leads to the definition of orientational and rotational neutrality.

Given a set  $\mathbf{R}_n = \{R_i\}_{i=1}^n$  of rotation matrices, the starting point of the discussion is the quantity  $\Delta R_i = R_i \bar{R}^T$ , which we denote the  $i$ 'th *matrix residual* of the sample  $\mathbf{R}_n$  with respect to its cosine average  $\bar{R} = \bar{R}_{cos}\{R_i\}$ . Consider the matrix

$$R_\Sigma \stackrel{\Delta}{=} \sum_{i=1}^n R_i \quad (6.33)$$

where  $R_i \in SO(3)$ . Then obviously we have

$$\sum_{i=1}^n \Delta R_i = R_\Sigma \bar{R}^T \quad (6.34)$$

The first, second and third row of  $R_\Sigma$  are the vectorial sums of all base vectors in the set in the  $x$ -,  $y$ - and  $z$ -directions, respectively, expressed in terms of the reference coordinate frame. If  $R_\Sigma$  turns out to be symmetric, this reflects certain interesting properties of  $\mathbf{R}_n$ . In the following, a geometric step-by-step argument is presented that leads to the introduction of these ideas.

First consider the trivial case when all  $R_i$  are  $3 \times 3$  identity matrices. Then  $R_\Sigma$  is a diagonal matrix; the first, second and third row of  $R_\Sigma$  is parallel to the  $x$ -,  $y$ - and  $z$ -axis, respectively, of the reference frame. Such a situation is illustrated in Figure 6.10a by means of a two-dimensional example with  $n = 2$ .

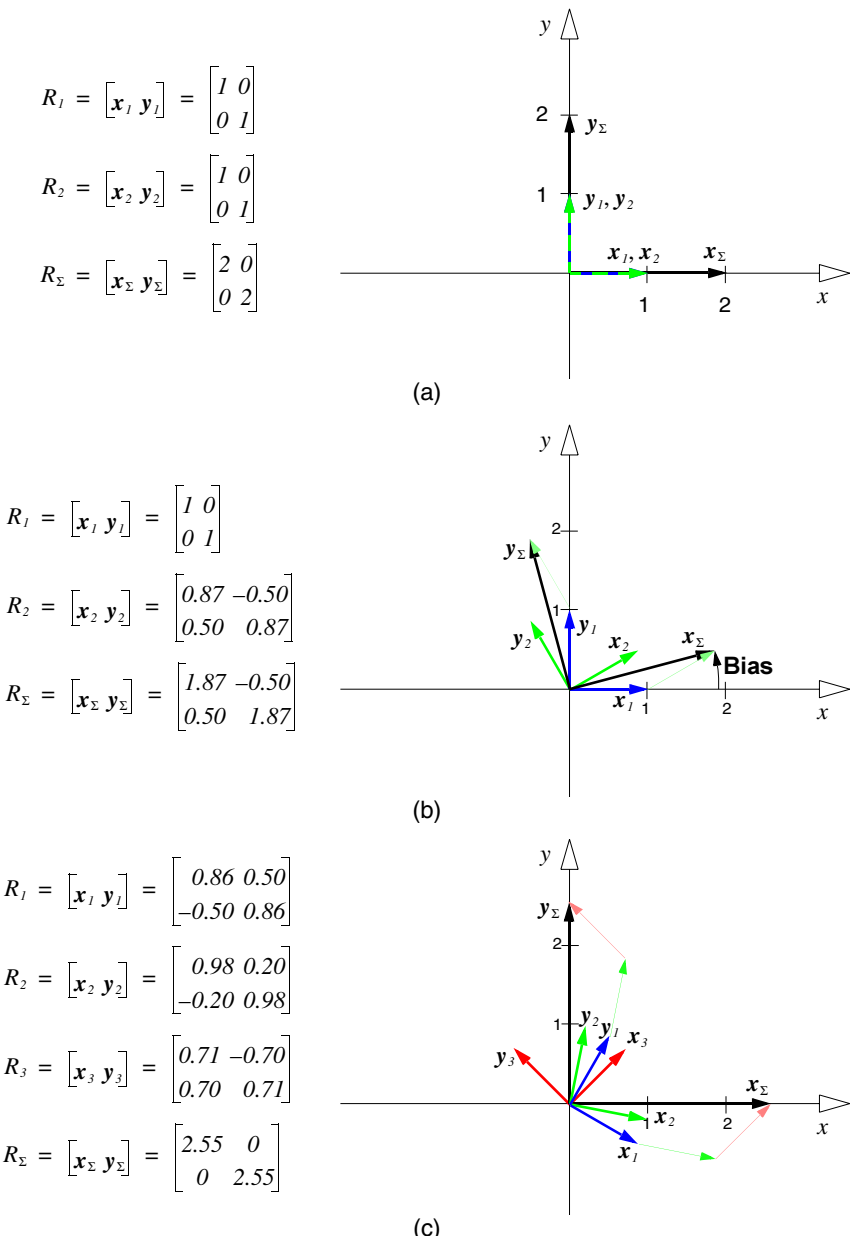


**Figure 6.10:** Rotational Neutrality; a geometric interpretation. The figures depict two-dimensional examples: Figure a is the trivial case where all  $R_i$  are identity matrices; Figure b depicts a case where one of the two matrices correspond to a positive rotation about the  $z$ -axis (perpendicular to the image plane) causing a rotational bias; Figure c shows a non-trivial rotationally neutral case where  $R_\Sigma$  is diagonal.

Next consider another case in which at least one of the elements of  $\mathbf{R}_n$  corresponds to a non-zero angle of rotation, i.e.  $\exists i \in \{1, 2, \dots, n\}$  such that  $R_i \neq I$ . In this case  $R_\Sigma$  generally is not diagonal. In fact, if  $\mathbf{R}_n$  as a whole, and thus the coordinate frames corresponding to this set, has a “rotational bias” in some direction, the rows of  $R_\Sigma$  should be expected to reflect this rotational bias. This situation is illustrated in Figure 6.10b.

Finally consider the case where the elements of  $\mathbf{R}_n$  are somewhat randomly distributed in  $SO(3)$  but in such a way that  $R_\Sigma$  is symmetric. Then,

$$\sum_{i=1}^n R_i = R_\Sigma = R_\Sigma^T = \sum_{i=1}^n R_i^T, \quad (6.35)$$

i.e.  $\mathbf{R}_n$  is distributed in such a way that if all the rotations  $\{R_i\}_{i=1}^n$  are “negated”, that is, carried out in the opposite direction (corresponding to transposing all the matrices), their rows and columns still add up to the same sum  $R_\Sigma$ . Now consider for a moment a set of vectors  $\mathbf{V}_n = \{\mathbf{v}_i\}_{i=1}^n$ ,  $\mathbf{v}_i \in \mathbb{R}^m$ , and their sum  $\mathbf{v}_\Sigma = \sum_{i=1}^n \mathbf{v}_i$ . If  $\mathbf{v}_\Sigma$  were invariant under negation of all the vectors  $\{\mathbf{v}_i\}_{i=1}^n$ , we would have

$$\mathbf{v}_\Sigma = \sum_{i=1}^n \mathbf{v}_i = \sum_{i=1}^n -\mathbf{v}_i = -\mathbf{v}_\Sigma \quad (6.36)$$

which implies  $\mathbf{v}_\Sigma = \mathbf{0}$ . This null vector is the zero element of  $\mathbb{R}^n$ ; if  $\mathbf{V}$  were a set of linear translations, their net effect would be no translation at all. Thus, the set  $\mathbf{V}$  can be said to possess a *neutral*ity with respect to translation, manifest by the fact that its arithmetic average  $\mathbf{v}_\Sigma/n$  is zero.

Translating these observations into  $SO(3)$ ,  $\mathbf{R}_n$  can be said to possess a neutral $\text{ity}$  with respect to rotation if  $R_\Sigma$  is symmetric. Figure 6.10c illustrates this situation by means of a two-dimensional example (in which case  $R_\Sigma$  actually becomes diagonal).

This gives rise to the following definition:

### Definition 6.7 Rotational and Orientational Neutral $\text{ity}$

*A set  $\mathbf{R}_n = \{R_i\}_{i=1}^n$  of rotation matrices is said to be rotationally neutral if and only if  $R_\Sigma$ , as defined in (6.33), is symmetric.*

*If  $\mathbf{R}_n$  represents the orientations of a set  $\mathbf{S}_n$  of coordinate frames,  $\mathbf{S}_n$  is said to be orientationally neutral if and only if  $\mathbf{R}_n$  is rotationally neutral.*

□

**Remark 6.6** The notion of rotational or orientational neutrality is a collective property of the set, not of each individual matrix or coordinate frame in the set. In fact, the only rotation matrices that are rotationally neutral on an individual basis are those corresponding to rotation angles that are integer multiples of  $\pi$ .  $\square$

Now assume that  $\mathbf{R}_n$  is rotationally neutral. It may then be legitimate to consider the identity matrix  $I$ , which is the zero element of SO(3) with respect to rotation, as being representative for the set. In particular, the identity matrix is a candidate average value for the set  $\mathbf{R}_n$ .

Next assume that  $\mathbf{R}_n$  is not rotationally neutral, but assume that there exists an  $\bar{\mathbf{R}} \in \text{SO}(3)$  such that the set  $\{\mathbf{R}_i \bar{\mathbf{R}}^T\}_{i=1}^n$  is rotationally neutral. Then it may be legitimate to consider  $\bar{\mathbf{R}}$  as being representative for the set  $\mathbf{R}_n$ . In particular,  $\bar{\mathbf{R}}$  is a candidate average value for  $\mathbf{R}_n$ . In fact the following holds:

**Theorem 6.2** Let  $\{\mathbf{R}_i\}_{i=1}^n$  be a set of rotation matrices and let  $\bar{\mathbf{R}} = \bar{\mathbf{R}}_{\text{cos}}\{\mathbf{R}_i\}$ . Then the set  $\{\mathbf{R}_i \bar{\mathbf{R}}^T\}_{i=1}^n$  is rotationally neutral.  $\square$

**Proof:** Finding the CA can be expressed as maximizing  $\text{tr}(\mathbf{R}_\Sigma \bar{\mathbf{R}}^T)$  subject to the constraint  $\bar{\mathbf{R}} \in \text{SO}(3)$ . Define

$$\mathbf{R}_\Sigma \stackrel{\Delta}{=} \begin{bmatrix} \mathbf{r}_{\Sigma 1}^T \\ \mathbf{r}_{\Sigma 2}^T \\ \mathbf{r}_{\Sigma 3}^T \end{bmatrix} \quad \mathbf{P} \stackrel{\Delta}{=} \begin{bmatrix} \mathbf{p}_1^T \\ \mathbf{p}_2^T \\ \mathbf{p}_3^T \end{bmatrix} \quad (6.37)$$

where  $\mathbf{p}_1, \mathbf{p}_2, \mathbf{p}_3 \in \mathbb{R}^3$ , and set  $\mathbf{r} = [\mathbf{r}_1^T, \mathbf{r}_2^T, \mathbf{r}_3^T]^T \in \mathbb{R}^9$  and  $\mathbf{p} = [\mathbf{p}_1^T, \mathbf{p}_2^T, \mathbf{p}_3^T]^T \in \mathbb{R}^9$ . Now the CA problem can be formulated as that of maximizing

$$f(\mathbf{p}) = \mathbf{r}^T \mathbf{p}$$

with respect to  $\mathbf{p}$ , subject to the constraints

$$\left. \begin{array}{l} g_1(\mathbf{p}) = \mathbf{p}_1^T \mathbf{p}_1 - 1 = 0 \\ g_2(\mathbf{p}) = \mathbf{p}_2^T \mathbf{p}_2 - 1 = 0 \\ g_3(\mathbf{p}) = \mathbf{p}_3^T \mathbf{p}_3 - 1 = 0 \end{array} \right\} \quad \text{Normality}$$

$$\left. \begin{array}{l} g_4(\mathbf{p}) = \mathbf{p}_1^T \mathbf{p}_2 = 0 \\ g_5(\mathbf{p}) = \mathbf{p}_1^T \mathbf{p}_3 = 0 \\ g_6(\mathbf{p}) = \mathbf{p}_2^T \mathbf{p}_3 = 0 \end{array} \right\} \quad \text{Orthogonality}$$
(6.38)

The associated gradients are

$$\begin{aligned} \nabla f(\mathbf{p}) &= [\mathbf{r}_{\Sigma_1}^T \ \mathbf{r}_{\Sigma_2}^T \ \mathbf{r}_{\Sigma_3}^T]^T \\ \nabla g_1(\mathbf{p}) &= [\mathbf{p}_1^T \ \mathbf{0}^T \ \mathbf{0}^T]^T \cdot 2 \\ \nabla g_2(\mathbf{p}) &= [\mathbf{0}^T \ \mathbf{p}_2^T \ \mathbf{0}^T]^T \cdot 2 \\ \nabla g_3(\mathbf{p}) &= [\mathbf{0}^T \ \mathbf{0}^T \ \mathbf{p}_3^T]^T \cdot 2 \\ \nabla g_4(\mathbf{p}) &= [\mathbf{p}_2^T \ \mathbf{p}_1^T \ \mathbf{0}^T]^T \\ \nabla g_5(\mathbf{p}) &= [\mathbf{p}_3^T \ \mathbf{0}^T \ \mathbf{p}_1^T]^T \\ \nabla g_6(\mathbf{p}) &= [\mathbf{0}^T \ \mathbf{p}_3^T \ \mathbf{p}_2^T]^T \end{aligned} \quad (6.39)$$

where  $\mathbf{0} \in \mathbb{R}^3$  is a null vector. Applying the Lagrange Multiplier method yields the equation

$$\nabla f(\mathbf{p}_{opt}) = \sum_{i=1}^6 \lambda_i \nabla g_i(\mathbf{p}_{opt}) \quad (6.40)$$

with some set of unknown constants  $\{\lambda_i\}_{i=1}^6 \subset \mathbb{R}$ . Substitution of (6.39) into (6.40) and subsequent rearrangement of the elements of  $\mathbf{p}$  into matrix form according to Equation (6.37) yields

$$R_\Sigma P_{opt}^T = \begin{bmatrix} 2\lambda_1 & \lambda_4 & \lambda_5 \\ \lambda_4 & 2\lambda_2 & \lambda_6 \\ \lambda_5 & \lambda_6 & 2\lambda_3 \end{bmatrix}. \quad (6.41)$$

This matrix is symmetric by construction, which concludes the proof.  
□

## 6.8 Appendix: Generalizations and Applications

### 6.8.1 The Cosine Average as an Orthogonalization Operator

As expressed in (6.6), the CA is based on the matrix  $R_\Sigma$ , the arithmetic sum of a set of rotation matrices. However, the discussion of the CA's existence and uniqueness properties does not depend on  $R_\Sigma$  being just that. In fact, *any* real  $3 \times 3$  matrix  $R_\Sigma$  will preserve the validity of the discussion, hence the basic concepts and techniques described for the CA can be applied more generally and the CA can be viewed as an optimal *orthogonalization operator* for real  $3 \times 3$  matrices.

In the following sections several applications of this operator are suggested and briefly discussed.

### 6.8.2 Filtering of Ordered Series of Rotations

One obvious generalization is to substitute a *weighted sum* for  $R_\Sigma$ , yielding the following operator:

$$\tilde{R}(\{R_i\}; \{c_i\}) = \arg \left( \max_{\bar{R} \in SO(3)} \left( \text{tr} \left( \left( \sum_{i=1}^n c_i R_i \right) \bar{R}^T \right) \right) \right) \quad (6.42)$$

where  $c_i \in \mathbb{R}$  and  $R_i \in SO(3)$ .

This operator covers many important applications, such as filters and other discrete-time dynamic systems. Figure 6.11 illustrates this in the form of a scalar n'th-order discrete-time Finite Impulse Response (FIR) filter working on real data and an equivalent filter working directly on data on  $SO(3)$ . Infinite Impulse Response (IIR) filters can be implemented with a similar scheme by introducing a feedback loop around one or more sample-and-hold elements.

The ability to do “traditional” signal processing on data in rotation matrix form is an important result. The discussion in Section 6.2.1 implies that linear component-wise filtering of Euler angles, orientation vectors or quaternions in effect represents non-linear orientation-dependent filtering of the underlying data set which inevitably will distort the data. In contrast, signal processing using (6.42) and a scheme similar to figure 6.11 works directly on the rotation matrices, and represents an isotropic approach with no non-linear distortion.

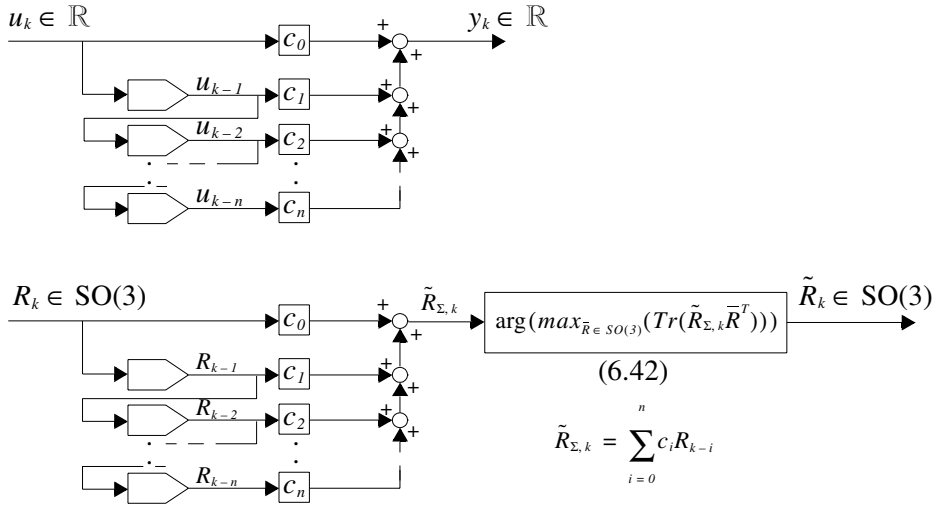


**Figure 6.11:** Schematic discrete-time FIR filters for real scalar data and for rotation matrix data. The structure of the real filter (upper diagram) and the  $SO(3)$  equivalent (lower diagram) are identical except for the additional application of equation (6.42) in the latter case.

### 6.8.3 Discrete Simulation of Rigid Body Orientation

In many contexts, matrices which are supposed to be elements of  $SO(3)$  are numerically distorted to become non-orthogonal. One relevant example is when performing dynamic simulation of systems involving rotational movement, like ships or satellites, where the kinematic differential equation

$$\dot{R}(t) = S(\omega(t))R(t) \quad (6.43)$$

is frequently employed; here,  $R(t) \in SO(3)$  represents the ship's or the satellite's instantaneous orientation at time  $t$ , the components of the 3-vector  $\omega(t) = [\omega_x(t), \omega_y(t), \omega_z(t)]^T$  are the object's instantaneous angular velocity about the  $x$ -,  $y$ - and  $z$ -axis, respectively, all with respect to a reference frame, and  $S(\omega)$  is the skew symmetric matrix

$$S(\omega) = \begin{bmatrix} 0 & -\omega_z & \omega_y \\ \omega_z & 0 & -\omega_x \\ -\omega_y & \omega_x & 0 \end{bmatrix}. \quad (6.44)$$

While (6.43) is strictly correct in the continuous case, simple discretization yields an approximation of the form

$$R_{k+1} \approx (I + S(\omega_k)\Delta t)R_k \quad (6.45)$$

in which case  $R_{k+1}$  is not a proper rotation matrix even if  $R_k$  is. Consequently,  $R_{k+1}$  needs to be projected onto  $SO(3)$  before proceeding to the next iteration lest the orientation estimate drifts off into a meaningless representation.

A straightforward solution which is optimal in the maximum cosines sense, is to apply the CA operator to each estimate. In the case of a simple Euler integration as in (6.45), this implies modifying the equation to read

$$R_{k+1} = \bar{R}_{\cos}((I + S(\omega_k)\Delta t)R_k). \quad (6.46)$$

#### 6.8.4 Dynamic State Estimation

Combining the ideas of the two previous subsections leads to the thought of a dynamic state estimator, e.g. a Kalman filter-like structure, working with rotation matrices. This provides a basis for potential improvement as compared to for instance quaternion-based Kalman filters, which neglect higher-order terms. A state estimator based on cosine statistics could provide optimal estimates of a rigid body's rotational movement, complemented by a traditional Kalman filter for estimation of translational motion. Relevant applications for such a structure would be vessel control in general, satellite and ocean vessels in particular.

A detailed study of this kind of state estimator is outside the scope of this thesis. It is noted, however, that the Kalman filter minimizes the variance of the state estimate error; similarly, an optimization criterion for an estimator tailored for  $SO(3)$  could be that it minimizes the cosine variance of the orientation estimate error.



## **Part III**

# **OPTIMAL WRIST PROSTHESIS KINEMATICS**

*There is much work to be done before upper limb prostheses rightfully are called arm replacements. But progress is occurring and advances are being made towards the goal of replacing the function and appearance of that marvellous tool, the human arm.*

*(Uellendahl, 2000)*



## **Chapter 7**

# **Experimental Results**

### **7.1 Introduction**

This chapter presents results obtained by applying the statistical methods of Chapter 6 to the data collected during the experiment described in Chapter 4. The wrist joint orientation of eight healthy subjects were measured during the performance of a set of ADL. The purpose of the present chapter is to identify implications of the resulting data set with respect to the optimal kinematics of passive or externally powered wrist prostheses.

The chapter is organized in the following way:

**Section 7.2** gives some introductory comments on the optimization problem at hand.

**Section 7.3** addresses the 0-DoF problem and derives the optimal kinematics of a wrist prosthesis without any powered joint functions. Consequently the results can be expressed in terms of the optimal alignment of the terminal device (hand) with respect to the forearm, which is shown to be corresponding to slight supination, extension and ulnar deviation.

**Section 7.4** derives similar results for the 1-DoF wrist, that is a wrist with a single joint axis. The results include the attitude of this optimal single axis with respect to the forearm and with respect to the terminal device.

Both Section 7.3 and 7.4 present results based on the total data set as well as results based on different groupings of the data (subjects, activities, age and sex). Appendix A contains complete tabulations and an extensive set of figures related to the results.

**Section 7.5** gives results pertaining to the control Range-of-Motion (ROM) activity and compares these with the results of previous studies, while

**Section 7.6** presents results related to measurement precision and noise.

Sections 7.5 and 7.6 are directly related to the quality and correctness of the ADL-related data, and give an indication of the technical validity of the present results.

## 7.2 Optimization: A Bird's Perspective

In general it is possible to fit any mathematical model to any set of data in an “optimal” way by means of estimating the model parameters that minimize or maximize some criterion, as long as the problem is not completely ill-posed. In light of the preceding chapters, fitting a zero-DoF model to a set of three-dimensional rotational data in the maximum cosines sense is equivalent to calculating the cosine average of the data, a problem which has a unique solution unless the data exhibits perfect rotational symmetry. Considering that the human wrist joint cannot be rotated more than approx.  $90^\circ$  in any direction, considerably less in most directions, rotational symmetry in the present sense is not possible to obtain and so the problem at hand is in fact guaranteed to have a unique solution with a high definiteness.

However, fitting a model to a set of data does not necessarily provide useful insight: fitting a linear function to a cloud of points in the plane does not imply that the data were generated by a linear relationship in the first place. The mere act of calculating a cosine average similarly does not give any useful insight in itself.

In order to assess the validity of the *grand average (GA)* wrist orientation (i.e. the 0-DoF model) and the *grand optimal kinematic parameters* calculated for the 1-DoF model as really being representative for the bulk of subjects and activities, it is necessary to study the variability of results between and within subgroups of the data. Although no general methodology exists for the analysis of variations (ANOVA) on  $\text{SO}(3)$ , an attempt is made in this chapter to examine the results in an ANOVA-like manner. In the absence of an established analytical methodology, however, the results of this examination are qualitative rather than quantitative.

## 7.3 The 0-DoF Problem

### 7.3.1 Grand Average Wrist Orientation During ADL

The GA wrist orientation was calculated as the cosine average for activities 1 through 15 (i.e. all the ADL activities) across all subjects and runs, with a definiteness of 0.88 and a cosine variance of 0.12. The latter corresponds to a cosine standard deviation of  $39.8^\circ$ .

In matrix form this GA orientation is given by

$$\bar{R}_{GA} = \begin{bmatrix} 1.00 & 0.08 & -0.06 \\ -0.08 & 0.99 & -0.13 \\ 0.05 & 0.13 & 0.99 \end{bmatrix}, \quad (7.1)$$

which differs from the identity matrix by an angle of  $9.25^\circ$  about the axis of rotation given by

$$\mathbf{k}_u = [0.8 \ -0.3 \ -0.5]^T \quad (7.2)$$

The corresponding clinical angles are

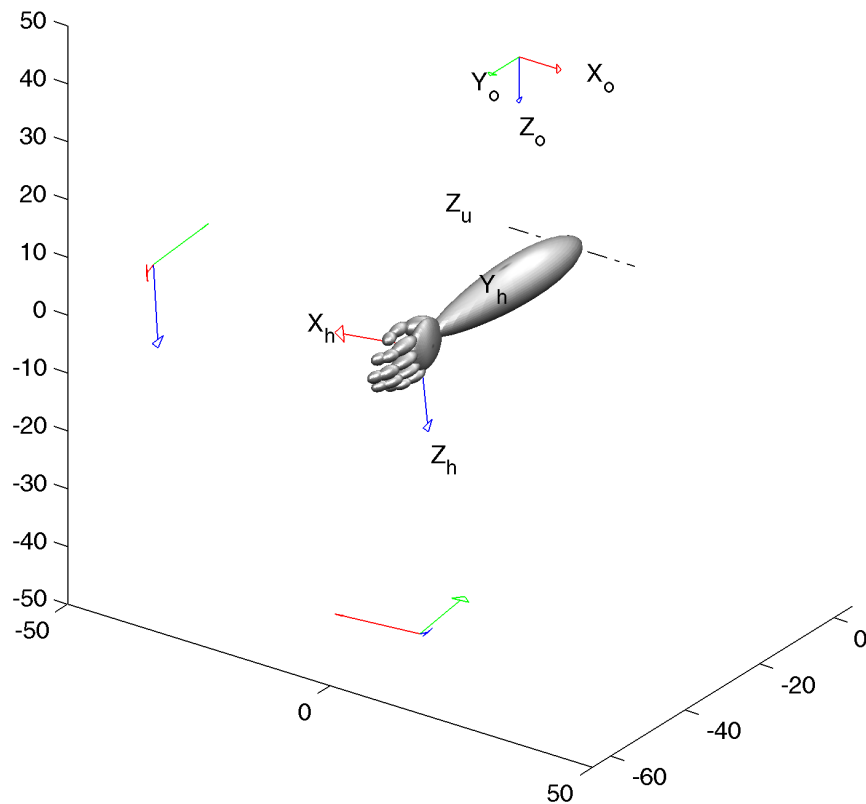
$$\begin{array}{ll} PSM: \theta = -3.3^\circ & \text{(pronation)} \\ FEM: \phi = 7.3^\circ & \text{(extension)} \\ RUD: \psi = -4.9^\circ & \text{(ulnar deviation)} \end{array} \quad (7.3)$$

Figure 7.1 depicts the wrist posture corresponding to this orientation. The broken line represents the elbow axis of rotation, with the symbol  $Z_u$  indicating the medial direction (cf. Figure 4.3). The hand-fixed coordinate axes are projected onto a horizontal and a vertical plane to aid in the three-dimensional interpretation of the figure.

### 7.3.2 Intra- and Inter-Group Variations

The cosine statistics were also calculated for each subject across all ADLs and for each ADL across all subjects. Furthermore, the subjects were divided into subgroups according to age and sex, and cosine statistics were calculated for each subgroup across all ADLs. The resulting quantities are listed in Table 7.1, where the first row displays the grand statistics given in the previous section. The second column shows the mean cosine standard deviation (SD) observed within each group. The column under the heading “Mean geodesic” displays the mean geodesic distance between the grand average and all group averages for each grouping, while the rightmost column shows the relative cosine variance of each set of group averages with respect to the GA.

Most within-group SDs agree remarkably well with the grand statistic in the first row, the within-activity SD being the only one with a markedly smaller value. Likewise, the mean distance from the GA is markedly greater for activities than for the other groupings, with a value two to four times that of the others. This apparent pattern suggests that each activity was performed using a relatively narrow set of postures, while the postures employed for one activity deviates from



**Figure 7.1:** Grand average wrist orientation during ADL.

**Table 7.1:** Summary of intra- and inter-group variations in the 0-DoF estimates.

<b>Grouping</b>	<b>Within-group</b>		<b>Between-group</b>
	<b>Mean</b> $SD_{cos}$ [°]	<b>Mean geodesic</b> [°]	$V_{cos}^{\bar{R}_{GA}}\{\bar{R}_{group}\}$
Grand	39.8	—	0.12
Subject	38.6	8.3	0.007
Activity	<b>32.1</b>	<b>19.9</b>	0.004
Age group	39.2	5.1	0.002
Sex	39.2	4.7	0.002

those employed for other activities. Figure 7.2 depicts two of the extreme activity-based average postures which deviates significantly from the GA shown in Figure 7.1.

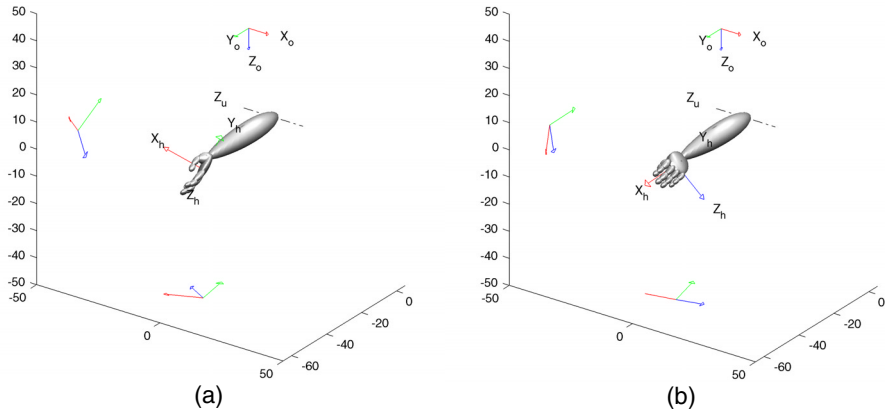


**Figure 7.2:** Largest activity-based average deviation from the grand average orientation. Activity 8 (pouring water) with the largest overall deviation (a) and activity 4 (slicing bread) with the largest deviation in a single clinical angle (b).

To further explore this relationship a separate analysis was carried out in order to allow explicit comparison of the dependency – if any – of the deviation from GA of the subject performing versus the activity performed. For each subject  $s$  and each activity  $a$  the cosine average  $\bar{R}_{s,a}$  of the corresponding data was calculated. Each bar of Figure 7.3a and b corresponds to the angular deviation from the GA of one of these subject-activity averages. In Figure 7.3a the data are sorted by the

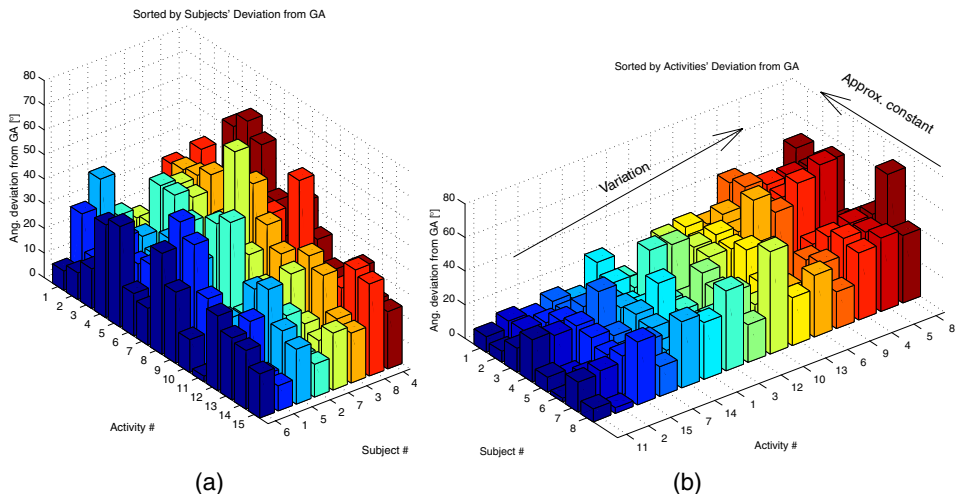


**Figure 7.3:** Angular deviation of subject-activity average from grand average. Sorted by mean deviation for each subject (a) and for each activity (b).

mean deviations associated with each subject (across all activities), while Figure 7.3b shows the data sorted by the mean deviations associated with each activity

(across all subjects). The latter chart suggests that each activity is more or less associated with a characteristic deviation from GA irrespective of which subject performs it, manifest by the wedge-like shape of the chart, although significant variations can be seen across the subjects. A similar relationship is far less apparent, if at all present, when the data are sorted by the mean deviation for each subject (Figure 7.3a).

## 7.4 The 1-DoF Problem

### 7.4.1 Terms and Conventions

In the following references are made to the *angular distance* or *deviation* between axes of rotation. This should be interpreted as the minimum angle of rotation that must be applied to a vector representing one of the axes in order to make it parallel to a vector representing the other axis, as illustrated in Figure 7.4. Note that the angular distance is independent of the sign of the vectors, and it is always in the interval  $[0, \pi/2]$ .

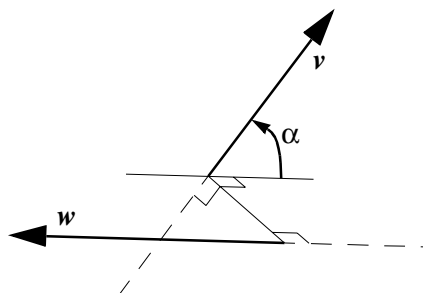


**Figure 7.4:** The concept of angular distance between two axes of rotation. The vectors  $v$  and  $w$  represent two axes an angular distance of  $\alpha$  apart.

It is recalled from Section 6.6.1 that the *angular residual* denotes the geodesic distance between a data point and its closest fit given the constraints implied by a certain kinematic model. Likewise, the *cosine residual* will denote the cosine of the angular residual. These concepts will be employed in the following to quantify the spread of data subsets with respect to an imposed kinematic structure.

### 7.4.2 Grand Optimal Kinematics

The optimal kinematic parameters with respect to all ADL-related data collected will be referred to collectively as the *grand optimal kinematics* and individually as the *grand axis of rotation* and the *grand rotational offset*, respectively. Symbols

related to the grand optimal kinematics are marked by the subscript “<sub>grand</sub>”. With reference to Figure 4.3, the grand axis of rotation was found to be represented by the coordinate vector

$$\mathbf{k}_{\text{grand}, u}^{\text{opt}} = \begin{bmatrix} -0.14 \\ 0.98 \\ -0.12 \end{bmatrix} \quad (7.4)$$

with respect to the forearm-fixed  $S_u$  frame, and by

$$\mathbf{k}_{\text{grand}, w}^{\text{opt}} = \begin{bmatrix} -0.23 \\ 0.95 \\ 0.23 \end{bmatrix} \quad (7.5)$$

with respect to the hand-fixed  $S_w$  frame. The rotational offset was found to correspond to an angle  $\beta_{\text{grand}}^{\text{opt}} = 9.0^\circ$  about the axis represented by

$$\mathbf{b}_{\text{grand}, w}^{\text{opt}} = \begin{bmatrix} 0.81 \\ 0.25 \\ -0.54 \end{bmatrix}. \quad (7.6)$$

The parameters  $\mathbf{k}_{\text{grand}, u}^{\text{opt}}$ ,  $\mathbf{b}_{\text{grand}, w}^{\text{opt}}$  and  $\beta_{\text{grand}}^{\text{opt}}$  now uniquely determine the kinematics of the corresponding wrist prosthesis via the model

$$\begin{aligned} R_u^w(\theta) &= R_u^{w^*} R_w^w \\ &= R_{\mathbf{k}_{\text{grand}, u}^{\text{opt}}, \theta} R_{\mathbf{b}_{\text{grand}, w}^{\text{opt}}, \beta_{\text{grand}}^{\text{opt}}}. \end{aligned} \quad (7.7)$$

Here  $R_u^w$  is the orientation with respect to the forearm-fixed frame  $S_u$  of an imaginary hand-fixed frame  $S_w$  resulting from rotating  $S_u$  through the angle  $\theta$  about  $\mathbf{k}_{\text{grand}, u}^{\text{opt}}$ , while  $R_w^w$  is the static orientation of  $S_w$  with respect to the hand-fixed frame  $S_w$  implied by the rotation angle  $\beta_{\text{grand}}^{\text{opt}}$  about the axis  $\mathbf{b}_{\text{grand}, w}^{\text{opt}}$  (cf. Figure 4.3, which illustrates the former and latter of these coordinates frames.).

Figure 7.5 depicts a left limb with some of the postures obtainable with this kinematic configuration. Note that the rotational offset

$$R_{\mathbf{b}_{\text{grand}, w}^{\text{opt}}, \beta_{\text{grand}}^{\text{opt}}} = \begin{bmatrix} 1.00 & 0.08 & -0.04 \\ -0.07 & 0.99 & -0.12 \\ 0.03 & 0.13 & 0.99 \end{bmatrix} \quad (7.8)$$

causes the wrist to be slightly extended even for  $\theta = 0$  (Figure 7.5a). In fact this “neutral” posture of the 1-DoF wrist is identical to the grand average posture of Section 7.3.1 for all practical purposes, their relative geodesic distance being less than  $1^\circ$ .

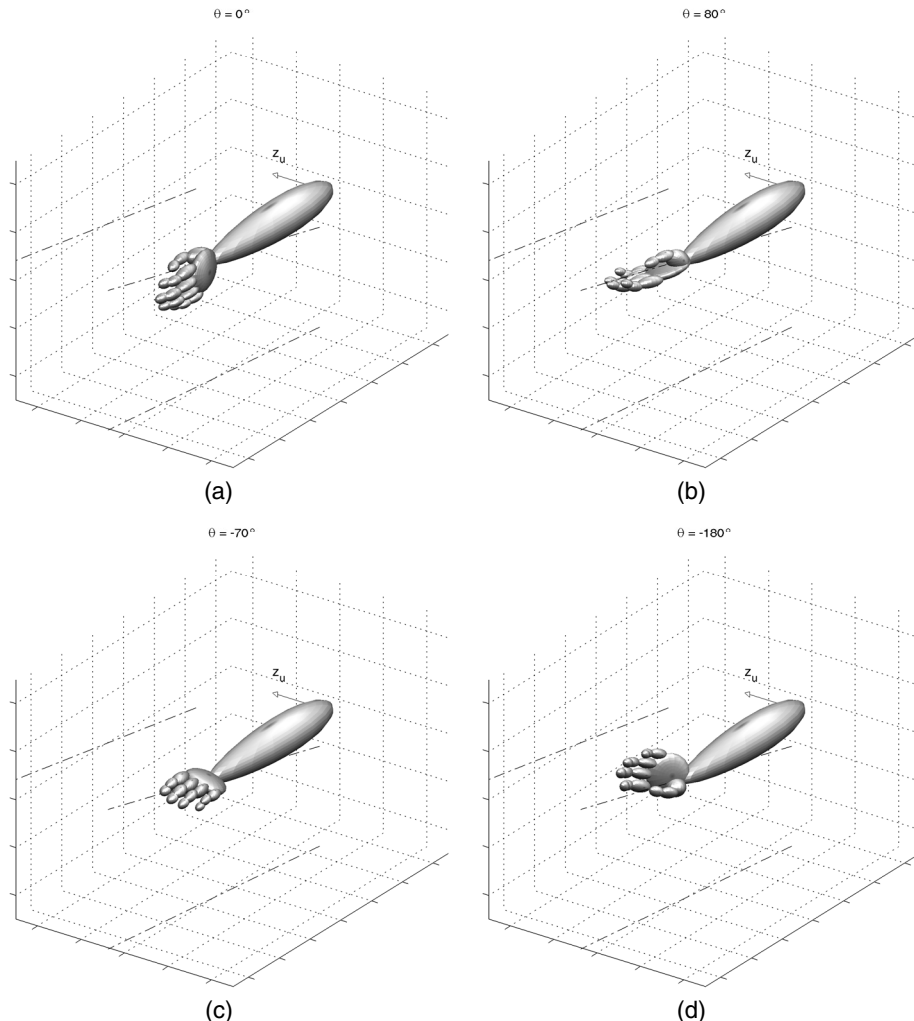


**Figure 7.5:** Postures obtainable with the grand optimal 1-DoF wrist kinematics. The angle  $\theta$  (cf. Equation (7.7)) corresponding to each posture is indicated above the figures. The dash-dotted line through the wrist indicates the axis of rotation, which is also projected onto the vertical and the horizontal plane. Figure (d) shows a posture well outside the range of a healthy wrist, but which is obtainable in a 1-DoF prosthesis without limited angular excursion.

### 7.4.3 Intra- and Inter-Group Variations

Like in the 0-DoF case, differences among activities, subjects, age groups and sexes with respect to the 1-DoF kinematic parameters were assessed. The parameters calculated for each data subset include the optimal single axis of rotation and the rotational offset. Since the 1-DoF model has a free variable, namely the angle of rotation  $\theta$ , the cosine average as such is of little use in comparing data sets. Instead within-group variations were quantified by means of the mean angular residual and the mean cosine residual. Likewise, between-group variations were sought captured through the computation of angular distance between the grand axis of rotation and that found for each group. Since the 1-DoF model used comprises a rotational offset, the optimal axis of rotation may not have the same attitude with respect to the forearm as to the hand, thus the angular deviation from the grand axis must be calculated with respect to both the forearm-fixed and the hand-fixed frame.

The quantities thus found are fully covered in Section A.2, Appendix A, while the most essential results are listed in Table 7.2. Starting at the bottom of the table, the sex-based and the age group-based axes of rotation are essentially identical to the grand axis, with mean deviations well below  $5^\circ$ . Consequently, the postures allowed by the corresponding kinematic constraints closely resemble those of Figure 7.5. While the subject-based results exhibit a slightly larger deviation from the grand optimal axis of rotation, again the activity-based results stand out as those with the largest between-group deviations, i.e. the largest differences from one group (activity) to another, and the smallest within-group variations.

**Table 7.2:** Summary of intra- and inter-group variations in the 1-DoF estimates. Each table cell contains the average over all relevant groups of the relevant quantity, e.g. the values listed for the mean angular residual are the average value for all subjects, activities, age groups and sexes, respectively. Mean residuals were not calculated for the grand optimal parameter set.

Grouping	Within-group mean residual		Between-group angular deviation in [ $^\circ$ ] from grand axis of rotation with respect to	
	Angular [ $^\circ$ ]	Cosine	$S_u$	$S_w$
Subject	28.2	0.84	9.8	8.3
Activity	21.6	0.89	26.1	25.9
Age group	27.7	0.84	1.9	3.9
Sex	28.3	0.84	1.0	1.0

## 7.5 Range of Motion

The primary rationale for including the Range of Motion (RoM) activity in the present experiment was to provide an indication as to whether the sockets and instrumentation actually did or did not reduce the wrist's range of motion. Table 7.3 shows the extreme values of the clinical angles measured during the RoM-activity, averaged across all relevant experimental runs (second row from the bottom, marked "entire data set"). For comparison the table also includes corresponding quantities reported by other investigators.

**Table 7.3:** Comparison of recorded wrist Range-of-Motion with previously reported data.

	Pro	Sup	PSM Range	Flx	Ext	FEM Range	UID	RaD	RUD Range
Brumfield et al. (1966) (male)				73	64	137			
Brumfield et al. (1966) (female)				82	65	147			
Sarrafian et al. (1977)				66	55	121			
Youm et al. (1978)						95	37	20	
Palmer et al. (1985)						133.3			40.5
Linscheid (1986)			150			140			60
Ruy et al. (1991)				79.1	59.3	138.4	37.7	21.1	58.7
Salvia et al. (1994) planar motion circumduction				61.8	55.1	144 116.9	35.4	22.8	56 58.2
van der Heijden and Hillen (1996)	72.5	70	142.5			144			
This study entire data set	71	86	157	60	61	121	50	41	91
ROIs only	71	86	157	59	61	121	35	37	71

The results for the FEM and PSM RoMs are in general agreement with the other studies. Neither do the results for the RUD angles indicate any restriction of the range of motion; on the contrary, the present RUD range appears to be significantly larger than that of previous studies. This discrepancy is so large that it calls for further investigation. For the following discussion it is noted that the disagree-

ment is in the order of  $10^\circ$  for ulnar deviation and  $30^\circ$  for radial deviation, hence common sources of “small” errors are unlikely to be the cause. The following discussion is based in part on observations made during the laboratory experiment and in part on previously published work by others.

Factors considered as a possible cause were incident noise and errors due to metal objects in the workspace; artefacts due to movement between the sensors and the Plaster-of-Paris sockets and between the sockets and the subjects’ body; and physical or mental factors related to the way the RoM activity was performed in relation to the wrist’s mechanical structure.

### ***Noise and Distortion***

No instructions were given to the subjects as to which body posture to assume during the RoM activity, hence each subject performed this activity in different parts of the workspace and at different angles with respect to the room. Consequently, random noise and magnetic field distortion are unlikely to cause systematic errors of the magnitude in question. Furthermore, the documented level of inherent noise (cf. Table 7.4, page 134) contraindicates such noise as the source of the discrepancy.

### ***Movement of the Sensors***

The sensors were firmly taped to the Plaster-of-Paris sockets and the sensor wires were arranged so as to minimize the tear and shear on them during the experiment. Thus, movement of the sensors with respect to the sockets cannot explain the results.

Another possible explanation is relative movement between the subject’s body and the sockets, as the latter were partly suspended in soft tissue. For the elbow socket, its extension in the proximal–distal direction combined with its tight fit effectively eliminates large angular movements in the FEM and the RUD planes. As for the hand socket, in extreme radial deviation the socket’s distal aspect may have been forced radially by unintentional abduction of the thumb and the index finger, causing the socket to deviate more than the hand. However, this inclination is counteracted by radially directed forces on the socket’s proximal aspect caused by tightened radial wrist and finger motor tendons and soft tissue being squeezed between the distal radius and the trapezium/thumb metacarpal. Similar effects occur in extreme ulnar deviation. From visual inspection of the phenomena in question, it is unlikely that the net effect of these contact forces can cause a systematic error as large as  $30^\circ$  in any direction.

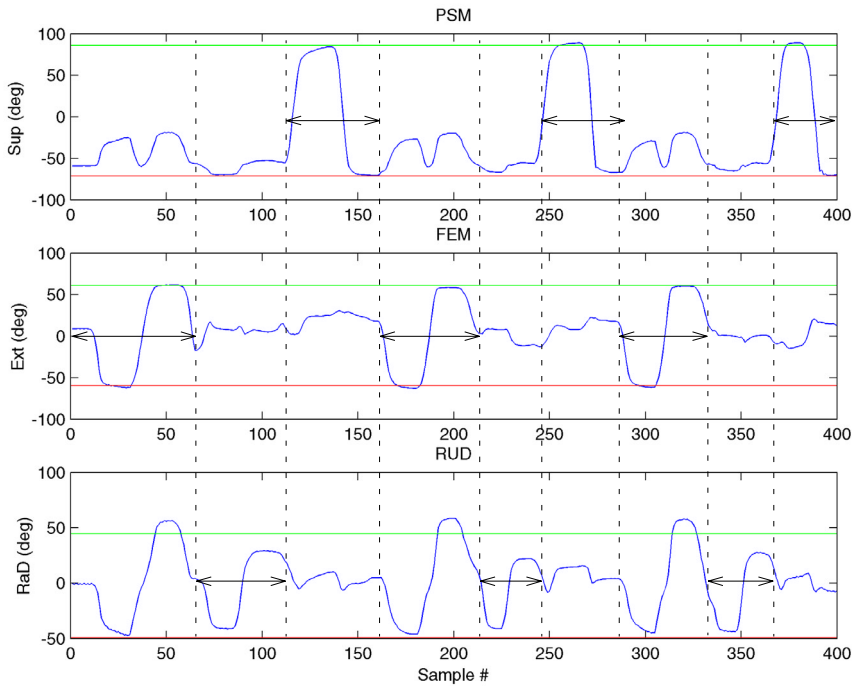


**Figure 7.6:** Example of clinical angles during RoM activity. The horizontal lines represent the average across all runs of the extreme angles measured in the positive and the negative directions, respectively. Labels on vertical axes indicate the positive direction of rotation in each plane; *Sup*=supination, *Ext*=extension, *RuD*=radial deviation. Vertical lines and arrows mark regions with predominantly PSM, FEM and RUD movement, respectively.

### Physiological and Mental Factors

Consider Figure 7.6, which presents the clinical angles as functions of sample number for a typical RoM experimental run, and Figure 7.7 which shows a scatter-plot of FEM angle vs. RUD angle for the same data set. The latter figure reveals two clusters of points with distinct properties, one being a central cluster (indicated by a dashed ellipse) near the neutral FEM angle. The second, diagonal cluster ranges from the lower left to the upper right of the plot, stemming from movements with high correlation between FEM and RUD angles. With respect to the following discussion, the data shown are qualitatively representative for the bulk of the RoM samples.

We can once again consider Figure 7.6, in which vertical lines and double-headed arrows are inserted to mark the regions with (predominantly) PSM, FEM and RUD activity, respectively. The subjects were not given any instructions regarding in which order to perform the three movements, therefore the regions were identified by visual inspection. The regions corresponding to PSM and FEM are easily identified as those with significant activity in the respective angles. The

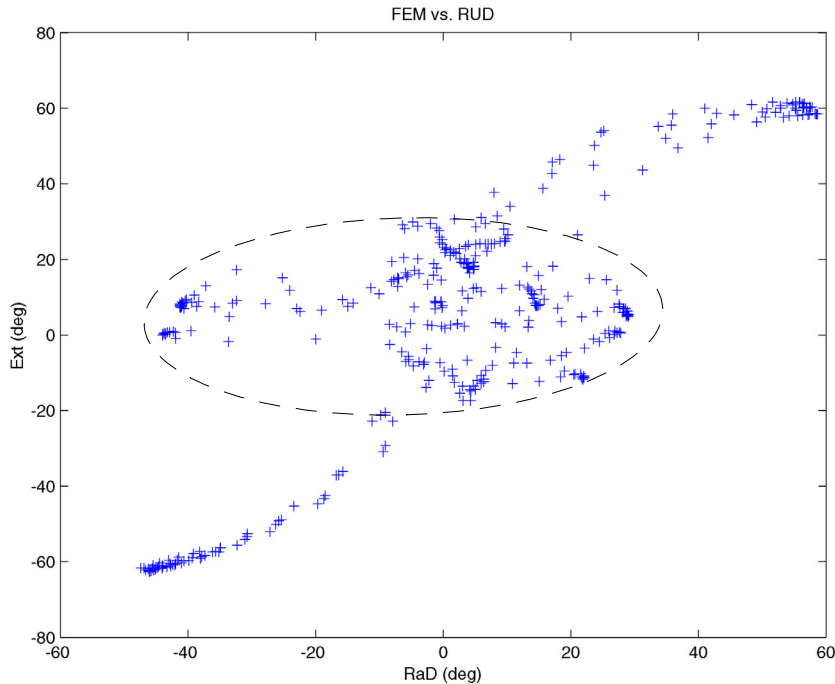


**Figure 7.7:** Scatter plot of FEM vs. RUD angles for the data in Figure 7.6. The ellipse marks the central cluster.

RUD regions then are necessarily what is left of the sample after the PSM and FEM regions are identified. By inspection of the figure it is obvious that the diagonal cluster of Figure 7.7 corresponds to the FEM regions of Figure 7.6, where flexion is consistently accompanied by ulnar deviation and extension by radial deviation.

Given that the RoM activity was performed as an active motion with no planar restrictions, the FEM–RUD correlation can be explained by the results of Saffar and Semaan (1994). These authors studied the morphology of the bones and tendons at the wrist and gave the following statement: “From direct visualization and cineradiography, one can see that a greater range of motion of the wrist is achieved in the oblique plane than in the R.U.D.”. The oblique plane referred to is the plane parallel to the long axis of the forearm that coincides with the tendon of the Flexor Carpi Ulnaris (FCU) and passes between the tendons of the Extensor Carpi Radialis Longus (ECRL) and Brevis (ECRB) (cf. Figure 7.8). Movement in this plane corresponds to extension–radial deviation (ERD) and flexion–ulnar deviation (FUD) and thus corresponds closely to the diagonal cluster in Figure 7.7; this is often referred to in the literature as the “dart thrower’s movement”. The shape of the ellipse in Figure 7.8 roughly suggests the relative wrist excursion in the different directions. For the present study it is assumed that because the sub-

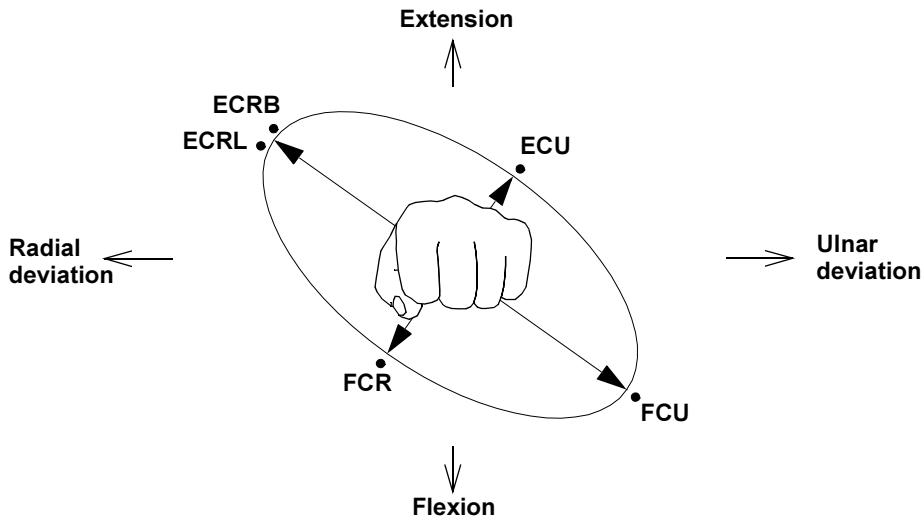


**Figure 7.8:** Muscles: the four groups of wrist motors according to Saffar and Semaan (1994). The labelled dots crudely indicate the position of each tendon and the arrows represent the direction of the forces exerted by the respective muscles on the carpus. The so-called oblique plane is that perpendicular to the image plane and coincident with the ellipse's long axis.

ject was simply instructed to achieve the largest possible FEM angles, (s)he unconsciously added a deviation component to maximize the range of FEM motion; hence the diagonal cluster of Figure 7.7.

Even more interesting than the FEM–RUD correlation is the fact that the largest deviation angles can be observed during the FEM regions, and not, as could be expected, during the RUD regions. Salvia et al. (1994) found statistically significant differences in FEM excursion for planar FEM motion and active circumduction, with the greater range in the planar case. In mathematical terms, if regarding the wrist's set of attainable orientations as a subspace of  $SO(3)$ , this result indicates that the bounds of this subspace is path dependent; in plain language: “how far you can go in a certain direction depends on how you got there”. The underlying causes of this phenomenon may be physiological, psychological or both. Physiologically, the reason why the healthy wrist does have excursion limits is the fact that at a certain point of excursion, interosseous contact forces and stress in ligaments and antagonistic tendons become large enough to balance the force generating ability of the agonists. At the spinal level, as tissue stress increases, sensory feedback from the involved structures will inhibit agonistic motor units and possibly recruit antagonistic action in order to hinder further excursion and thus prevent damage. Eventually the sensory feedback even reaches a conscious level in the brain and is perceived as discomfort or pain. Such discomfort causes mental distraction from the task of moving the wrist, and reduces the motivation for further action. As the reader may readily verify,

extreme circumduction is typically associated with more discomfort than extreme planar motion; in circumduction the entire path of motion is uncomfortable, while in planar motion only the extreme end points are associated with such sensation. This argument may explain the results of Salvia et al. (1994). More importantly, it provides a possible explanation of why the maximum RUD excursion found in the present study exceeds that reported for studies involving planarly restricted motion or circumduction.

To assess the correctness of this explanation, the PSM, FEM and RUD regions, or Regions-of-Interest (ROI), in each RoM recording were manually extracted from the data. The average maximum angles were then recalculated using only the relevant ROI in each case. The resulting quantities are listed in the bottom row of Table 7.3 (labelled “ROIs only”), and show a significantly better agreement with previous reports than the numbers based on the entire data set. As evident from Figure 7.6, the FEM angle was kept relatively still during the RUD regions, indicating an approximately planar RUD motion. Average FEM angle during these regions across all subjects was found to be  $15^\circ$  of extension. The FEM angle corresponding to the average wrist orientation across the same data was  $22^\circ$ .

## 7.6 Measurement Error Quantified

It is recalled from Section 4.2.5 that an instrumented rigid beam was used for quantifying the inherent measurement noise and other sources of error in the laboratory set-up. The beam was moved within the motion tracking system’s workspace while the relative movement between two motion sensors attached to the beam was measured. Since only relative orientation is considered in the present experiment, the relative rotational movement between the two sensors provides a direct measure of the errors involved.

The results of this procedure are summarized in Table 7.4. The standard deviation values listed in the table are traditional statistics based on scalar angular values, not cosine statistics, because the results related to the cosine statistics were not available at the time these numbers were computed. Considering the small values recorded for the maximum angular error (third column), traditional statistics provide adequate approximations in this case.

Runs 1–6 quantify the intrinsic noise level of the laboratory, i.e. the noise induced by computer equipment, fluorescent lights, the MotionStar system itself and any source external to the laboratory, while runs 7–8 represents this background noise with the addition of any potential laser induced components.

The error magnitudes calculated for runs 1–4 were remarkably constant. This affects the interpretation of the other measurements, in that differences in noise levels can most likely be attributed to known differences in measurement conditions.

**Table 7.4:** Quantification of measurement errors under various movement velocities and under the influence of different potential sources of disturbances.

Run #	Conditions	Maximum error [°]	Standard deviation [°]
1	Beam at rest on table Lasers off	0.18	0.03
2		0.18	0.03
3		0.12	0.03
4		0.26	0.03
5	Beam at rest in forearm support Lasers off	0.22	0.05
6		0.23	0.06
7	Beam at rest in forearm support Lasers on	0.22	0.05
8		0.28	0.05
9	Beam movements resembling ADLs <sup>a</sup> Lasers off	3.04	0.60
10		2.86	0.40
11	Beam movements unnaturally fast <sup>b</sup> Lasers off	8.66	1.34
12		11.31	2.25

- a. The instrumented beam was moved in ways and at translational and angular velocities assumed to be representative for ADLs.
- b. Beam velocities notably higher in run 12 than in run 11.

Neither the angular standard deviations nor the maximum angular errors measured with the lasers turned on (runs 7–8) differed from those measured with the lasers turned off under otherwise identical conditions (runs 5–6). Thus, the lasers can be assumed not to have significant influence on measurement precision. A slight but clearly insignificant difference was observed for the figures from different locations within the laboratory workspace, i.e. on the table (runs 1–4) as compared to in the forearm support (runs 5–8).

The maximum errors and standard deviation recorded during ADL-like movements (runs 9–10) were approx. an order of magnitude larger than those for sensors at rest (runs 5–8). This confirms the presumption that the authentic ADL measurements might be contaminated with movement artefacts. However, the error standard deviation found during ADL-like movements were an order of magnitude smaller than the 5° calibration error allowed; even the maximum instantaneous error recorded during these runs did not exceed this limit.

Runs 11–12, during which the beam was moved excessively fast and jerky, yielded maximum error values three to four times higher than those for ADL-like movements, while error standard deviations were two to six times higher. The latter figures were still less than half of the maximum calibration error allowed. As these figures can be regarded as a conservative upper limit for the measurement error standard deviation of authentic ADLs, one can conclude that intrinsic noise and movement artefacts are small compared to the calibration uncertainty. Thus the dominant limiting factor for the overall measurements precision is the calibration process.



# Chapter 8

## Discussion and Conclusion

While the original goal of this work was to provide empirical evidence to support or reject certain assumptions about the healthy wrist and the prosthetic wrist, developing and understanding the statistical tools for analysing the data became a major issue during the course of the work. These theoretical results constitute significant parts of this thesis, both with respect to volume and contributions, and are the first to be discussed.

### 8.1 Rotation Statistics

#### 8.1.1 Differential Rotations vs. General Rotational Data

Traditionally, statistics have been applied mostly to differential (small) rotations. In biomechanics this is typically done for purposes such as estimation of smooth movements from more or less noisy landmark position data. A somewhat similar paradigm exists in motion control science, where data are typically smoothed by means of a dynamic state estimator while a relatively high sampling frequency justifies the assumption that angular differences between adjacent data points are small. Several simplifications apply for such data, and the need for general rotation-specific statistical methods has not been critical.

It has been demonstrated that basic statistical operations, like taking the average, may give bizarre results if applied to general sets of rotational data. Starting from a mainly geometrical point of view, a set of unambiguous statistical operators has been derived that take series of rotation matrices as their arguments. The operator named the *cosine average*, which is equivalent to the maximum likelihood estimator for the mean of a matrix Fisher distributed set, is shown to be completely independent of the choice of reference coordinate frame; it is *isotropic* in its effect. In certain cases of rotationally symmetric data the cosine average problem does not have a unique solution, a phenomenon associated with rotations as such

rather than with the operator. A novel concept, the *definity*, has been introduced as a simple scalar measure of how close a given data set is to this situation. The *cosine variance* and the corresponding *cosine standard deviation* constitute simple measures of data dispersion. Together the cosine statistics provide a simple toolbox for performing unambiguous basic statistical analyses of general data sets on SO(3).

### 8.1.2 Suggestions for Future Research

The research literature related to orientation statistics is sparse. Basic results have been applied in the field of crystallography and to a very limited extent in the study of human kinematics, but the bulk of the material published is strictly theoretical. While acknowledging the importance of in-depth theoretical understanding, there seems to be a potential for simple methodologies that can be applied to real-world data and thus provide deeper understanding of the underlying real-world processes. One example is the (admittedly very limited) ANOVA-inspired analysis applied in this thesis. An ultimate goal may be to develop a framework for hypothesis testing and assessment of statistical significance on SO(3) without strict prior assumptions with respect to the data set.

The cosine average can be applied to any set of real  $3 \times 3$  matrices as a general orthogonalization operator. As such this may have applications far beyond those demonstrated in this thesis, and a suggested issue for further research is time-domain filtering of three-dimensional rotation sequences. The concept may even be extended to an SO(3)-specific Kalman filter-like construct based on minimizing the cosine variance of the rotational estimation error, though no attempt has been made to assess the tractability of the resulting mathematics.

## 8.2 Wrist Prosthesis Kinematics

### 8.2.1 People are Alike but Activities are Different

Optimal kinematic parameters have been identified for the passive (0-DoF) wrist prosthesis in terms of the optimal alignment of the hand with respect to the forearm. The grand average orientation, taken across the entire ADL-related data set, corresponds to a pronation angle of  $3^\circ$ , an extension of  $7^\circ$  and  $5^\circ$  of ulnar deviation. This is a moderate posture somewhat close to the centre of the healthy wrist's range of motion, and it matches fairly well the practice of many limb fitting centres.

Similarly the optimal axis of rotation and rotational offset of a single-DoF active wrist prosthesis has been calculated. It turned out that the “neutral posture” of this optimal joint is virtually identical to the grand average orientation found for the

0-DoF case. The joint's axis of rotation crudely corresponds to the prosupination axis, but its obliquity with respect to the forearm is large enough to cause significant wrist extension in the pronated configuration.

The analysis of different sub-groupings of the data set revealed two main trends.

1. Both in the 0-DoF and the 1-DoF case, the dispersion of the results was greater between activities performed than between subjects performing. Likewise, the data within each activity showed less dispersion than in the data associated with each subject or subject subgroup. In plain language this implies that different people utilize their wrists in similar fashions for the same activity, but the wrist is employed differently for different tasks. Thus, if specialized prosthetic devices were to be designed on the basis of these results, these should be optimized for specific applications or application categories rather than for specific users. This is hardly a surprising result, and supports present practice in the prosthetics industry.
2. Despite significant differences in the attitudes of rotation axes optimized for different tasks, the majority of the wrist axes identified showed the same *general* attitude with respect to the forearm: from a dorsal and ulnar position on the proximal side of the wrist to a ventral (palmar) and radial position distally.

No significant differences were found between age groups or between sexes.

### 8.2.2 Validity of the Results

Considerable effort has been put into the experimental design in order to assure a certain quality and relevance of the results. However, there are inevitably issues that are open to discussion in this respect.

#### *Technical Considerations*

The quality of the motion data collected depends heavily on the proper attachment and alignment of the motion sensors with the subject's body. Initial and final alignment is assured by the special calibration procedure used, at least within a very few degrees ( $^{\circ}$ ). It can be argued that this procedure does not guarantee proper alignment during the course of each experimental run, because the plaster sockets used for sensor attachment are partly suspended in soft tissue. However, apart from serving as sensor attachment devices, a second – and perhaps more important – role of the plaster sockets was to limit the range of limb motion to that obtainable when using a below-elbow externally powered hand prosthesis. The elbow socket thus resembled a (distally open-ended) transradial prosthesis inner socket. A real prosthesis socket is subject to forces (and thus displacements with respect to the body) caused by the terminal device's interaction with the environment, while such forces were necessarily absent in the present plaster sockets.

However, forces from the underlying tissue in the (simulated) residual limb would be similar in the real and the simulated cases. To conclude, the forces acting on real and simulated prosthesis sockets are different to some extent, so the rotational relationship between the socket and the (simulated) residual limb during movements may be different. By conjecture, considering the tight fit of the socket and the condition of the tissue in question, these deviations are not significant in comparison with other sources of error. It should be noted, however, that any such deviations may constitute systematic errors and thus offset the final results. As for the plaster gauntlet applied to the hand, the presence of soft tissue is less of a problem although forces from the restricted thumb and fingers may have caused transient misalignment.

### ***The Simulated Prosthesis***

An important assumption has been that under the experimental conditions, subjects utilize their hand and wrist as if the hand were an electric prosthetic hand. In retrospect it is felt that the mechanical restrictions of movement and grip postures provided a fairly realistic set of postures. However, the simulated prostheses of this project had virtually all sensing and proprioceptive abilities intact, giving the subjects a dramatically better control of their grip function than can presently be achieved in a prosthesis. Broad tape applied to the fingers merely reduced the fine sense of touch, while gross contact forces, joint angles and musclotendon stress continued to be integral parts of the subjects' sensorimotor system. It should therefore be expected that the simulated amputees in this study performed the ADL with a far greater confidence than real prosthesis users would, which is likely to influence the way the ADL were performed. Local anaesthesia was at one time considered for disabling hand afferent nerves and intrinsic muscles, but this idea was not pursued due to technical, medical and ethical considerations. It is strongly recommended that this option be considered if the concept of simulated prostheses is employed for future prosthetics research.

### ***Representativeness***

An issue not mentioned so far is the effects of the tremendous adaptability exhibited by humans. The subjects of this study were all inexperienced "amputees", and had limited time to adapt their normal limb utilization to the modified functionality offered by the simulated prosthesis. Philosophically, this may have led to a more "objective" limb utilization, unbiased by the compensatory movement patterns typically exhibited by users of real "sub-optimal" wrist prostheses. On the other hand, adaptation of movement patterns to specific limb or prosthesis properties is believed to take place in order to optimize the overall utilization of the limb with respect to some – possibly unconscious, abstract and highly subjective – criterion. Thus, subjects more familiar with the (simulated) prosthesis might display different wrist utilization from those of this study, possibly leading to even

better “optimal wrist prosthesis kinematics” than that calculated from the present data set. The relative importance of these conflicting arguments remains unknown. Nevertheless, these and similar considerations should be kept in mind when interpreting the present findings. Ultimately, the theoretical optimality of the kinematic parameters calculated does not guarantee that a wrist device designed accordingly will actually be judged by the users to be better than devices with other kinematic properties. This is because the user’s perception of the device will also account for cosmesis, control system, control interface and other aspects of the prosthesis not explicitly considered in this study.

Only a limited number of activities and subjects could be included in the experiment. It has long since been argued that the very concept of activities of daily living (ADL) is poorly defined and inaccurately interpreted by many investigators. Furthermore, the majority of published results related to wrist function during ADL is focused on the effects of pathological conditions and surgical procedures other than amputation, and thus not necessarily relevant to this study. Therefore the selection of activities was carried out with limited consideration of previous research but with a correspondingly high degree of focus on actually spanning a relevant range of basic movements. The close cooperation with occupational therapists during the experimental design phase is believed to have significantly contributed to the appropriateness of the experiment as a whole. The results are only valid to the extent that a relevant set of activities were actually selected. Also, cultural and social differences obscure the level of confidence with which the results can be generalized to other anthropological groups than that studied here, namely otherwise healthy adult unilateral below-elbow amputees of western industrialized societies.

### ***The Original Hypothesis Revisited***

In Chapter 3 the purpose of the present study was stated to be the evaluation of the following null hypothesis:

*A powered wrist prosthesis with an exclusive forearm rotation (i.e. prosupination movement) is at least as kinematically functional as a device with any other single axis of rotation*

against the alternative hypothesis

*For a powered one-DoF wrist prosthesis there exists at least one axis of rotation which is more kinematically functional than the forearm rotation.*

The results just discussed lead to a twofold conclusion: for some activities the null hypothesis should be rejected, while for others it should clearly be kept.

### 8.2.3 Suggestions for Future Research

A suggested follow-up of this study is to apply clustering techniques in order to identify data subsets, such as subsets related to different activities, with equal or similar properties with respect to kinematic parameters. If significant clustering is unveiled, the following secondary outcome might be foreseen.

- A wrist prosthesis may be developed with a single powered joint axis but with additional passive functions that allow the user to reconfigure (for example by using the contralateral hand) the prosthesis according to the kinematic requirements of the task at hand. The clustering analysis may then provide the basis for optimizing the passive functions.
- Clustering ADL-related data according to kinematic requirements may lead to a deeper understanding of the spectrum of tasks undertaken in everyday life. Ultimately this may provide the basis for improved criteria with respect to the selection of activities for studies like this one.

The most obvious future research issue, however, is the clinical assessment of an actual powered wrist prosthesis with an oblique axis of rotation based on the present findings. Application of an established hand function test combined with a user survey may give a definite answer as to whether the “optimal” axis of rotation actually represents a significant functional improvement in wrist prosthesis design.

*Because when it all comes down to Daily Living,  
the Proof of the Prosthesis is in the Performance.*

# References

- Abboudi, R. L., Glass, C. A., Newby, N. A., Flint, J. A., and Craelius, W. (1999). A biomimetic controller for a multifinger prosthesis. *IEEE Transactions on Rehabilitation Engineering*, 7:121–129.
- Alderson, S. W. (1952). Shoulder harness for artificial arms. US Patent 2,592,842.
- Almström, C. (1977). An electronic control system for a prosthetic hand with six degrees of freedom. Research Laboratory of Medical Electronics, Chalmers University of Technology, Göteborg, Sweden.
- An, K. N., Chao, E. Y., Cooney, W. P., and Linscheid, R. L. (1979). Normative model of human hand for biomechanical analysis. *Journal of Biomechanics*, 12:775–788.
- An, K. N., Ueba, Y., Chao, E. Y., Cooney, W. P., and Linscheid, R. L. (1983). Tendon excursion and moment arm of index finger muscles. *Journal of Biomechanics*, 16:419–425.
- Andrews, J. G. (1984). On the specification of joint configurations and motions. *Journal of Biomechanics*, 17(2):155–158.
- Arbib, M. A., Iberall, T., and Lyons, D. (1985). Coordinated control programs for control of the hands. In Goodwin, A. W. and Darian-Smith, editors, *Hand function and the neocortex. Experimental Brain Research Supplemental 10*, 111–129. Springer-Verlag, Berlin.
- Ariel, G. B., Buijs, R. J. C., Penny, A., and Chung, S. G. (2000). Visualizing orientation using quaternions. In *Proceedings of the Sixth International Symposium on the 3D Analysis of Human Movement*, Cape Town, South Africa, 21–24. International Society of Biomechanics.
- Armstrong, T. J. and Chaffin, D. B. (1978). An investigation of the relationship between displacements of the finger and wrist joints and the extrinsic finger flexor tendons. *Journal of Biomechanics*, 11:119–128.

- Atkins, D. J., Heard, D. C. Y., and Donovan, W. H. (1996). Epidemic overview of individuals with upper-limb loss and their reported research priorities. *Journal of Prosthetics and Orthotics*, 8(1):2–11.
- Atkins, D. J. and Meier III, R. H., editors (1989). *Comprehensive Management of the Upper-limb Amputee*. Springer Verlag, New York.  
ISBN 0-387-96779-6, 3-540-96779-6
- Barker, T., Nicol, A., Kelly, I., and Paul, J. (1996). Three-dimensional joint co-ordination strategies of the upper limb during functional activities. *Proceedings of the Institution of Mechanical Engineers [H]*, 210(1):17–26.
- Bergantz, D. and Barad, H. (1988). Neural network control of cybernetic limb prostheses. In *Proceedings of the IEEE Engineering in Medicine and Biology Society 10th Annual International Conference*, 1486–1487. IEEE Engineering in Medicine & Biology Society. Track 16: Neural Networks.
- Bingham, C., Chang, T., and Richards, D. (1992). Approximating the matrix Fisher and Bingham distributions: Applications to spherical regression and procrustes analysis. *Journal of Multivariate Analysis*, 41:314–337.
- Bowler, J. H. and Michael, J. W., editors (1992). *Atlas of Limb Prosthetics*. Mosby-Year Book, Inc, St. Luis, MO. 2nd edition.
- Box, G. E. P., Hunter, W. G., and Hunter, J. S. (1978). *Statistics for Experimenters*. Wiley Series in Probability and Mathematical Statistics. John Wiley & Sons.  
ISBN 0-471-09315-7.
- Brand, P. W., Beach, R. B., and Thompson, D. E. (1981). Relative tension and potential excursion of muscles in the forearm and hand. *Journal of Hand Surgery*, 6(3):209–219.
- Brand, P. W., Cranor, K. C., Rouge, B., and Ellis, J. C. (1975). Tendon and pulleys at the metacarpophalangeal joint of a finger. *Journal of Bone and Joint Surgery*, 57-A(6):779–784.
- Brumfield, R., Nickel, V., and Nickel, E. (1966). Joint motion in wrist flexion and extension. *Southern Medical Journal*, 59:909–910.
- Brumfield, R. H. and Champoux, J. A. (1984). A biomechanical study of normal functional wrist motion. *Clinical Orthopaedics and Related Research*, (187):23–25.
- Buchholz, B. and Armstrong, T. J. (1992). A kinematic model of the human hand to evaluate its prehensile capabilities.  
*Journal of Biomechanics*, 25(2):149–162.

- Buchholz, B., Armstrong, T. J., and Goldstein, S. A. (1992). Anthropometric data for describing the kinematics of the human hand. *Ergonomics*, 35(3):261–273.
- Carlsson, J. D. and Tromby, C. A. (1983). The effect of wrist immobilization on performance of the Jebsen hand function test. *The American Journal of Occupational Therapy*, 37:169–175.
- Chao, E. Y. S. (1980). Justification of triaxial goniometer for the measurement of joint rotation. *Journal of Biomechanics*, 13:989–1006.
- Chappell, P. H. and Kyberd, P. J. (1991). Prehensile control of a hand prosthesis by a microcontroller. *Journal of Biomedical Engineering*, 13:363–369.
- Childress, D., Grahn, E., Weir, R., Heckathorne, C., and Uellendahl, J. (1993). Modification of a Bock electric hand for E.P.P. control by exteriorized tendons. In *Proceedings, 19th Annual Meeting & Scientific Symposium of the American Academy of Orthotists and Prosthetists*, page 13, Las Vegas, Nevada. American Academy of Orthotists and Prosthetists, AAOP.
- Cupo, M. E. and Sheredos, S. J. (1998). Clinical evaluation of a new, above-elbow, body-powered prosthetic arm: a final report. *Journal of Rehabilitation Research and Development*, 35:431–446.
- de Lange, A., Kauer, J. M. G., and Huiskes, R. (1985). Kinematic behavior of the human wrist joint: A roentgen-stereophotogrammetric analysis. *Journal of Orthopaedic Research*, 3:56–64.
- de Visser, H. and Herder, J. L. (2000). Force-directed design of a voluntary closing hand prosthesis. *Journal of Rehabilitation Research and Development*, 37:261–271.
- Deutsch, S. and Deutsch, A. (1993). *Understanding the Nervous System. An Engineering Perspective*. IEEE Press, New York. ISBN 0-87942-296-3.
- Group Representations in Probability and Statistics, volume 11 of *Lecture Notes – Monograph Series*. Institute of Mathematical Statistics, Hayward, CA.

Doshi, R., Yeh, C., and LeBlanc, M. (1998). The design and development of a gloveless endoskeletal prosthetic hand. *Journal of Rehabilitation Research and Development*, 35:388–395.

Downs, T. D. (1972). Orientation statistics. *Biometrika*, 59:665–676.

- Egeland, O. and Sagli, J. R. (1993). Coordination of motion in a spacecraft manipulator system. *The International Journal of Robotics research*, 12(4):366–379.
- Ervik, S.-M., Kippernes, A., Mathisen, T., Møgedal, L. H., Opsahl, S., and Stadtler, H. G. (1996). Selection of activities for a laboratory experiment. Project report, School of Health Education, Department of Occupational Therapy, Sør-Trøndelag University College, Norway. In Norwegian.
- Farry, K., Fernandez, J., Abramczyk, R., Novy, M., and Atkins, D. (1997). Applying genetic programming to control of an artificial arm. In *Conference Proceedings, 1997 MyoElectric Controls/Powered Prosthetics Symposium, MEC'97*, 50–55, Inst. of Biomedical Engineering, University of New Brunswick, Fredericton, NB, Canada.
- Fraser, C. M. (1998). An evaluation of the use made of cosmetic and functional prostheses by unilateral upper limb amputees. *Prosthetics and Orthotics International*, 22(3):216–223.
- Gow, D., Geggie, C., Douglas, W., Philipson, L., and Petterson, S.-O. (1993). A simple electrical prosthesis for transcarpal absence of the hand in children - the REACH hand. Paper 19.3 in *Proceedings of the 2nd European Conference of Advances in Rehabilitation Technology, ECART*, Stockholm, Sweden.
- Gow, D. J., Douglas, W., Geggie, C., Monteith, E., and Stewart, D. (2001). The development of the Edinburgh modular arm system. *Journal of Engineering in Medicine (Part H)*, 215(3):291–298.
- Graham, B., Adkins, P., Tsai, T. M., Firrell, J., and Breidenbach, W. C. (1998). Major replantation versus revision amputation and prosthetic fitting in the upper extremity: a late functional outcomes study. *Journal of Hand Surgery [Am]*, 23:783–791.
- Grood, E. S. and Suntay, W. J. (1983). A joint coordinate system for the clinical description of three-dimensional motions: Application to the knee. *Journal of Biomechanical Engineering*, 105(2):136–144.
- Hahn, P. and Krimmer, H. (1995). Quantitative and qualitative investigation of the distal interphalangeal link. In Boheman, N., editor, *Second Triennial International Hand and Wrist Symposium. Proceedings*, 97–98, San Fransisco, California. Mayo Clinic/Mayo Foundation, American Foundation for Surgery of the Hand.
- Haugland, M. and Sinkjaer, T. (1999). Interfacing the body's own sensing receptors into neural prosthesis devices. *Technology and Health Care*, 7:393–399.

- Hazelton, F. T., Smidt, G. L., Flatt, A. E., and Stephens, R. I. (1975). The influence of wrist position on the force produced by the finger flexors. *Journal of Biomechanics*, 8:301–306.
- Herberts, P., Almström, C., and Caine, K. (1978a). Clinical application study of multifunctional prosthetic hands. *The Journal of Bone and Joint Surgery*, 60-B(4):552–560.
- Herberts, P., Almström, C., and Caine, K. (1978b). Evaluation of a multifunctional hand prosthesis. *Scandinavian Journal of Rehabilitation Medicine*, Supplement No. 6:144–150.
- Hjermstad, G. (1996). Centre of competence for congenital limb deficiency and acquired arm amputation. Report STF78 A96402, SINTEF Unimed Rehab, Oslo, Norway. ISBN 82-595-9462-5. In Norwegian.
- Holgers, K. M. and Branemark, P. I. (2001). Immunohistochemical study of clinical skin-penetrating titanium implants for orthopaedic prostheses compared with implants in the craniofacial area. *Scandinavian Journal of Plastic and Reconstructive Surgery and Hand Surgery*, 35(2):141–148.
- Hollister, A., Buford, W. L., Myers, L. M., Giurintano, D. J., and Novick, A. (1992). The axes of rotation of the thumb carpometacarpal joint. *Journal of Orthopaedic Research*, 10(3):454–460.
- Hudgins, B., Scott, R. N., and Parker, P. A. (1992). An adaptive multifunction myoelectric control system. In *Proceedings, Seventh World Congress of ISPO*, page 308, Chicago, Illinois. International Society for Prosthetics and Orthotics.
- Humbert, M., Gey, N., Muller, J., and Esling, C. (1996). Determination of a mean orientation from a cloud of orientations. Application to electron back-scattering pattern measurements. *Journal of Applied Crystallography*, 29:662–666.
- Humbert, M., Gey, N., Muller, J., and Esling, C. (1998). Comment on determination of a mean orientation from a cloud of orientations. Application to electron back-scattering pattern measurements. *Journal of Applied Crystallography*, 31:485.
- Humphreys, F. J., Bate, P. S., and Hurley, P. J. (2001). Orientation averaging of electron backscattered diffraction data. *Journal of Microscopy*, 201(Pt 1):50–58.

- Iberall, T. and Fagg, A. H. (1996). Neural network models for selecting hand shapes, chapter 12 in Wing, A. M., Haggard, P. and Flanagan, J. R., editors, *Hand and Brain: The Neurophysiology and Psychology of Hand Movements*, 243–264. Academic Press, Inc., San Diego, California.
- Isidori, A. and Nicolo, F. (1966). A device for the detection and measurement of some parameters of myoelectric potentials. Report 11, Electrotechnical Institute, University of Rome, Italy.
- Jacobs, R., Branemark, R., Olmarker, K., Rydevik, B., VanSteenberghe, D., and Branemark, P. I. (2000). Evaluation of the psychophysical detection threshold level for vibrotactile and pressure stimulation of prosthetic limbs using bone anchorage or soft tissue support. *Prosthetics and Orthotics International*, 24(2):133–142.
- Jackson, W. T., Hefzy, M. S., and Guo, H. (1994). Determination of wrist kinematics using a magnetic tracking device. *Medical Engineering and Physics*, 16:123–133.
- Jebesen, N. H., Taylor, N., Trieschmann, R. B., Trotter, M. J. and Howard, L. A. (1969). An objective and standardized test of hand function. *Archives of Physical Medicine and Rehabilitation*, 50:311–319.
- Jerregard, H., Nyberg, T., and Hildebrand, C. (2001). Sorting of regenerating rat sciatic nerve fibers with target-derived molecules. *Experimental Neurology*, 169(2):298–306.
- Jones, F. W. (1941). *The Principles of Anatomy as Seen in the Hand*. Baillière, Tindall & Cox, London, 2nd edition.
- Kaufman, K. R., An, K.-N., and Chao, E. Y. S. (1989). Incorporation of muscle architecture into the muscle length-tension relationship. *Journal of Biomechanics*, 22(8/9):943–948.
- Kelly, M. F., Parker, P. A., and Scott, R. N. (1990a). Myoelectric signal analysis using neural networks. *IEEE Engineering in Medicine and Biology Magazine*, 61–64.
- Kelly, M. F., Parker, P. A., and Scott, R. N. (1990b). The Application of Neural Networks to Myoelectric Signal Analysis: A Preliminary Study. *IEEE Transactions on Biomedical Engineering*, 37(3):221–230.
- Khatri, C. G. and Mardia, K. V. (1977). The von Mises-Fisher matrix distribution in orientation statistics. *Journal of the Royal Statistical Society. Series B*, 39(1):95–106.

- 
- Knutsen, H. et al. (Group 6, candidate 4, 19, 21, 25, 30, and 40) (1997). With the arm in focus. Project report, School of Health Education, Department of Occupational Therapy, Sør-Trøndelag University College, Norway. In Norwegian.
- Krieger Lassen, N. C., Juul Jensen, D., and Conradsen, K. (1994). On the statistical analysis of orientation data. *Acta Crystallographica*, A50:741–748.
- Kuruganti, U., Hudgins, B., and Scott, R. (1995). Two-channel enhancement of a multifunction control system. *IEEE Transactions on Biomedical Engineering*, 42(1):109–115.
- Kyberd, P. J. (1990). *Algorithmic Control of a Multifunction Hand Prosthesis*. PhD thesis, University of Southampton, UK.
- Kyberd, P. J., Chappell, P. H., and Nightingale, J. M. (1987). Sensory control of a multifunction hand prosthesis. *Biosensors*, 3:347–357.
- Kyberd, P. J., O.'Holland, Chappell, P. H., Bagwell, P., and Snaith, M. (1994). Marcus: A two degree of freedom prosthesis with hierarchical grip control. *IEEE Transactions on Rehabilitation Engineering*, 3(1):65–69.
- Kyberd, P. J., Beard, D. J., and Morrison, J. D. (1997). The population of users of upper limb prostheses attending the Oxford limb fitting service. *Prosthetics and Orthotics International*, 21(2):85–91.
- Lamoreaux, L. and Hoffer, M. M. (1995). The effect of wrist deviation on grip and pinch strength. *Clinical Orthopaedics and Related Research*, (314):152–155.
- Landsmeer, J. M. F. and Long, C. (1965). The mechanism of finger control based on electromyograms and location analysis. *Acta Anatomica*, 60:330–347.
- Lemay, M. and Crago, P. (1996). A dynamic model for simulating movements of the elbow, forearm, and wrist. *Journal of Biomechanics*, 29(10):1319–1330.
- Leow, M. E., Kour, A. K., Ng, W. K., and Pho, R. W. (1999). Creating a model for fabricating a partial hand glove prosthesis using the realigned casts of the contralateral digits. *Prosthetics and Orthotics International*, 23:72–74.
- Levy, P. (1939). L'addition des variables aléatoires définies sur une circonférence. *Bulletin de la Société Mathématique de France*, 67:1278–1302.
- Lie, E. (1944). *Anatomy for Artists*. Aschehoug, Oslo, Norway. In Norwegian.

- Light, C. M. and Chappell, P. H. (2000). Development of a lightweight and adaptable multiple-axis hand prosthesis. *Medical Engineering and Physics*, 22:679–684.
- Lindanger, T. K. and Jøsang, T. (1997). Optimization of a prosthetic wrist with a single degree-of-freedom. Project report, Department of Engineering Cybernetics, Norwegian University of Science and Technology, Norway. In Norwegian.
- Linscheid, R. L. (1986). Kinematic considerations of the wrist. *Clinical Orthopaedics and Related Research*, (202):27–39.
- Loeb, G. E., Peck, R. A., Moore, W. H., and Hood, K. (2001). Bion system for distributed neural prosthetic interfaces. *Medical Engineering and Physics*, 23(1):9–18.
- Long, II, C., Conrad, P. W., Hall, E. A., and Furler, S. L. (1970). Intrinsic-extrinsic muscle control of the hand in power grip and precision handling. *Journal of Bone and Joint Surgery*, 52-A(5):853–867.
- Lovely, D. F., Hudgins, B. S., and Scott, R. N. (1985). Implantable myoelectric control system with sensory feedback. *Medical & Biological Engineering & Computing*, 23:87–89.
- Lundborg, G. and Rosen, B. (2001). Sensory substitution in prosthetics. *Hand Clinics*, 17:481–488.
- MacKenzie, C. L. and Iberall, T. (1994). *The Grasping Hand*. Number 104 in Advances in Psychology. North-Holland/Elsevier Science, Amsterdam. ISBN 0-444-81746-8.
- Mann, K. A., Werner, F. W., and Palmer, A. K. (1989). Frequency spectrum analysis of wrist motion for activities of daily living. *Journal of Orthopaedic Research*, 7(2):304–306.
- Momentum (2001). "No matter what leg he got out of bed with first, it was never the right one...". Booklet about voluntary peer support groups, Norwegian Association for Arm and Leg Prostheses Users, Grinistubben 6, N-1359 Eiksmarka, Norway. In Norwegian.
- Moore, J. A., Ellis, R. E., Pichora, D. R., and Hollister, A. M. (1993). A kinematic technique for describing wrist joint motion: Analysis of configuration space plots. *Journal of Engineering in Medicine, Proceedings of the Institution of Mechanical Engineers, Part H*, 207:211–218.
- Napier, J. R. (1956). The prehensile movements of the human hand. *Journal of bone and joint surgery. British volume*, 38B:902–913.

- Nelson, D. L., Mitchell, M. A., Groszewski, P. G., Pennik, S. L., and Manske, P. R. (1994). Wrist range of motion in activities of daily living. In Schuind, F. et al., editors, *Advances in the Biomechanics of the Hand and Wrist*, 329–334. Plenum Press, New York.
- Näder, M. (1995). Development of myoelectric upper limb prostheses: A glance at the past and a glimpse of the future. In *Conference Proceedings, 1995 MyoElectric Controls Symposium, MEC'95*, 2–8, Inst. of Biomedical Engineering, University of New Brunswick, Fredericton, NB, Canada.
- O'Driscoll, S. W., Horii, E., Ness, R., Cahalan, T. D., Richards, R. R., and An, K.-N. (1992). The relationship between wrist position, grasp size, and grip strength. *Journal of Hand Surgery*, 17A:169–177.
- Ohshima, J., Yamamoto, T., and Matsuoka, K. (1994). On an estimation of the location of the axes of wrist joint movements. In Sheppard, N. F., Eden, M., and Kantor, G., editors, *Proceedings of the 16th Annual International Conference of the IEEE Engineering in Medicine and Biology Society*, volume 16, 333–334, Piscataway, NJ.
- Okuno, R., Yoshida, M., and Akazawa, K. (1996). Development of biomimetic prosthetic hand controlled by electromyogram. In *AMC Proceedings of the 1996 4th International Workshop on Advanced Motion Control, AMC'96. Part 1*, 103–108, Tsu, Japan. IEEE.
- O'Neill, O. R., An, K. N., Morrey, B. F., and Chao, E. Y. S. (1988). Interrelation of shoulder and elbow kinematics (abstract). *Journal of Biomechanics*, 21(10):860.
- Palmer, A. K. and Werner, F. W. (1984). Biomechanics of the distal radioulnar joint. *Clinical Orthopaedics*, (187):26–35.
- Palmer, A. K., Werner, F. W., Murphy, D., and Glisson, R. (1985). Functional wrist motion: A biomechanical study. *Journal of Hand Surgery*, 10A(1):39–46.
- Philipson, L. (1985). Adaptable myoelectric prosthetic control with functional visual feedback using microprocessor techniques. *Medical & Biological Engineering & Computing*, 23:8–14.
- Prentice, M. J. (1986). Orientation statistics without parametric assumptions. *Journal of the Royal Statistical Society. Series B*, 48(2):214–222.
- Raikova, R. (1992). A general approach for modelling and mathematical investigation of the human upper limb. *Journal of Biomechanics*, 25(8):857–867.

- Rancourt, D., Rivers, L.-P. and Asselin, J. (2000). Using orientation statistics to investigate variations in human kinematics. *Applied Statistics, Part 1*, 49:81–94.
- Randström, B. (1996). Personal correspondence. CENTRI AB, Järfälla, Sweden.
- Reiter, R. (1948). Eine neue Elektrokunsthand. *Grenzgebiete der Medizin*, 1(4):133–135.
- Ruy, J., Cooney, W. P., Askew, L. J., An, K.-N., and Chao, E. Y. S. (1991). Functional ranges of motion of the wrist joint. *Journal of Hand Surgery*, 16A(3):409–419.
- Saffar, P. and Semaan, I. (1994). *The Study of the Biomechanics of Wrist Movements in an Oblique Plane – A Preliminary Report*, volume 256 of *NATO Advanced Science Institutes Series A: Life Sciences*, 305–311. Plenum Press, NATO Advanced Research Workshop, Brussels.
- Salvia, P., Klein, P., David, J. H., and Rooze, M. (1994). The envelope of active wrist circumduction - an in vivo electrogoniometric study. In Schuind, F. et al., editors, *Advances in the Biomechanics of the Hand and Wrist*, 313–328. Plenum Press, New York.
- Salvia, P., Woestyn, L., David, J. H., Feipel, V., Van, S., Jan, S., Klein, P., and Rooze, M. (2000). Analysis of helical axes, pivot and envelope in active wrist circumduction. *Clinical Biomechanics*, 12(2):103–111.
- Samson, C., LeBorgne, M., and Espiau, B. (1991). *Robot Control: The Task Function Approach*. Number 22 in Oxford Engineering Science Series. Oxford University Press, Oxford, UK. ISBN 0-19-853805-7.
- Sarrafian, S. K., Melamed, J. L., and Goshgarian, G. M. (1977). Study of wrist motion in flexion and extension. *Clinical Orthopaedics and Related Research*, (126):153–159.
- Schlesinger, G., editor (1919). *Ersatzglieder und Arbeitshilfen*. Springer Verlag, Berlin.
- Schulz, S., Pylatiuk, C., and Brethauer, G. (2001). A new ultralight anthropomorphic hand. In *Proceedings of the International Conference on Robotics & Automation*, 2437–2441, Seoul, Corea. IEEE.
- Shannon, G. F. (1976). A comparison of alternative means of providing sensory feedback on upper limb prostheses. *Medical and Biological Engineering*, 289–294.

- Shannon, G. F. (1979). A myoelectrically-controlled prosthesis with sensory feedback. *Medical & Biological Engineering & Computing*, 17:73–80.
- Sheehan, F. T. and Mitiguy, P. (1999). In regards to the "ISB recommendations for standardization in the reporting of kinematic data". *Journal of Biomechanics*, 32(10):1135–1136. Letter to the Editor.
- Simpson, D. C. (1973). The control and supply of a multi-movement externally powered upper limb prosthesis. In *Proceedings, 4th International Symposium on External Control of Human Extremities*, 247–254.
- Simpson, D. C. (1974). The choice of control system for the multimovement prosthesis: extended physiological proprioception (E.P.P.), chapter 15 in *The Control of Upper-Extremity Prostheses and Orthoses*, 146–150. Thomas.
- Sollerman, C. and Ejeskär, A. (1995). Sollerman hand function test. a standardised method and its use in tetraplegic patients. *Scandinavian Journal of Plastic and Reconstructive Surgery and Hand Surgery*, 29(2):167–176.
- Spong, M. W. and Vidyasagar, M. (1989). *Robot Dynamics and Control*. John Wiley & Sons. No ISBN.
- Stavdahl, O. (1995). Summary: Krukenberg procedure. Posted to the St Johns University Amputee Mailing List *amputee@sjuvm.stjohns.edu* and the The Orthotics and Prosthetics ListServer *oandp-l@lists.ufl.edu* as a summary of recent discussions on the subject [cited 16 Jun 1995].  
Available from Internet: <<http://www.oandp-l.org/>> or  
<<http://amputee-online.com/amputee/ampsources.html#MAILING LISTS>>.
- Stavdahl, O., Bondhus, A. K., Pettersen, K. Y., and Malvig, K. E. (2002). Optimal statistical operators for 3-dimensional rotational data: Geometric interpretations and application to prosthesis kinematics. *Robotica*. In press.
- Stavdahl, O., Gronningsaeter, A., and Malvig, K. E. (1997a). Ultrasound based estimation of muscle contraction. In *Conference Proceedings, 1997 Myo-Electric Controls/Powered Prosthetics Symposium, MEC'97*, 65–70, University of New Brunswick, Fredericton, NB, Canada.
- Stavdahl, O., Hermansson, L., Pettersson, S.-O., Kristensen, K.-T., and Malvig, K. E. (1997b). Evaluation of built-in lithium ion batteries used as energy source for externally powered upper-limb prostheses. In *Conference Proceedings, 1997 MyoElectric Controls/Powered Prosthetics Symposium, MEC'97*, 7–12, University of New Brunswick, Fredericton, NB, Canada.

- Stavdahl, O., Witsoe, E., and Malvig, K. (1995). ProPosition(TM): A proportional myoelectric hand prosthesis control system with internal position feedback. In *Abstracts of the 8th World Congress of ISPO*, Melbourne, Australia, 1995, page 32.
- Stephens, M. A. (1979). Vector correlation. *Biometrika*, 66(1):41–48.
- Stroyan, M. and Wilk, K. E. (1993). The functional anatomy of the elbow complex. *Journal of Orthopaedic and Sports Physical Therapy*, 17(6):279–288. Clinical Commentary.
- Tønnevold, N.-O. (2002). Norwegian world sensation gives new hope to arm amputees. *MOMENTUMnytt*, (1):14–15. In Norwegian.
- Tura, A., Lamberti, C., Davalli, A., and Sacchetti, R. (1998). Experimental development of a sensory control system for an upper limb myoelectric prosthesis with cosmetic covering. *Journal of Rehabilitation Research and Development*, 35:14–26.
- Uellendahl, J. E. (2000). Upper extremity myoelectric prosthetics. *Physical Medicine and Rehabilitation Clinics of North America*, 11(3):639–652.
- van der Heijden, E. P. A. and Hillen, B. (1996). A two-dimensional kinematic analysis of the distal radioulnar joint. *Journal of Hand Surgery*, 21B(6):824–829.
- van der Meer, A., van der Veel, F. R. and Lee, D. N. (1995). The functional significance of arm movements in neonates. *Science*, 267:693–695.
- Veldpaus, F. E., Woltring, H. J., and Dortmans, L. J. M. G. (1988). A least-squares algorithm for the equiform transformation from spinal marker co-ordinates. *Journal of Biomechanics*, 21(1):45–54.
- Weir, R. F., Heckathorne, C. W., and Childress, D. S. (2001). Cineplasty as a control input for externally powered prosthetic components. *Journal of Rehabilitation Research and Development*, 38:357–363.
- Weiss, T., Miltner, W. H., Adler, T., Bruckner, L., and Taub, E. (1999). Decrease in phantom limb pain associated with prosthesis-induced increased use of an amputation stump in humans. *Neuroscience Letters*, 272:131–134.
- Werner, F. (2001). Wrist and hand coordinate systems. Personal Correspondence.

- 
- Werner, F. and Buchholz, B. (1994). Wrist and hand [online]. Proposal, constitutes a part of the ISB Recommendations for Standardization in the Reporting of Kinematic Data. The International Society of Biomechanics [cited 2002-11-06].  
Available from Internet: <<http://www.isbweb.org/standards/wrist.html>>.
- Woltring, H. J. (1994). 3-D attitude representation of human joints: a standardization proposal. *Journal of Biomechanics*, 27(12):1399–1414.
- Woltring, H. J., Huiskes, R., and de Lange, A. (1985). Finite centroid and helical axis estimation from noisy landmark measurements in the study of human joint kinematics. *Journal of Biomechanics*, 18(5):379–389.
- Wood, A. T. A. (1993). Estimation of the concentration parameters of the Fisher matrix distribution on  $\text{SO}(3)$  and the Bingham distribution on  $S_q$ ,  $q \geq 2$ . *The Australian journal of statistics*, 35:69–79.
- Wu, G. and Cavanagh, P. R. (1995). ISB recommendations for standardization in the reporting of kinematic data. *Journal of Biomechanics*, 28:1258–1261.
- You, Y., Gillespie, T. E., Flatt, A. E., and Sprague, B. L. (1978). Kinematic investigation of normal MCP joint. *Journal of Biomechanics*, 11:109–118.
- Youm, Y., McMurtry, R. Y., Flatt, A. E., and Gillespie, T. E. (1978). Kinematics of the wrist. (I). An experimental study of radio-ulnar deviation and flexion-extension. *The Journal of Bone and Joint Surgery*, 60-A(4):423–431.



## **Appendix A**

# **Tabulated Experimental Results**

This appendix gives extensive tables related to the experimental results of Chapter 7. The tables present statistical quantities and optimal kinematic parameter values calculated for the various groupings of the raw data. Figures are added to aid in the interpretation of the tabulated data.

## A.1 0-DoF Optimal Wrist

### A.1.1 Subject-based Analysis

Table A.1 lists the results of a subject-based analysis. Under the heading “Within-subject” are listed the definity, cosine variance and cosine standard deviation associated with each subject average  $\bar{R}_s$ , which is the cosine average calculated for subject s across all activities (ADL).

The column labelled “Geodesic” shows each subject’s angular distance from the grand average (GA) in terms of the angle  $\angle(\bar{R}_s, \bar{R}_{GA})$ , i.e. the *between-subject deviation*. The three rightmost columns show the difference in supination, extension and radial deviation, respectively, between each subject’s average orientation and the GA.

**Table A.1:** Subject-wise angular deviations from grand average. Largest angular deviations in boldface. All angles (columns 4–8) in  $^\circ$ , remaining quantities dimensionless.

Subj #	Within-subject			Between-subject ( $V_{cos}^{\bar{R}_{GA}}\{\bar{R}_s\} = 0.007$ )			
	Def	$V_{cos}$	$SD_{cos}$	Geodesic	Supination	Extension	Radial deviation
1	0.92	0.08	32.1	6.9	6.8	-0.9	-0.3
2	0.83	0.12	40.0	5.0	2.8	-3.8	1.9
3	0.87	0.13	41.7	2.0	-0.9	-0.3	-1.8
4	0.84	0.11	38.1	<b>17.6</b>	<b>-8.6</b>	-2.1	<b>14.3</b>
5	0.89	0.11	38.0	4.2	4.0	1.3	0.5
6	0.89	0.11	38.2	7.4	2.8	<b>5.9</b>	4.1
7	0.89	0.12	40.5	13.5	-0.5	5.2	-12.6
8	0.86	0.12	40.3	10.2	-7.7	-4.4	-5.7
<b>Mean</b>	0.87	0.11	38.6	8.3			

The between-subject deviation ranges from  $2^\circ$  for subject three to  $18^\circ$  for subject four, while the largest deviation in any clinical angle is  $14^\circ$  (subject four). The shown between-subject variance  $V_{cos}^{\bar{R}_{GA}}\{\bar{R}_s\}$  is the relative variance of all subject’s averages with respect to the GA.

Figure A.1 depicts the posture corresponding to the overall most deviant subject’s average.

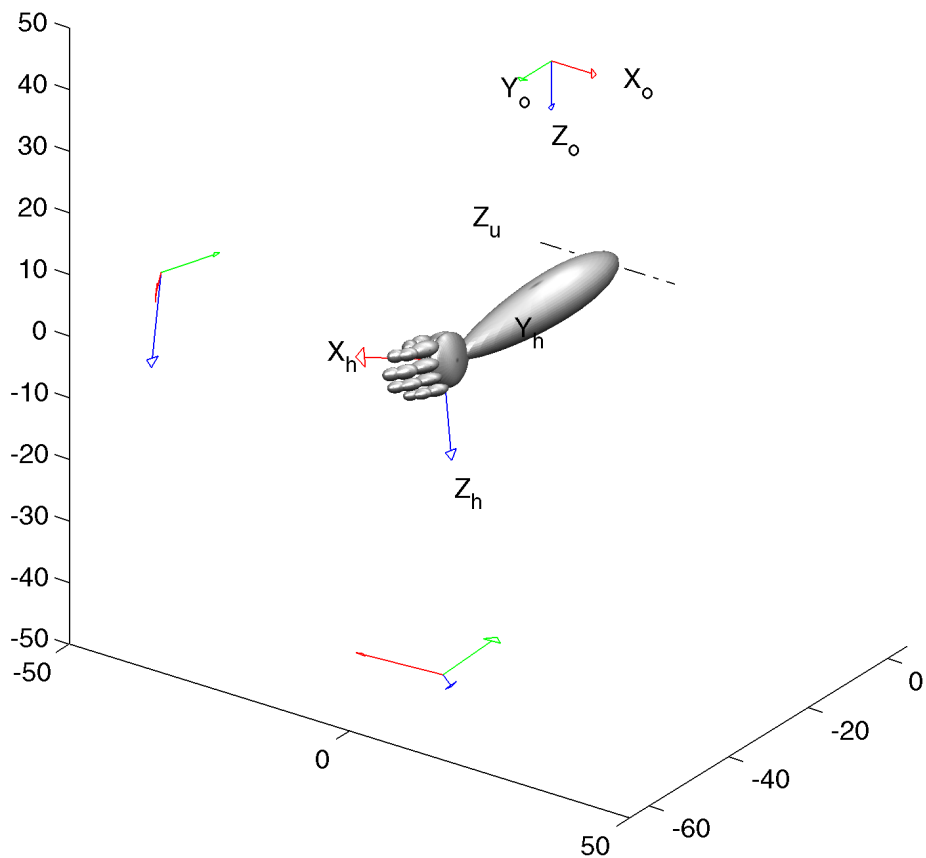


**Figure A.1:** Largest subject-based deviation from grand average orientation. The figure depicts the average wrist orientation of subject 4 over all ADL; cf. Table A.1 for numerical values.

### A.1.2 Activity-based Analysis

Table A.2 lists results of an activity-based analysis for all the ADL. Under the heading “Within-activity” are listed the definiteness, cosine variance and cosine standard deviation associated with each activity average  $\bar{R}_a$ , that is the cosine average calculated for activity  $a$  across all subjects.

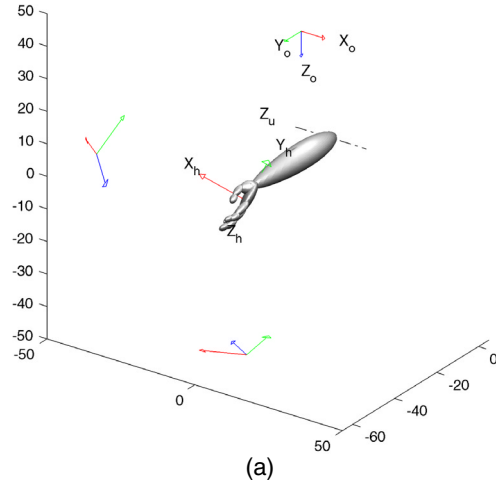
The column labelled “Geodesic” shows each activity’s angular distance from the GA in terms of the angle  $\angle(\bar{R}_a, \bar{R}_{GA})$ , i.e. the *between-activity deviation*. The three rightmost columns show the difference in supination, extension and radial deviation, respectively, between each activity’s average orientation and the GA in the same fashion as for the subject averages in Table A.1. The overall between-

**Table A.2:** Activity-wise cosine statistics and angular deviations from grand average. Largest angular deviations in boldface. All angles (columns 5–9) in  $^\circ$ ; remaining quantities dimensionless.

#	Description	Within-activity			Between-activity ( $V_{cos}^{\bar{R}_{GA}}\{\bar{R}_a\} = 0.04$ )			
		Def	$V_{cos}$	$SD_{cos}$	Geo-desic	Supi-nation	Exten-sion	Radial deviation
1	Zip-lock	0.95	0.05	25.8	21.5	15.7	-14.8	-0.9
2	Pants	0.96	0.06	28.0	1.8	-0.8	-0.7	-1.5
3	Knife and fork	0.85	0.12	41.2	13.7	-13.8	0.4	-2.0
4	Slicing bread	0.97	0.04	23.1	38.6	<b>-38.9</b>	1.5	-4.5
5	Spreading butter	0.94	0.08	31.8	35.3	-34.7	6.3	-0.0
6	Milk carton	0.94	0.06	28.8	27.9	-17.2	11.6	<b>15.3</b>
7	Stirring in pot	0.96	0.04	23.6	10.9	-0.8	7.1	-8.3
8	Pouring water	0.92	0.10	36.5	<b>39.8</b>	31.9	13.0	-14.0
9	Scissors	0.96	0.08	33.5	31.1	30.3	1.7	-3.8
10	Broom	0.84	0.11	38.6	10.9	-9.1	4.2	3.1
11	Clothesline	0.95	0.06	28.7	0.3	-0.0	-0.3	0.1
12	Sweater	0.92	0.10	37.3	22.3	20.5	-8.8	-0.8
13	Button shirt	0.96	0.05	26.0	28.3	19.2	<b>-17.1</b>	11.5
14	Threaded lid	0.86	0.10	37.2	6.1	-0.3	-2.6	5.5
15	Dishwashing	0.84	0.12	41.2	9.4	-3.4	3.7	-8.5
<b>Mean</b>		0.92	0.08	32.1	19.9			

activity deviation ranges approximately from  $0^\circ$  to  $40^\circ$ , while the largest deviation in any clinical angle is close to  $39^\circ$ . The shown ‘between-activity variance’  $V_{cos}^{\bar{R}_{GA}}\{\bar{R}_a\}$  is the relative variance of all activities’ averages with respect to the GA. Figure A.2 depicts the postures corresponding to the largest overall deviation and the largest clinical angle-based deviations from the GA.

Av., Pouring water from pot with lid, all subj.



Av., Slicing bread, all subj.

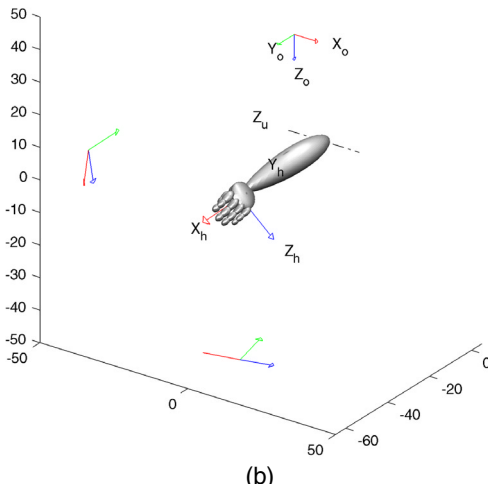


**Figure A.2:** Largest activity average-wise deviation from grand average orientation. Activity 8 (pouring water) with the largest overall deviation (a); Activity 4 (slicing bread) with the largest deviation in a single clinical angle (b). Cf. Table A.2 for numerical values.

### A.1.3 Subject/Activity-based Analysis

Table A.3 lists the angular deviation of each subject-activity average  $\bar{R}_{s,a}$  (i.e. the cosine average of all data related to subject  $s$  and activity  $a$ ) from the GA. The table contains the numerical basis for Figure 7.3.

**Table A.3:** Geodesic angular distance of subject-activity average from grand average. Largest deviation for each activity (subject) is underlined (written in boldface). All angles in  $^{\circ}$ .

Act. #	Subject #								Mean
	1	2	3	4	5	6	7	8	
1	28.2	21.8	14.3	19.3	<b><u>39.4</u></b>	7.9	18.0	33.8	22.8
2	13.4	13.9	7.7	<u>22.6</u>	4.9	10.7	19.4	3.3	12.0
3	12.4	13.9	42.2	17.8	18.0	16.2	25.9	<u>47.6</u>	24.3
4	29.7	45.1	43.5	<u>57.7</u>	27.3	37.6	42.7	39.9	40.4
5	22.7	44.9	47.5	<b><u>63.6</u></b>	23.3	40.7	41.2	43.7	41.0
6	25.7	37.5	32.9	<u>57.7</u>	33.5	17.2	10.6	36.6	31.5
7	15.1	13.9	23.7	<u>38.6</u>	18.3	14.8	26.7	17.6	21.1
8	<b>50.8</b>	44.4	<b>54.9</b>	24.0	31.6	<b>40.9</b>	<u>70.8</u>	40.2	<b>44.7</b>
9	45.3	<b><u>48.7</u></b>	42.0	45.5	1.9	28.8	32.7	21.8	33.3
10	27.1	15.0	33.9	34.1	15.8	13.3	23.3	<b><u>60.9</u></b>	27.9
11	9.2	6.4	14.1	<u>25.2</u>	8.8	2.1	17.7	7.6	11.4
12	3.3	21.8	<u>40.5</u>	13.9	35.5	30.3	36.0	22.4	25.5
13	29.0	25.6	36.3	33.8	<u>39.1</u>	25.1	19.5	28.3	29.6
14	10.9	13.1	22.3	24.0	26.0	23.7	16.3	<u>39.3</u>	22.0
15	10.2	13.3	20.3	23.3	22.2	17.9	23.1	<u>37.4</u>	21.0
<b>Mean</b>	22.2	25.3	31.7	<u>33.4</u>	23.0	21.8	28.3	32.0	27.2

### A.1.4 Age Group-based analysis

The eight subjects were divided into three groups based on age:

1. age 60 and above (subjects 1 and 8, n=2),
2. age between 30 and 40 (subjects 2...5, n=4), and
3. below 30 years of age (subjects 6 and 7, n=2).

Table A.4 lists the results of an age group-based analysis. Under the heading “Within-group” are listed the definitiy, cosine variance and cosine standard deviation corresponding to each age group’s average  $\bar{R}_{ag}$  (i.e. the cosine average calculated for each age group across all activities).

The column labelled “Geodesic” shows each age group’s angular distance from the GA in terms of the angle  $\angle(\bar{R}_{ag}, \bar{R}_{GA})$ , i.e. the *between-group deviation*. The three rightmost columns show the difference in supination, extension and radial deviation, respectively, between each age group’s average orientation and the GA.

**Table A.4:** Age group-wise variations. All angles (columns 4–8) in  $^{\circ}$ , remaining quantities dimensionless.

Age group [years]	Within-group			Between-group ( $V_{cos}^{\bar{R}_{GA}}\{\bar{R}_{ag}\} = 0.002$ )			
	Def	$V_{cos}$	$SD_{cos}$	Geodesic	Supi-nation	Exten-sion	Radial deviation
60–	0.89	0.10	37.1	4.0	-0.2	-2.5	-3.1
30–40	0.86	0.12	40.3	4.1	-0.6	-1.5	3.7
–29	0.89	0.12	40.1	7.2	1.1	<b>5.6</b>	-4.2
<b>Mean</b>	<b>0.88</b>	<b>0.11</b>	<b>39.2</b>	<b>5.1</b>			

The between-group deviation ranges from  $4^{\circ}$  to  $7^{\circ}$ , while the largest deviation in any clinical angle is  $5.6^{\circ}$  (shown in boldface). The “between-group variance”  $V_{cos}^{\bar{R}_{GA}}\{\bar{R}_a\}$  is the relative cosine variance of all age groups’ averages with respect to the GA.

### A.1.5 Sex-based Analysis

The total group of subjects included five females and three males. Table A.5 lists the results of a sex-based analysis. Under the heading “Within-sex” are listed the definiteness, cosine variance and cosine standard deviation corresponding to each sex’ average  $\bar{R}_{gen}$  (i.e. the cosine average calculated for each sex across all activities).

The column labelled “Geodesic” shows each sex’ angular distance from the GA in terms of the angle  $\angle(\bar{R}_{gen}, \bar{R}_{GA})$ , i.e. the *between-sexsex deviation*. The three rightmost columns show the difference in supination, extension and radial deviation, respectively, between each age sex’ average orientation and the GA. The

**Table A.5:** Sex-wise variations. All angles (columns 4–8) in  $^{\circ}$ , remaining quantities dimensionless.

<b>Sex</b>	<b>Within-sex</b>			<b>Between-sex (<math>V_{cos}^{\bar{R}_{GA}}\{\bar{R}_{gen}\} = 0.002^{\circ}</math>)</b>			
	<i>Def</i>	$V_{cos}$	$SD_{cos}$	<b>Geodesic</b>	<b>Supi-nation</b>	<b>Exten-sion</b>	<b>Radial deviation</b>
Female	0.88	0.12	40.4	3.5	-0.4	1.6	-3.2
Male	0.86	0.11	38.0	5.8	0.5	-2.7	<b>5.1</b>
<b>Mean</b>	0.87	0.11	39.2	4.7			

largest deviation in any clinical angle is approx.  $5^{\circ}$  (shown in boldface). The “between-sex variance”  $V_{cos}^{\bar{R}_{GA}}\{\bar{R}_{gen}\}$  is the relative cosine variance of both sexes’ averages with respect to the GA.

## A.2 1-DoF Optimal Wrist

### A.2.1 Subject-based Analysis

The optimal axis of rotation  $\mathbf{k}_{s,u}^{opt}$  and rotational offset ( $\mathbf{b}_{s,w}^{opt}, \beta_s^{opt}$ ) calculated for each subject  $s$  across all ADLs are listed in Table A.6. The vector  $\mathbf{k}_w^{opt}$  is the optimal axis of rotation decomposed in the hand-fixed frame  $S_w$ . The table is redundant in that  $\mathbf{k}_{s,w}^{opt}$  can be calculated from the other parameters. It is included because  $\mathbf{k}_{s,u}^{opt}$  and  $\mathbf{k}_{s,w}^{opt}$  have straightforward physical interpretations and – together with the definitions of the forearm- and the hand-fixed coordinate frames – uniquely define the kinematics of the optimal 1-DoF wrist with respect to the associated data set.

**Table A.6:** Optimal kinematic parameters for each subject. For interpretation of the parameters cf. Sections 5.4.2 and 6.6.2.

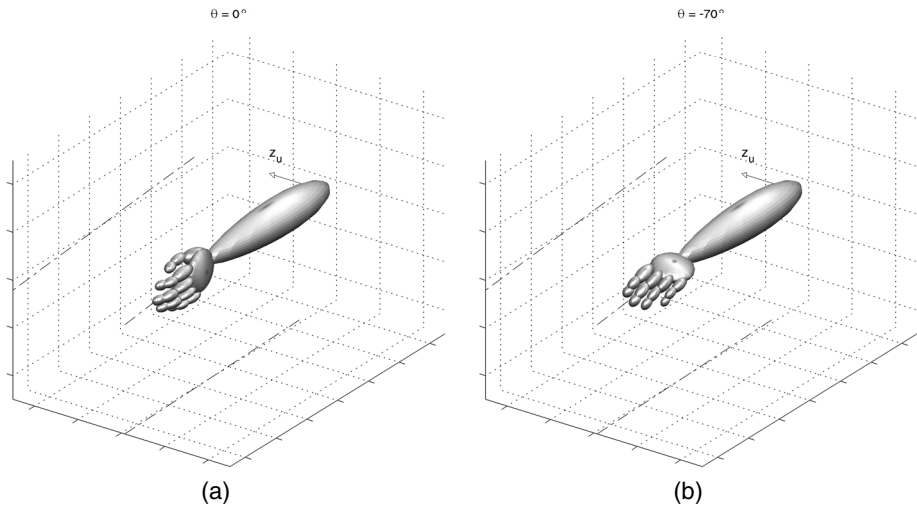
Subject #	Kinematic Parameters			
	$\mathbf{k}_{s,u}^{opt}$	$\mathbf{k}_{s,w}^{opt}$	$\mathbf{b}_{s,w}^{opt}$	$\beta_s^{opt} [^\circ]$
1	$[-0.1 \ 1.0 \ 0.0]^T$	$[0.0 \ 1.0 \ 0.1]^T$	$[0.7 \ 0.4 \ -0.6]^T$	9.0
2	$[-0.2 \ 1.0 \ 0.0]^T$	$[-0.1 \ 1.0 \ 0.1]^T$	$[0.8 \ -0.1 \ -0.7]^T$	4.5
3	$[0.1 \ 1.0 \ 0.0]^T$	$[0.2 \ 1.0 \ 0.2]^T$	$[0.7 \ -0.4 \ -0.6]^T$	10.4
4	$[-0.4 \ 0.9 \ -0.3]^T$	$[-0.4 \ 0.8 \ -0.3]^T$	$[0.3 \ -0.7 \ 0.6]^T$	15.7
5	$[-0.2 \ 1.0 \ -0.1]^T$	$[-0.2 \ 1.0 \ 0.1]^T$	$[0.9 \ 0.0 \ -0.4]^T$	9.8
6	$[-0.2 \ 1.0 \ -0.1]^T$	$[-0.2 \ 1.0 \ 0.1]^T$	$[1.0 \ 0.0 \ -0.1]^T$	13.1
7	$[0.0 \ 1.0 \ -0.1]^T$	$[0.3 \ 0.9 \ 0.2]^T$	$[0.6 \ -0.1 \ -0.8]^T$	21.4
8	$[-0.2 \ 1.0 \ -0.2]^T$	$[0.0 \ 1.0 \ -0.2]^T$	$[0.3 \ -0.7 \ -0.7]^T$	15.6

Table A.7 summarizes the variations within and across subjects with respect to the 1-DoF approximation.

The two parameter sets whose axis of rotation deviates the most from the grand axis of rotation with respect to the forearm and the hand, respectively (marked with boldface in the table) give rise to the postures and axes shown in Figures A.3 and A.4. The axis of rotation of subject 3 closely resembles a prosupination axis, while that of subject 4 is oblique and causes significant wrist extension at negative  $\theta$  angles (Figure A.4b).

**Table A.7:** Variations in subject-based optimal 1-DoF kinematics. Cosine quantities dimensionless, all remaining quantities in  $^{\circ}$ .

Subject #	Within-subject mean residual		Between-subject angular deviation from grand axis of rotation with respect to	
	Angular	Cosine	$S_u$	$S_w$
1	22.2	0.90	9.5	9.7
2	31.2	0.81	7.3	10.6
3	30.7	0.83	14.7	<b>13.3</b>
4	30.6	0.82	<b>18.8</b>	6.3
5	27.4	0.86	6.6	4.8
6	26.7	0.85	4.2	8.0
7	27.5	0.84	9.3	4.3
8	29.6	0.83	8.1	9.8
<b>Mean</b>	28.2	0.84	9.8	8.3



**Figure A.3:** Axis and postures for optimal 1-DoF parameters based on subject 3. This subject's axis of rotation exhibited the largest angular deviation from the grand axis with respect to the hand-fixed frame. Axis of rotation and its projections are shown with dashdot-style lines.

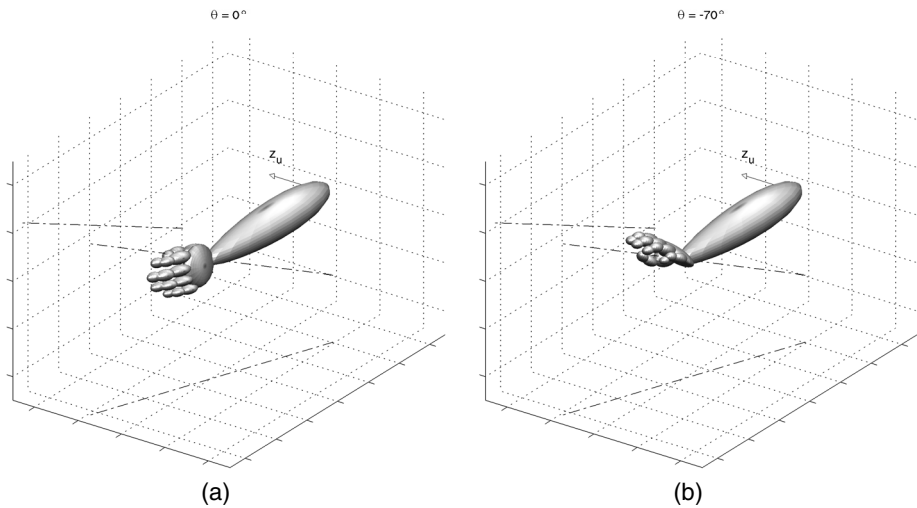


**Figure A.4:** Axis and postures for optimal 1-DoF parameters based on subject 4. This subject's axis of rotation exhibited the largest angular deviation from the grand axis with respect to the forearm-fixed frame. Axis of rotation and its projections are shown with dashdot-style lines.

### A.2.2 Activity-based Analysis

The optimal axis of rotation  $\mathbf{k}_{a,u}^{opt}$  and rotational offset ( $\mathbf{b}_{a,w}^{opt}, \beta_a^{opt}$ ) calculated for each activity  $a$  across all subjects are listed in Table A.8. .

**Table A.8:** Optimal kinematic parameters for each activity. For interpretation of the parameters cf. Sections 5.4.2 and 6.6.2.

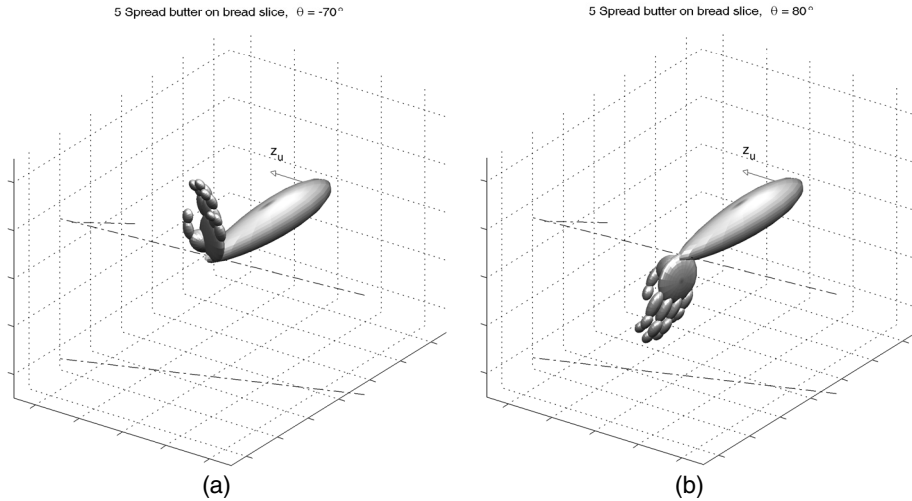
#	Description	Kinematic Parameters			
		$\mathbf{k}_{a,u}^{opt}$	$\mathbf{k}_{a,w}^{opt}$	$\mathbf{b}_{a,w}^{opt}$	$\beta_a^{opt} [^\circ]$
1	Zip-lock	$[-0.6 \ 0.8 \ -0.2]^T$	$[-0.6 \ 0.8 \ -0.2]^T$	$[-0.5 \ 0.8 \ -0.4]^T$	10.1
2	Pants	$[-0.5 \ 0.9 \ -0.2]^T$	$[-0.6 \ 0.8 \ -0.3]^T$	$[0.7 \ -0.6 \ -0.4]^T$	12.9
3	Knife and fork	$[0.1 \ 1.0 \ 0.2]^T$	$[0.0 \ 1.0 \ 0.1]^T$	$[0.5 \ -0.8 \ -0.3]^T$	18.0
4	Slicing bread	$[-0.3 \ 0.7 \ -0.6]^T$	$[-0.8 \ 0.5 \ -0.3]^T$	$[0.2 \ -0.9 \ -0.3]^T$	38.0
5	Spreading butter	$[-0.1 \ 0.3 \ -0.9]^T$	$[-0.7 \ 0.1 \ -0.7]^T$	$[0.4 \ -0.9 \ 0.2]^T$	43.5
6	Milk carton	$[-0.3 \ 0.9 \ -0.3]^T$	$[-0.3 \ 0.8 \ -0.5]^T$	$[0.5 \ -0.7 \ 0.4]^T$	31.5
7	Stirring in pot	$[0.1 \ 0.9 \ -0.4]^T$	$[-0.1 \ 0.8 \ -0.6]^T$	$[0.7 \ 0.0 \ -0.7]^T$	20.2
8	Pouring water	$[0.5 \ 0.9 \ -0.1]^T$	$[0.2 \ 1.0 \ -0.1]^T$	$[0.4 \ 0.7 \ -0.6]^T$	38.9
9	Scissors	$[-1.0 \ 0.2 \ 0.0]^T$	$[-0.9 \ 0.0 \ -0.4]^T$	$[0.2 \ 0.9 \ -0.4]^T$	30.3
10	Broom	$[0.0 \ 1.0 \ -0.2]^T$	$[-0.1 \ 0.9 \ -0.4]^T$	$[0.7 \ -0.7 \ 0.0]^T$	17.6
11	Clothesline	$[-0.2 \ 1.0 \ -0.2]^T$	$[-0.3 \ 0.9 \ -0.3]^T$	$[0.8 \ -0.3 \ -0.5]^T$	8.6
12	Sweater	$[-0.3 \ 1.0 \ 0.0]^T$	$[-0.4 \ 0.9 \ 0.0]^T$	$[-0.1 \ 0.9 \ -0.3]^T$	16.0
13	Button shirt	$[-0.8 \ 0.6 \ -0.1]^T$	$[-0.6 \ 0.8 \ -0.2]^T$	$[-0.4 \ 0.8 \ 0.4]^T$	18.3
14	Threaded lid	$[-0.1 \ 1.0 \ -0.1]^T$	$[-0.1 \ 1.0 \ -0.1]^T$	$[0.8 \ -0.6 \ 0.1]^T$	5.9
15	Dishwashing	$[-0.1 \ 1.0 \ -0.2]^T$	$[-0.4 \ 0.9 \ -0.3]^T$	$[0.6 \ -0.3 \ -0.7]^T$	17.9

Table A.9 summarizes the variations within and between activities with respect to the 1-DoF approximation.

The parameter sets whose axis of rotation has the largest components in the  $x$ - and the  $z$ -direction (activity 5 and 9), respectively, give rise to the postures and axes shown in Figures A.5–A.6.

**Table A.9:** Variations in activity-based optimal 1-DoF kinematics. All angles (columns 2, 4 and 5) in  $^{\circ}$ , remaining quantities dimensionless.

ADL		Within-activity mean residual		Between-activity angular deviation from grand axis of rotation with respect to	
#	Description	Angular	Cosine	$S_u$	$S_w$
1	Zip-lock	17.7	0.93	28.7	25.7
2	Pants	17.5	0.93	20.7	22.1
3	Knife and fork	29.1	0.81	24.0	23.1
4	Slicing bread	15.4	0.94	36.9	41.2
5	Spreading butter	23.1	0.90	62.4	64.1
6	Milk carton	18.8	0.92	16.6	16.4
7	Stirring in pot	13.8	0.94	19.6	23.1
8	Pouring water	23.3	0.87	38.9	23.9
9	Scissors	19.0	0.91	<b>72.7</b>	<b>74.2</b>
10	Broom	28.2	0.82	6.4	9.8
11	Clothesline	18.6	0.92	6.4	6.2
12	Sweater	23.5	0.88	11.2	13.8
13	Button shirt	17.2	0.94	41.9	26.3
14	Threaded lid	28.8	0.84	3.3	8.0
15	Dishwashing	30.5	0.81	2.3	10.2
<b>Mean</b>		21.6	0.89	26.1	25.9



**Figure A.5:** Axis and postures for optimal 1-DoF parameters based on activity 5. This activity's axis of rotation had the largest  $z$ -component with respect to both the forearm-fixed and the hand-fixed coordinate frame. The resulting range motion resembles that of a “dart-thrower’s motion” as described by Palmer et al. (1985). This activity also exhibited the largest angular offset between forearm and hand. Axis of rotation and its projections are shown with dashdot-style lines.

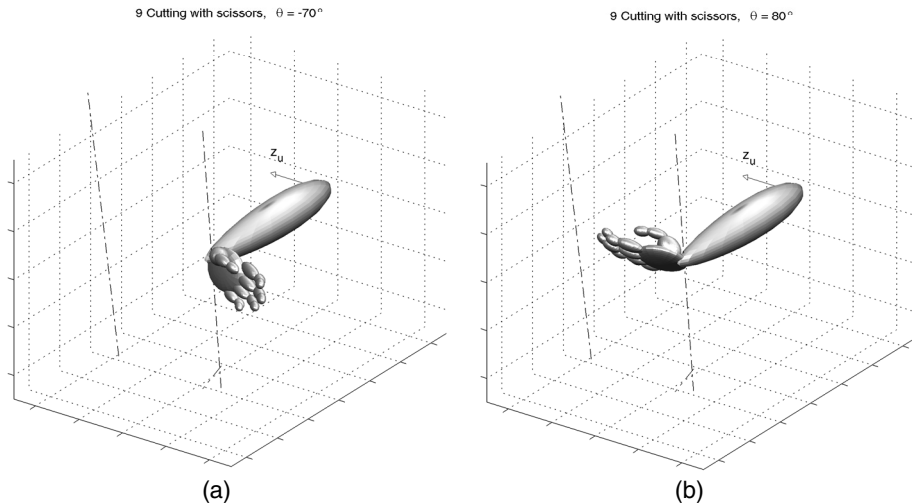


**Figure A.6:** Axis and postures for optimal 1-DoF parameters based on activity 9. This activity’s axis of rotation had the largest  $x$ -component with respect both the forearm-fixed and the hand-fixed coordinate frame, and the resulting range of motion is crudely restricted to that of wrist flexion and extension. This activity also exhibited the largest angular deviation from the grand axis of rotation with respect to both forearm and hand. Axis of rotation and its projections are shown with dashdot-style lines.

### A.2.3 Age Group-based Analysis

The optimal axis of rotation  $\mathbf{k}_{ag,u}^{opt}$  and rotational offset  $(\mathbf{b}_{ag,w}^{opt}, \beta_{ag}^{opt})$  calculated for each age group  $ag$  across all activities are listed in Table A.10. Table A.11 summarizes the variations within and across age groups with respect to the 1-DoF approximation.

**Table A.10:** Optimal kinematic parameters for each age group. For interpretation of the parameters cf. Sections 5.4.2 and 6.6.2.

Age group [years]	Kinematic Parameters			
	$\mathbf{k}_{ag,u}^{opt}$	$\mathbf{k}_{ag,w}^{opt}$	$\mathbf{b}_{ag,w}$	$\beta_{ag}^{opt} [\circ]$
60–	$[-0.1 \ 1.0 \ -0.1]^T$	$[-0.3 \ 0.9 \ -0.2]^T$	$[0.5 \ -0.3 \ -0.8]^T$	9.8
30–40	$[-0.2 \ 1.0 \ -0.1]^T$	$[-0.2 \ 1.0 \ -0.2]^T$	$[0.8 \ -0.5 \ -0.1]^T$	7.0
–29	$[-0.1 \ 1.0 \ -0.1]^T$	$[-0.2 \ 0.9 \ -0.3]^T$	$[0.8 \ -0.1 \ -0.5]^T$	15.9

**Table A.11:** Variations in age group-based optimal 1-DoF kinematics. All angles (columns 2, 4 and 5) in  $^\circ$ , remaining quantities dimensionless.

Age group [years]	Within-group mean residual		Between-group angular deviation from grand axis of rotation with respect to	
	Angular	Cosine	$S_u$	$S_w$
60–	25.9	0.86	1.2	3.0
30–40	30.1	0.83	2.1	2.5
–29	27.2	0.84	<b>2.5</b>	<b>6.1</b>
<b>Mean</b>	27.7	0.84	1.9	3.9

The parameter set whose axis of rotation deviates the most from the grand optimal axis, namely that corresponding to subjects below 30 years of age, gives rise to the postures and axes shown in Figure A.7. Note that since the deviation from the grand axis is small, age group-specific kinematics is virtually identical to that of the grand optimal parameter set (cf. Figure 7.5).

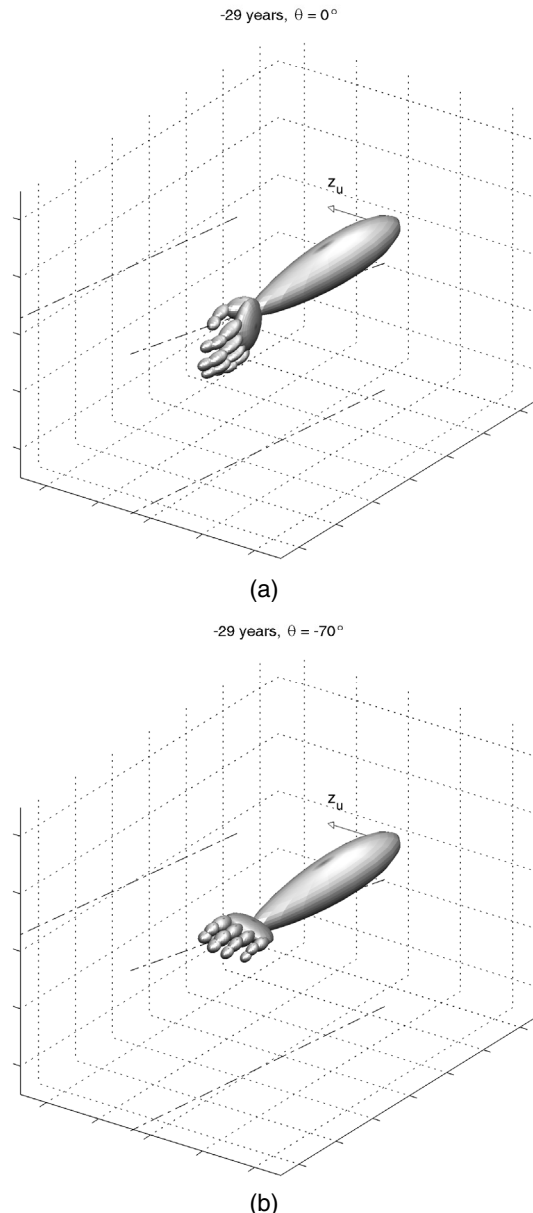


**Figure A.7:** Axis and postures for optimal 1-DoF parameters for subjects below 30 years of age. This age group's axis of rotation showed the largest angular deviation from the grand axis with respect to both forearm and hand. Axis of rotation and its projections are shown with dashdot-style lines.

### A.2.4 Sex-based Analysis

The optimal axis of rotation  $\mathbf{k}_{sex, u}^{opt}$  and rotational offset ( $\mathbf{b}_{sex, w}^{opt}, \beta_{sex}^{opt}$ ) calculated for each sex  $sex$  across all activities are listed in Table A.12. Variations within and across sexes with respect to the 1-DoF approximation are summarized in Table A.13.

**Table A.12:** Optimal kinematic parameters for each sex. For interpretation of the parameters cf. Sections 5.4.2 and 6.6.2.

Sex	Kinematic Parameters			
	$\mathbf{k}_{sex, u}^{opt}$	$\mathbf{k}_{sex, w}^{opt}$	$\mathbf{b}_{sex, w}^{opt}$	$\beta_{sex}^{opt} [^\circ]$
Female	$[-0.1 \ 1.0 \ -0.1]^T$	$[-0.2 \ 0.9 \ -0.2]^T$	$[0.7 \ -0.3 \ -0.6]^T$	12.4
Male	$[-0.2 \ 1.0 \ -0.1]^T$	$[-0.2 \ 1.0 \ -0.2]^T$	$[0.8 \ -0.6 \ 0.1]^T$	6.3

**Table A.13:** Variations in sex-based optimal 1-DoF kinematics. All angles (columns 2, 4 and 5) in  $^\circ$ , remaining quantities dimensionless.

Sex	Within-sex mean residual		Between-sex angular deviation from grand axis of rotation with respect to	
	Angular	Cosine	$S_u$	$S_w$
Female	28.3	0.84	0.7	0.7
Male	28.3	0.84	1.4	1.4
<b>Mean</b>	<b>28.3</b>	<b>0.84</b>	<b>1.0</b>	<b>1.0</b>

The two parameter sets whose axis of rotation deviates the most from the grand axis of rotation with respect to the forearm and the hand, respectively, give rise to the postures and axes shown in Figures A.8 and A.9.

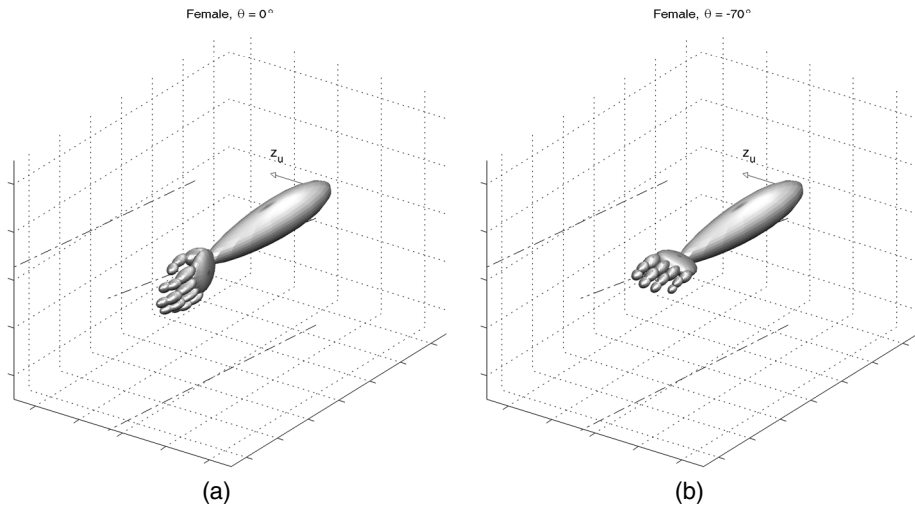


**Figure A.8:** 1-DoF model optimized for female subjects. Axis of rotation and example postures.

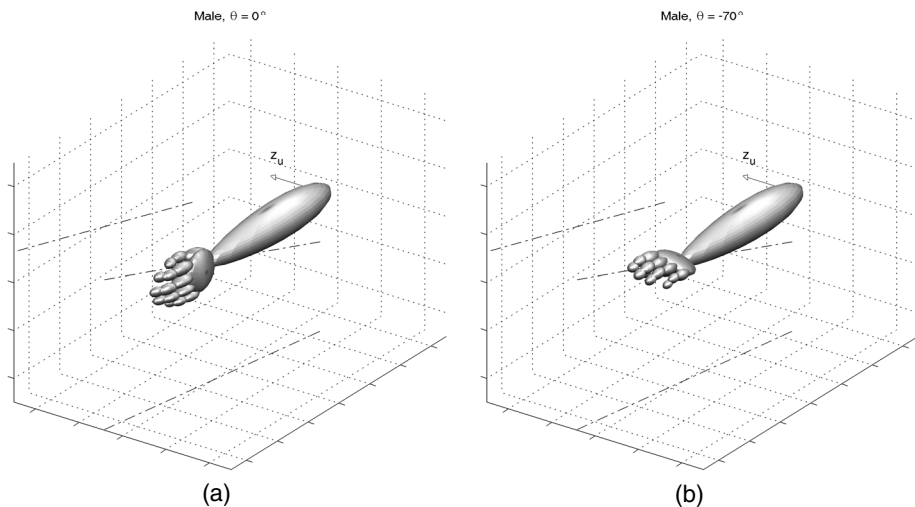


**Figure A.9:** 1-DoF model optimized for male subjects. Axis of rotation and example postures.